Universidade do Minho

Escola de Engenharia

Tiago João Silva Sousa Azevedo Costa

Analysis of internal combustion engines towards the improvement of its efficiency

Tese de Mestrado
Ciclo de Estudos Integrados Conducentes ao
Grau de Mestre em Engenharia Mecânica

Trabalho efetuado sob a orientação do
Professor Doutor Jorge José Gomes Martins

Coorientação do
Professor Doutor Francisco Brito

Outubro de 2014

DECLARAÇÃO

Nome

Tiago João Silva Sousa Azevedo Costa
_____

Endereço electrónico: tcostavn@gmail.com _____ Telefone: 919030668 ____ / _____

Número do Bilhete de Identidade: 13913590 _____

Título dissertação □/tese □

 Analysis of Internal Combustion Engines towards the improvement of its efficiency _____

_____

_____

Orientador(es):

Professor Doutor Jorge Martins e Professor Doutor Francisco Brito _____

_____ Ano de conclusão: 2014 _____

Designação do Mestrado ou do Ramo de Conhecimento do Doutoramento:

 Mestrado Integrado em Engenharia Mecânica _____

Nos exemplares das teses de doutoramento ou de mestrado ou de outros trabalhos entregues para prestação de provas públicas nas universidades ou outros estabelecimentos de ensino, e dos quais é obrigatoriamente enviado um exemplar para depósito legal na Biblioteca Nacional e, pelo menos outro para a biblioteca da universidade respectiva, deve constar uma das seguintes declarações:

1. É AUTORIZADA A REPRODUÇÃO INTEGRAL DESTA TESE/TRABALHO APENAS PARA EFEITOS DE INVESTIGAÇÃO, MEDIANTE DECLARAÇÃO ESCRITA DO INTERESSADO, QUE A TAL SE COMPROMETE;

2. É AUTORIZADA A REPRODUÇÃO PARCIAL DESTA TESE/TRABALHO (indicar, caso tal seja necessário, nº máximo de páginas, ilustrações, gráficos, etc.), APENAS PARA EFEITOS DE INVESTIGAÇÃO, , MEDIANTE DECLARAÇÃO ESCRITA DO INTERESSADO, QUE A TAL SE COMPROMETE;

3. DE ACORDO COM A LEGISLAÇÃO EM VIGOR, NÃO É PERMITIDA A REPRODUÇÃO DE QUALQUER PARTE DESTA TESE/TRABALHO

Universidade do Minho, ____/____/_____

Assinatura: _____

Acknowledgements

The author wishes to thank the following persons for their support during all the work herein described:

Jorge Martins, PhD

Francisco Brito, PhD

Bernie Bon

Analysis of internal combustion engines towards the improvement of its efficiency

Abstract

This work discusses ways for internal combustion engine efficiency improvement using unconventional technologies and mechanisms. A low consumption engine developed to participate in the Eco-Marathon Shell contest was used as a basis for this study.

The first part of this work details the steps of the design and thermodynamic analysis of a high efficient internal combustion engine, with special emphasis on the crankshaft system. The second part analyses the inlet port to enhance production of turbulence by swirl, creating high combustion speeds. To perform this task the use of two software programs was required, SolidWorks, and CONVERGE. The modelling tests included normal engine cycle operation, performing all 4 strokes.

An unconventional crankshaft was studied to improve combustion efficiency. The main goal was to generate constant volume combustion to increase combustion efficiency and eliminate negative work done over the piston before top dead centre. CONVERGE, which includes the combustion model SAGE, was used to determinate the heat release rate during constant volume combustion.

The purpose of the third part of this work was to calculate the potential for heat recovery of the combustion chamber and exhaust valve walls in order to run the engine as "quasi-adiabatic", by using a direct water injection added (to cool down the wall surface) after the end of combustion.

Finally, all the results of the features were analysed, presented, illustrated and compared using the engine cycle P-V diagram, which clearly shows the overall amount of work produced by the thermodynamic cycle performed with the internal combustion engine. Although more work and study has to be done in order to quantify all the variables involved to produce the most efficient cycle, it is expected that the thermal efficiency might reach values close to 50%.

Análise de motores de combustão interna para a melhoria da sua eficiência

Resumo

Este trabalho discute formas de melhorar a eficiência de motores de combustão interna, utilizando tecnologias e mecanismos não convencionais. Um motor de baixo consumo desenvolvido para participar na competição Eco-Marathon Shell foi utilizado como base para o presente estudo.

A primeira parte deste trabalho detalha as etapas de projeto e análise termodinâmica de um motor de combustão interna de alta eficiência, com especial destaque para a sua cambota. A segunda parte analisa a conduta de admissão para aumentar a produção de turbulência por swirl, criando velocidades de combustão elevadas. Para executar esta tarefa foi necessário o uso de dois programas de software, SolidWorks, e CONVERGE. As simulações incluem a operação normal do ciclo do motor, realizando os 4 tempos.

Uma cambota não convencional foi estudada para melhorar a eficiência da combustão. O objetivo principal foi gerar combustão a volume constante para aumentar a eficiência de combustão e eliminar o trabalho negativo feito sobre o pistão antes do ponto morto superior. O CONVERGE, que inclui o modelo de combustão SAGE, foi usado para determinar a taxa de libertação de calor durante a combustão a volume constante.

O objetivo da terceira parte deste trabalho foi calcular o potencial de recuperação de calor das paredes da câmara de combustão e válvulas de escape para um funcionamento do motor como ''quase-adiabático'', usando injeção direta de água (para arrefecer o superfície de parede), após o final da combustão.

Por fim, todos os resultados foram analisados, apresentados e comparados através do diagrama P-V do ciclo do motor, mostrando o montante global do trabalho produzido pelo ciclo termodinâmico realizado pelo motor. Mais estudo e trabalho tem de ser feito de modo a quantificar todas as variáveis envolvidas para produzir o ciclo mais eficiente, no entanto é esperado que a eficiência térmica possa atingir valores próximos de 50%.

Table of contents

List of Figures

x

List of tables

Symbols

a - Efficiency factor

A - Area

c_v - Specific heat at constant volume

c_p - Specific heat at constant pressure

d - Pipe diameter

D - Cylinder bore

h - Heat transfer coefficient

$\bar{h}$ - Medium heat transfer coefficient

k - Thermal conductivity

l - Cell width

L - Pipe length

m - Mass

$\dot{m}$ - Mass flow rate

M - Form factor

MFB - Mass fraction burned

n - Polytrophic index

Nu - Nusselt number

Q - Heat transfer

$\dot{Q}$ - Heat flux

Re - Reynolds number

S - Swirl number

Sp - Mean piston speed

t - Time

T - Temperature

α - Thermal diffusivity

W - Work

Δw - Water injection duration

x - Dilution mass fraction

ε - Droplet heat transfer effectiveness

μ - Dynamic viscosity

η - Efficiency

θ - Crank angle

ρ - Density

Ω - Angular speed

Subscripts

air – Fresh air/intake mixture

comb – Combustion

drop – Droplet

f – Final

flow – Air flow

gas – Remaining hot gases

i – Initial

in – Inlet

inj – Injected

out – Outlet

tot – Total

vap – Vapour

Abbreviations

AFR – Air fuel ratio

ATDC – After top dead center

BDC – Bottom dead center

BTDC – Before top dead center

CA – Crankshaft angle

CAD – Computer aided design

CFD – Computer fluid dynamics

CNC – Computer numeric control

CR – Compression ratio

CVC – Constant volume combustion

DISP – Displacement

EGR – Exhaust gas recirculation

HEHC – High efficiency hybrid cycle

ICE – Internal combustion engine

IVO – Intake valve opening

LIVC – Early intake valve closure

MBT – Maximum brake torque

MFB – Mass fraction burn

NeCCoRC – Nested coaxial counter rotating cam

OEE – Over-expanded engine

QCV – Quasi-constant volume

STL – STereoLithography

TDC – Top dead center

TTW – Tank-To-Wheel

VSE – Variable stroke engine

WFR – Water fuel ratio

WOT – Wide open throttle

WTW – Well-To-Wheel

1. Introduction

The society is more and more focused on the quest for efficiency in order to reduce waste in every aspect of life [1]. The same is happening in the automotive industry and particularly concerning internal combustion engines (ICEs), where the wasted energy and pollutant emissions are still quite significant [2]. Nowadays we are witnessing a paradigm shift on the automotive industry towards electric mobility which has a good potential for efficiency improvement. Still, on a life cycle analysis perspective (Well-To-Wheel - WTW) the efficiency and emission record of electric vehicles will depend also on the efficiency and emissions of the electricity production and transport. ICEs might sometimes be less pollutant and aggressive to the environment as long as their efficiency (Tank-To-Wheel - TTW) is high. Indeed, when electricity is produced from thermal power station, the overall WTW efficiency might be lower when compared to efficient vehicles using ICEs.

However ICEs suffers from fairly low efficiency due to theoretical thermodynamic limitations of ideal cycles as well as additional energy losses due to deviations from ideal cycles such as heat transfer from the hot burning gases to the combustion chamber walls, among many others [2]. From the theoretical 62% efficiency of the Otto cycle typically only 30% of the fuel energy is converted into useful work; 35% is lost as heat by the cooling system, and another 35% is lost within the exhaust gases [3]. Therefore there is still a long way to achieve really efficient ICEs.

A lot of effort in engine research and development in recent years has been dedicated to the use of technologies such as Variable Compression Ratio, Variable Valve Timing or Charge Stratification in order to maximize efficiency. This highlights to current general tendency to create and design engines that work under different conditions depending on the demand, with constant improvement of fuel consumption.

The studies performed in this work aim to provide innovative ways of improving ICE efficiency using unconventional technologies and mechanisms, differently than what is being actually developed by the big automotive industries. Nonetheless, the objective is always the decrease of fuel consumption and thus the efficiency enhancement of engines using novel technologies.

Some of the sources of inefficiencies or losses in the spark ignition ICEs are presented in Table 1. The several technical solutions studied in this work aim to minimize those losses. The table also

shows some of the ways way that those technologies can improve engine performance by reduction of the referred losses.

Table 1 - Reduction of different losses for improved fuel economy.

	Over-expansion	Water injection	Isochoric combustion	Turbulence Enhancement	Combustion chamber design
Exhaust to ambient	x	x			
Combustion duration			X	x	x
Heat losses		x			x

The present work presents the potential benefits of unconventional ways to increase engine efficiency, by using two different crankshaft designs, a hypotrochoid crankshaft and a cam crankshaft. Direct water injection, turbulence generation in the intake channel and combustion chamber design. All these features are studied using a base engine called the UMotor.

In the following section (Chapter 2) an analysis will be made to these technologies, focusing on the achievements reached in the past years in terms of engine thermal efficiency and other performance measures. Additionally is presented a detailed description of the UMotor development, an overview of the commercial computer fluid dynamics (CFD) software and a 0D model, created in Matlab Simulink, used to perform the present studies.

Chapter 3 contains the detailed efficiency improvement analysis of all the features proposed. Starting with the over-expansion using the hypotrochoid crankshaft of the UMotor, the piston friction using the unconventional crankshaft is calculated. Then the thermodynamic efficiency of the UMotor is calculated using the 0D engine model. On the combustion efficiency improvement, a CFD simulation using the UMotor combustion chamber is performed to quantify the combustion efficiency improvement using turbulence generation, improved combustion chamber design and two spark plugs. Constant volume combustion, using a cam crankshaft, was also simulated using the CFD software in order to determinate and quantify the combustion and thermodynamic efficiency improvement. A combustion 0D model developed by the author, in order to be

implemented on a wall temperature model, is detailed and validated using the CFD software. The chapter is finalized with a wall temperature model description along with the direct water injection feature to cool the combustion chamber and valve walls.

Chapter 4 shows all the features results comparison using the engine cycle Pressure-Volume (P-V) diagram calculated using the 0D engine model in Matlab Simulink.

2. State of the art

2.1 Combustion Chamber Design

The combustion chamber shape is extremely important to achieve high combustion efficiency. Therefore a lot of importance has been put on the combustion chamber design over the years of engine research. Initially the cylinder head was little more than a cover for the cylinder where the simplest configuration was the side valve engine with the inlet and exhaust valves together at one side of the cylinder. The most successful combustion chamber for the side valve engine was the Ricardo turbulent head [4]. This design was the result of extensive experimental studies aimed at improving combustion.

Nowadays there are many different combustion chamber shapes. The principal characteristics of the combustion chamber that will change the combustion efficiency of an ICE are:

- Compactness;
- Spark plug position;
- Controlled wall temperature;
- Gas exchange area, and valve position;
- Turbulence generation intensity;
- Intake and exhaust channels position.

The first four characteristics are inherent to the combustion chamber design. The last two are related to the intake and exhaust channels design and the valve system. The objectives of those chamber design characteristics which are related to engine efficiency and emissions are [3]:

- Fast combustion process, with low cycle by cycle variability;
- Minimum heat loss to the combustion chamber walls;
- Low fuel octane index requirement.

To achieve those major design objectives some considerations have to be taken in the design procedure of a combustion chamber [3]:

- Minimization of the distance travelled by the flame front; by minimising the distance between the spark plug and the end gas, combustion will be as fast as possible reducing

the time available for the chain reactions that lead to knock to occur. This implies that, for geometrically similar engines, those with the smallest diameter cylinders will be able to use the highest compression ratios;

- The exhaust valve and spark plug should be close together; the exhaust valve is very hot (possibly incandescent) so it should be positioned as far from the end gas as possible to avoid inducing knock or pre-ignition;

- Turbulence generation; there should be sufficient turbulence to promote a rapid combustion. However, too much turbulence will lead to excessive heat transfer to the chamber walls and also very fast combustion is noisy;

- The end gas should be in a cool part of the combustion chamber; the small clearance between the cylinder head and the piston in the squish area forms a cool region. Since the inlet valve is cooled during the induction stroke, it too can be positioned at the end gas region.

The advancements achieved in the knowledge of the fundamentals of spark ignition engine combustion, in cylinder gas motion, and heat transfer allow nowadays to perform a rigorous procedure for evaluating these factors and develop an optimized combustion chamber. This procedure leads to an optimum combustion chamber design with the following features:

- Compact (low surface/volume ratio) using under-square engines (stroke larger than the bore) as these have combustion chambers with a better surface to volume ratio;
- Central spark plug, or two spark plugs per cylinder;
- Flame front area increasing with its progression (hemispherical combustion chamber);
- Valves position so as to increase the gas exchange area, and exhaust valves not excessively big in order to increase the cooling efficiency;
- High turbulence generation without penalizing volumetric efficiency.

Very often the production and economic considerations rather than the thermodynamic considerations will determine the type of combustion chamber used. In the case of low production volume, custom-built engines used in high level motorsport competitions, this factor is normally not that relevant.

A study done by S. G. Poulos [5] shows the effect of four different chamber geometries on flame front area, and thus on combustion efficiency (Figure 1).

| Open | Disc | Hemi | Bowl-in-piston |
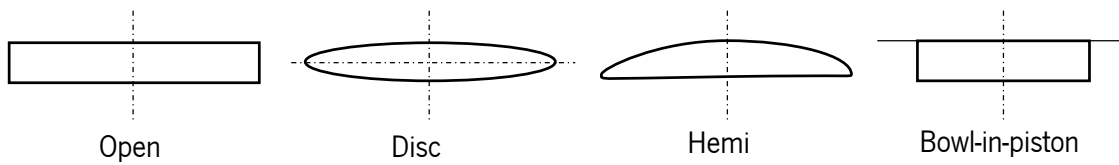
Figure 1 - Four different combustion chamber geometry's.

The bowl-in-piston chamber gives flame surface areas which are 30 to 45 percent larger than those obtained with the disc chamber under equivalent conditions around top dead centre (TDC). The hemispherical and open chamber showed gains of about 30 percent relatively to the equivalent disc configuration. For a given chamber shape, the flame area depends even more significantly on plug location. Shifting the plug from a side to a central location may increase the peak flame area by 150 percent [5]. When it is not possible to locate the plug centrally, 2 plugs should be placed at the sides.

The hemispherical chamber with a centre location plug has the fastest combustion process, relatively to burn rate results for different chamber geometries. This type of combustion chamber shows good compactness which, coupled with large valve diameters, allows a good compromise between power and combustion stability at low speeds. There is normally a small amount of squish provided at either side of the valve ports. Nevertheless, more squish can be created, if necessary, by using a raised or domed piston-crown (Figure 2).
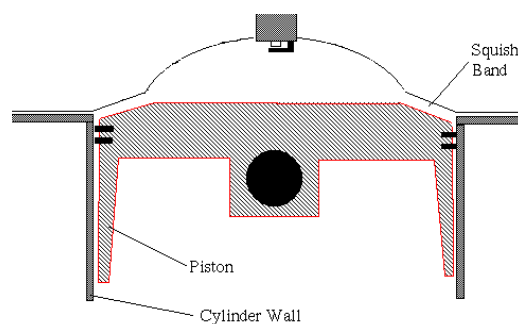
Figure 2 - Hemispherical combustion chamber and piston with squish band.

Brunt [6] in his doctoral thesis on combustion chamber design showed that:

- The cylinder pressure and mass burn (combustion) rate can be significantly altered by changing the chamber design. The design parameters having the greatest effect are the

number of spark plugs, spark plug location, and compression ratio and chamber shape. Chambers producing high combustion rates were found to have reduced cyclic dispersion;

- For lean burn engines, dual spark plugs designs were shown to provide improved performance over single spark plug designs. With single ignition, a bowl in piston arranged such that it provides about 60% of squish area associated with a centrally located spark plug should provide reasonable lean mixture performance.

Several papers have been published showing the effects of using dual spark plugs. Caris et al [7] has presented results showing that dual spark plugs can provide a considerable reduction in burn time, whilst Quader [8] has confirmed that both spark plug location and the existence of an extra spark plug have a large effect on combustion duration and on the lean limit. Oblander et al [9] shown that a reduction in combustion duration and cyclic dispersion could be obtained with two spark plugs.

Nakajima et al [10] compared the results from a compact wedge chamber with a ''fast burn'' engine of a zero squish, hemispherical head, and dual ignition design. The results show that the dual ignition design is superior to the squish design concerning combustion rate, cyclic dispersion and exhaust gas recirculation (EGR) tolerance.

2.2 Turbulence Generation

There are several important parameters to allow the development of an efficient, fast and complete combustion in ICEs. These parameters can be related to the engine design or engine command, combustion chamber design, compression ratio, turbulence or ignition advance, air fuel ratio (AFR), mixture preparation level, load and engine speed.

It's important to have a fast start of combustion, and a fast burn rate. If the combustion duration is instantaneous, it falls within the constant volume combustion theoretical cycle which has high thermal efficiency.

If combustion happens within a stationary mixture (no fluid movement and turbulence), an extremely slow burn will take place. That couldn't occur at medium to high engine speeds. On practice, because of the fact that the mixture has to travel through channels and valves, and it is compressed on the cylinder, high turbulence is expected just before combustion occurs. In this case combustion can be 10 times faster than one occurring within a stationary mixture [2].

To enhance the efficiency of an ICE it is important to optimize its thermal efficiency, which is obtained at the highest possible compression ratio. But if the compression ratio is too high there is a chance that knock will occur, which should be avoided. A solution for this problem is to promote a very fast combustion, to reduce the time available for that phenomenon to occur.

Sufficient large-scale turbulence (kinetic energy) is needed at the end of the compression stroke to promote a rapid combustion. This turbulence will result in a better mixing process of air and fuel and it will also enhance the flame development. However, too much turbulence leads to excessive heat transfer from the gases to the cylinder walls and may create problems of flame propagation [11-13]. The key to efficient combustion is to have enough turbulence in the combustion chamber prior to ignition. This turbulence can be created by the design of the intake port [11].

There are two types of structural (large scale) turbulence that are recognizable in an engine; swirl and tumble (Figure 3). Both are created during the intake stroke. Swirl is defined as the charge that rotates concentrically around the axis of the cylinder. Tumble is defined as the in-cylinder flow that is rotating around an axis perpendicular to the cylinder axis.
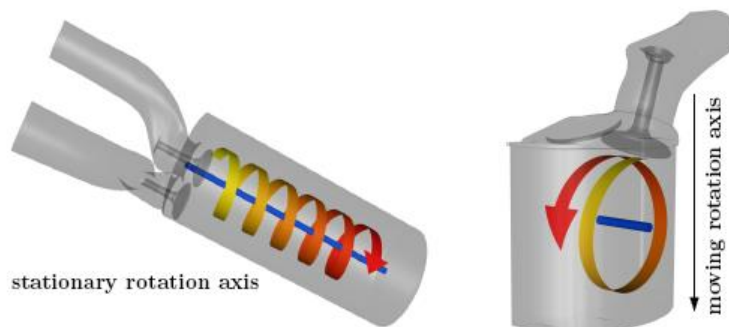
Figure 3 - Difference between swirl (left) and tumble (right).

While tumble is generally existent in 4-valve pent roof combustion chambers, swirl is more common in 2-valve heads [12]. If the inlet flow is brought into the cylinder with an initial angular momentum, it will create swirl [11] [12].

As mentioned above, turbulence should not be too high or it could lead to excessive heat transfer from the mixture to the cylinder walls and even flame propagation problems [14]. Furthermore, a very high swirl is not desirable as the kinetic energy for the flow is obtained at the expense of a reduced volumetric efficiency. Finally, it may be said that an optimal swirl ratio is not only good for optimum combustion but also for an optimal emission reduction [12].

There are two ways of creating swirl, by valve design and by intake design [3]. The design needs a shape that creates turbulence during the intake stroke that still lasts during the compression stroke.

Commonly two designs can be used to create swirl: the direct port and the helical port [3] (Figure 4). These ports basically differ in their shape around the valve stem. The helical port concept relies on the assumption that the flow upstream of the valve curtain is induced into rotation and therefore enters the combustion chamber with an angular momentum along the valve stem axis. This in turn should result in a higher fluid rotation within the cylinder. The idea of a helical port is that the air is already rotating prior to entering the cylinder, because of the inlet port design. The rotation is achieved by forcing the air around the valve stem, so that an angular momentum along the cylinder axis is created as the charge enters the cylinder. The swirl of a direct port relies solely on the interaction of flow and cylinder walls.

Figure 4 - Direct port (left) and helical port (right).

Helical ports normally have a higher discharge coefficient than direct ports for equivalent swirl levels [3]. Another advantage of helical ports is that they are not that sensitive to shape defects that may occur due to the casting process. Also, a helical port produces more swirl than a direct port. There is a further constrain for the intake port design which is the manufacturing (casting) requirements.

Experimental studies [15] [16] show that swirl has large-scale effects on flow fields, flame size, shape, stability, and combustion intensity, which are affected by the degree of swirl. This degree of swirl usually is characterized by the swirl number, S, which is a non-dimensional number representing the ratio of the axial flux of angular momentum to the axial flux of axial momentum. The swirl number aims to provide a relative measure of the strength of circulating flow inside the cylinder following the air intake. S ranges below or above 0.5 are considered to be low and high swirl levels, respectively [3].

10

During induction, the generated turbulence may be swirl or tumble, depending on the flow pattern, while during the end of compression there is a different kind of turbulence that may be induced, called squish. The squish effect happens at TDC when the piston crown comes very close to the cylinder head (Figure 5). The mixture is suddenly ''squished'' out within the combustion chamber, creating turbulence.
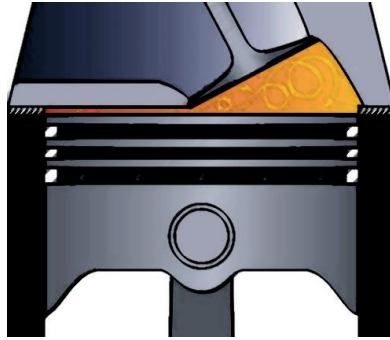
Figure 5 - Squish effect.

Swirl may also be generated in twin inlet valve engines, by deactivating one of the intake valves or intake passages during induction (using port de-activation throttles [15]). The use of high swirl ratios increases the heat release rate during combustion, reducing the combustion duration. At the same time, the heat transfer ratio increases with a reduction in the thermal efficiency of the engine. However there are benefits in the reduction of HC emissions, due to a more complete combustion.

Nagayama et al [16] measured flame speeds using two ionisation probes and compared four combustion chambers combining both squish area and swirl. They found that both squish and swirl increased the flame speed and that maximum speeds were achieved when the squish and swirl were combined. It is interesting to note that squish was effective in increasing the flame speed during both the initial and the main combustion phases.

2.3 Over-expansion

The majority of the engines used in the automobile industry around the world are based on the Otto cycle. When the exhaust valve of this kind of engines opens, there is still a fair amount of energy in the cylinder, in the form of pressure and temperature (enthalpy) of the exhaust gases that is lost through the exhaust blow-out [2] [3] [17].

With an over-expanded cycle engine, in which the expansion stroke is longer than the intake stroke, it is possible to significantly reduce this wasted energy, enhancing the efficiency of the engine [2].

11

A type of over-expansion concept using charge intake to increase the lower torque resulted by the over-expansion was patented by Ralph Miller, an American engineer, in the 1940s, but the concept was proposed earlier by Atkinson.

The Atkinson cycle takes all the exhaust gas enthalpy by performing expansion to atmospheric pressure. The Miller cycle only takes part of that enthalpy being also super-charged. The over-expanded engines are called Atkinson or Miller even if none of this denominations are completely true. On this work only the over-expanded denomination will be used.

Previous work by the laboratory of thermal engines of the University of Minho has shown the potential for over-expansion, especially when combined with optimized compression ratios [18] [14] [19] [20] [21], with a Patent having been issued [22]. The over-expansion was achieved with a Late Intake Valve Closure (LIVC) strategy, in which the effective intake and compression strokes are reduced while keeping unaltered the expansion (and exhaust) stroke. This strategy is highly attractive in terms of simplicity. Its main disadvantage is that this reduction of the intake stroke induces a proportional reduction in engine power. An alternative would be to increase the expansion stroke instead of decreasing the compression stroke. This is only possible by having physically different compression and expansion strokes using a non-conventional crank mechanism [23]. This is the approach chosen for the present work.

The P-V diagram presented on Figure 6 shows the efficiency gain of the theoretical over-expanded cycle in relation to the more usual Otto cycle [14]. This gain is presented by the grey area limited by the points 4,5,6,1. In fact, these P-V diagram areas actually represent work ($\int P \cdot dV$).
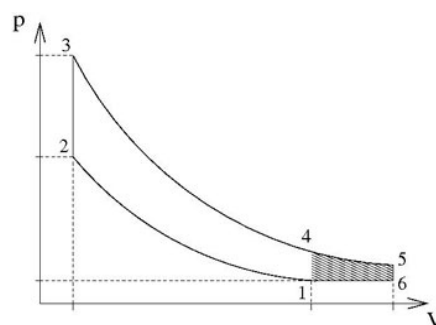
Figure 6 - Miller cycle P-V diagram.

Real Miller cycle engines (with supercharging) were produced by Mazda in the 1980s. They had a fixed LIVC and were supercharged. In 1993, Mazda introduced in the market a supercharged Miller cycle gasoline engine as an answer to the requirement of CO_2 emissions reduction [24].

12

An ICE linked to an electric motor by a planetary gear system (Toyota Hybrid System) was fitted by Toyota on its car model Prius [25]. The ICE had a displacement of 1497cc, with a geometric compression ratio of 13.5:1, but the effective compression ratio was limited to the range of 4.8:1 to 9.3:1 by using variable valve timing to time the intake valve closing between 80° and 120° after bottom dead centre (ATDC). In order to minimize friction losses the engine speed was lowered. The specific fuel consumption was reduced to a level of 230 g/kWh.

Another method for realizing over-expansion is by crankshaft offset. This consists on deviating the axis of the crankshaft relatively to the axis of the cylinder. By doing this, the piston motion is modified and the cycle strokes duration is changed, depending on the side to which the crankshaft is offset.

The "High Efficiency Hybrid Cycle" (HEHC) used on the X Engine [26], borrows elements from Otto, Diesel, Atkinson and Rankine cycles (Figure 7). It is a rotary engine with some particular features. Air is compressed and introduced in a separate combustion chamber where fuel is injected and combustion occurs under truly isochoric conditions. After the combustion is complete, the burned gases are expanded in a separate expansion chamber, which has an expansion ratio higher than the compression ratio of the compression chamber. The HEHC engine is reported to be two to three times more fuel efficient than today's engines over an automotive drive cycle (from 17-25% to over 50% efficiency) [27].
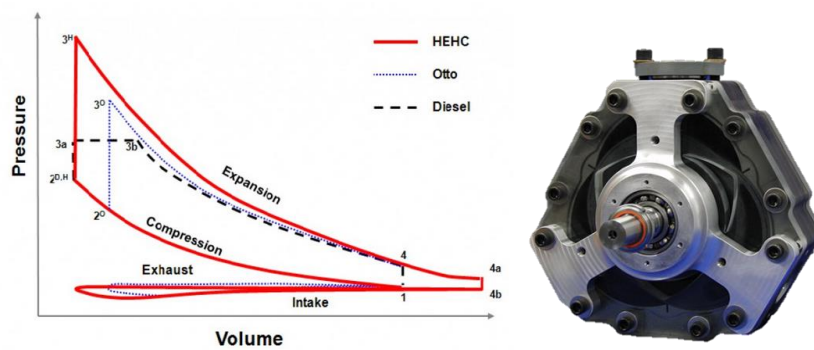
Figure 7 - HEHC P-V diagram comparison with Otto and Diesel cycles and the X Engine [26].

Finally, the split cycle engines are the ones which separate the 4 strokes (intake, compression, power and exhaust) of conventional engines in to two separate paired strokes to occur in two separate cylinders, namely compression and power cylinders. Scuderi split cycle engine (Figure 8) was named after the concept proposed by Carmelo Scuderi [28]. The engine works the same way

as split cycle engines with slight modifications in order to overcome the drawbacks of the ordinary split cycle engines. The over-expanded cycle on this engine is a function of its architecture where the compression stroke volume is smaller than the power stroke volume.
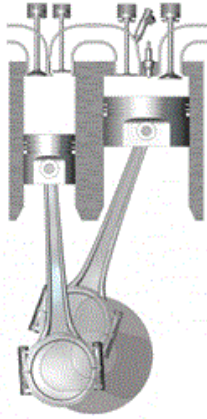
Figure 8 - Scuderi split cycle engine [28].

2.4 Constant Volume Combustion

The theoretic Otto cycle includes processes of isentropic compression and expansion and isochoric (constant volume) supply and loss of heat. The graphical presentation of the ideal Otto cycle is illustrated on Figure 9 with the P-V and T-S diagrams.
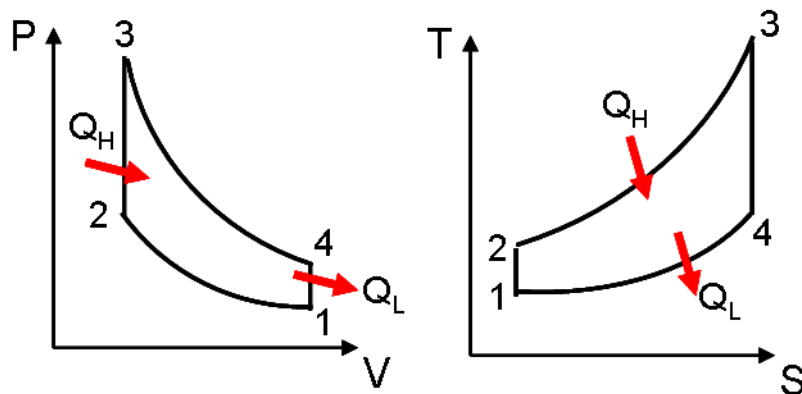
Figure 9 - Otto cycle P-V and T-S diagrams.

1 – 2   Isentropic process. The gas is compressed by the work done. The compression stroke begins at bottom dead centre (BDC) and is an isentropic, i.e., adiabatic, process.

2 – 3   Isochoric process. The air fuel mixture burns instantaneously at TDC. All heat release (combustion) takes place at constant volume at TDC.

14

3 – 4   Isentropic process. The gas is expanded, producing work. The expansion stroke begins at TDC and is an isentropic and adiabatic, process.

4 – 1   Isochoric process. The loss of heat shown in the T-S diagram crossing the 4-1 line. A heat rejection process (exhaust) occurs at constant volume at BDC. The constant volume process is thermodynamically efficient. It is called a constant volume process because the heat supply (representing the real combustion phenomenon) occurs at a constant volume. The thermal efficiency of this process follows:

$$\eta = \frac{W}{Q_0} = 1 - \frac{|Q_{1-4}|}{Q_{2-3}} = 1 - \frac{T_4 - T_1}{T_3 - T_2} = 1 - \frac{T_1 \frac{T_4}{T_1} - 1}{T_2 \frac{T_3}{T_2} - 1} \qquad (1)$$

In conventional engines, because of the piston movement created by the crankshaft, the heat supply would have to occur infinitely fast, i.e. abruptly. However, that is not realistically feasible unless an unconventional crank mechanism is used.

In fact, real cycles applied in ICE cannot achieve the levels of performance suggested by ideal thermodynamic cycles. One of the main differences has to do with heat release (combustion) timing, which does not occur isochorically. In fact, the combustion starts way before the piston reaches the TDC and takes place during a significant part of the downward stroke of the piston. The traditional design of ICEs using a crank connecting rod system simply does not allow the constant volume combustion to take place, significantly reducing the efficiency of the cycle.

Comparing with the theoretical Otto cycle (Figure 9) with the real Otto cycle (Figure 10) there are some differences that can be described and understood on the following label of Figure 10.
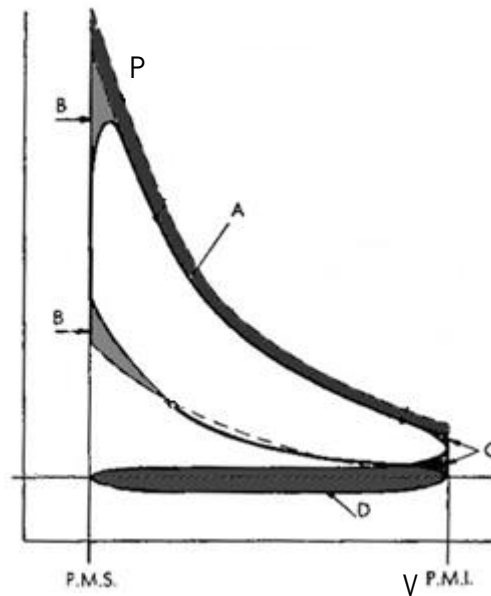
Figure 10 - Real Otto cycle P-V diagram.

A – Heat transfer during combustion and power stroke.

B – Non instantaneous combustion (non isochoric).

C – Exhaust valve opening.

D – Pressure drop between intake and exhaust strokes.

The use of a conventional crankshaft limits the type of movement that aims to give the piston, being necessary to create different mechanisms to fulfil this function. The possibility of effectively stopping the piston at TDC for some time while the crankshaft continues its rotation allows for constant volume combustion.

The main advantages of producing a near constant volume combustion relate to increasing maximum pressure near TDC even using a smaller spark advance value, which leads to higher efficiency and higher work produced. The disadvantages lies in the need to use unconventional systems in spite of the crankshaft which in turn are quite complex.

Multiple link mechanisms [29] and crankless cam-driven engines can be used to significantly modify the conventional piston motion, either by slowing the piston speed near TDC or by effectively stopping the piston motion at TDC during some crankshaft angle (CA) degrees (DWELL). The characteristics of crankless cam-driven engines allow the replacement of the conventional crankshaft, being possible to induce whatever a piston movement is desired. This allows to focus

16

on the study of different movements of the piston during combustion, using various DWELL amplitudes at TDC to effectively implement a constant volume combustion strategy.

One of the works proposed in this field [30] implemented the constant volume combustion by stopping the piston at TDC during 20 CA degrees. The crankshaft design was not presented by the author. The engine efficiency improvement relatively to a conventional crankshaft was reported to be 11% at full throttle.

Another author [31] performed quasi constant volume (QCV) combustion by using a high torque, high bandwidth, permanent magnet electric drive system attached to the crankshaft. The system enabled strong reductions in piston velocity around TDC (Figure 11). A quasi constant volume combustion was thus been successfully achieved, leading to an improvement in the pressure integral of the cycle of 11% relatively to the conventional cycle.
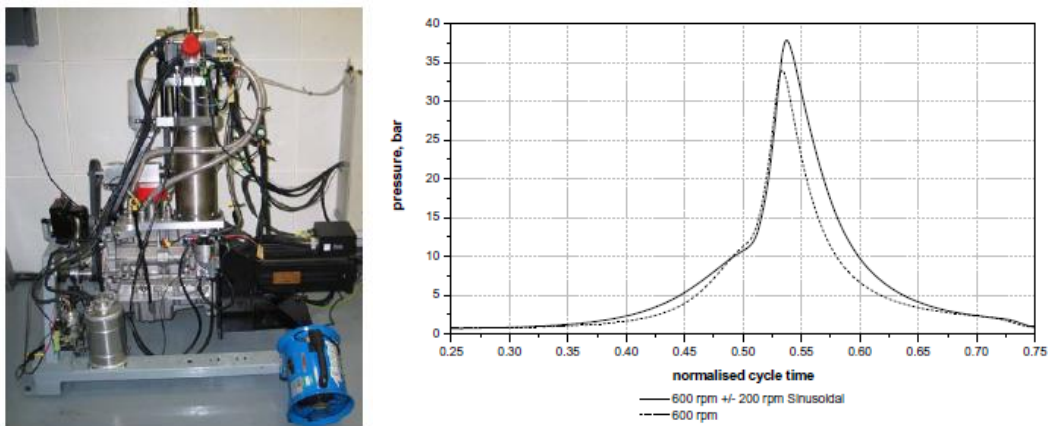
Figure 11 - Single cylinder research engine used and the fired cylinder pressure graph with conventional and QCV cycles [31].

A zero dimensional model was used by Doric [32] to investigate the combustion performance of a four cylinder petrol engine with unconventional piston motion. The kinematic scheme of the crankshaft used is very similar to a conventional crankshaft mechanism. Different piston motions near TDC were performed and overall, the obtained pressure integral of the combustion cycle was about 4% higher than that of the conventional cycle.

ICVC and APC engines [29] used complex linkage mechanisms to allow the piston displacement to change moderately around TDC and increase the degree of constant volume in order to improve the thermal efficiency. The results showed that the heat loss increased and the thermal efficiency did not improve. The author stated that the higher heat loss came from the fact that high pressure and temperature around TDC were maintained for a longer period of time. Nevertheless, in order

to reduce heat loss a direct injection engine was operated as stratified charge combustion and a degree of constant volume increased, leading to an increase of thermal efficiency of 1.1 points topping at 42.7%.

In conclusion, the following statement by Blair [11] is presented, as it illustrates well why this feature should be extensively studied:

"It's clear that the ideal Otto cycle is ineffective in simulating combustion in a spark-ignition engine, compared to data measured in a real engine. The problem is simply that an engine cannot conduct combustion at constant volume, i. e., instantaneously at TDC, because a real burning process takes time, the piston keeps moving, and the cylinder volume changes. If this latter problem could be remedied by keeping the piston stationary at TDC while combustion took place and then moving it down on the power stroke when all is burned, the imep and power would increase by some 50%. So also would the thermal efficiency improve as it would require no more fuel per cycle. Needless to add, many have tried to induce stop-go piston motion characteristics into both 2 stroke and 4 stroke ICEs. So far none has succeeded, using a plethora of mechanical contraptions on linkages, or at least none are known to be in mass production. The tone of this comment may imply that I think that they never will succeed, not so as I have accepted long ago that there is no limit to human inventiveness. To the contrary, I would actually encourage the world's inventors to keep on trying to accomplish this ICE equivalent of the search for the Holy Grail." Gordon P. Blair.

2.5 Direct Water Injection

The ideal Otto cycle consist of isentropic compression, combustion, isentropic expansion and gas exchange and does not include any form of heat transfer. In contrast to the case with other types of heat engine, heat transfer in the ICE is totally undesirable.

Heat transfer plays an important role in the conceptual and detail design of the engine. The strong heat release within the engine would lead to excessive thermal loading of some engine components, if some sort of cooling would not be employed. But conventional engine cooling normally affects thermal efficiency, because the thermal load retrieved from the engine for this purpose will not be used to produce mechanical work.

The development of new ceramic materials [33] able to withstand high temperatures has raised the question of whether it could one day be possible to discard engine cooling altogether and build

18

an adiabatic engine with zero heat loss. The cyclic nature of the ICE process hinders efforts in this direction considerably, so that the ideal situation of an adiabatic engine is virtually unachievable. At best, a thermally insulated engine would result, where indeed no net heat would be lost through the walls, but would be stored within the insulating material during the combustion process only to be transfer back to the gas during the gas exchange phase.

A few years ago some so-called adiabatic engines were developed [2]. They were not truly adiabatic (they had minor heat losses) but did have greatly reduced heat loss at the combustion chamber. They usually had no coolant jacket or finned surfaces, and the only heat losses were those related with convection at the external surface of the engine. This resulted in much hotter internal engine components and losses in brake power output, as the intake air was immensely heated by the hot walls and its density was therefore significantly reduced, affecting volumetric efficiency.

Because they had no cooling system (water pump, water jacket, finned surfaces, etc.) adiabatic engines could be made smaller and lighter than conventional engines. Vehicles could be made more aerodynamic with a lower drag coefficient because there would be no need for a radiator. This also gives greater flexibility for engine location and positioning.

The adiabatic engines proposed in those times were all compression ignition engines. The concept cannot be used in spark ignition engines because the hot cylinder walls would heat the air-fuel mixture too quickly and knock would be a prevailing problem.

Nevertheless, the concept of an adiabatic engine in the sense of an engine that does not have significant thermal losses to the outside (except through the exhaust gases) could still be achieved by internally cooling the engine walls. This could be done by using direct water injection, and it would allow spark ignition engines to virtually operate as adiabatic engines. This strategy makes a lot of sense on an energy efficient point of view, since the energy retrieved from the walls with this method may be converted into useful work through phase change and expansion. This internal heat recovery concept is known as internal regeneration.

The injection of water into a combustion engine is not a new concept. During World War II, water injection was extensively used in both Allied and Axis aircraft. These aircrafts were all powered by piston engines, and most were supercharged. In the 1940s NACA (the predecessor to NASA) reported extensively on ICE water injection experiments [34-37].

In 1983, Renault started using water injection at the intake system of their turbocharged 1.5 litre Formula 1 engine, after the inter-cooler. The system used a 12 litre tank and a dedicated control unit. An electric pump, pressure regulator and pressure sensor were used. It was reported that the inlet air temperature reduction achieved with this strategy was 10 to 12 °C, dropping the intake air temp from around 60 to 50 °C [38].

The injection of water in the intake manifold is sometimes used, in turbocharged engines, to increase power output avoiding engine overheating and knock. Water or a mixture of water and methanol is injected into the intake manifold (Figure 12) lowering the temperature of the mixture. This allows the increase of boost pressure, compression ratio and ignition advance, all leading to the improvement of torque, power and even efficiency. Water injection can also be used in normally aspirated engines to increase charge density and the ability to use higher ignition advance values without the onset of knock.
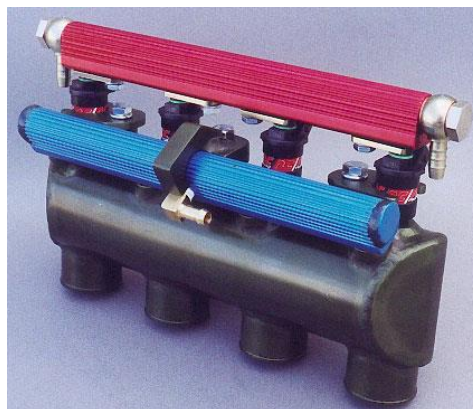
Figure 12 - Engine intake manifold with fuel (red) and water (blue) injectors with common rail.

Water injection is still currently object of study, namely in diesel engines in order to reduce the production of NOx and even a slight increase in power due to the expansion of the water vapour [39].

The production of mechanical work obtained from separate the expansion of water injected directly into the cylinder has been examined in several works [40-42]. These engines are called 6 stroke engines, and are based on a 4 stroke engine with 2 additional strokes. After the normal expansion of a 4 stroke engine, part of the burned gases are exhausted, while the other part is compressed again. The fifth stroke occurs with the injection of water directly into the remaining exhaust gases at high temperature. Water vaporizes producing another power stroke due to its increase in

pressure. The sixth and last stroke is the exhaust of water vapour and remaining exhaust gases to the atmosphere.

Those authors only studied the interaction of water and the hot gases but did not examine the interaction of water particles with the walls of the combustion chamber and cylinder, as they used a ''conventional'' externally water cooled engine.

There are several patents related to water injection in ICEs [43-64]. Some of these patents are related to rather particular or unconventional engines like the split cycle [43], where water injection may be added more easily. Others are related to water injection systems to be implemented in conventional ICEs.

Recently, a numerical and experimental work acceded direct water injection during the compression stroke [65]. Water spray characterization of a multi-hole injector under pressures and temperatures which are representative of engine relevant conditions was investigated for naturally aspirated and boosted engine conditions. The experimental conditions included a range of injection pressures of 34, 68, and 102 bar and ambient temperatures ranging from 30 to 200°C, which includes flash-boiling and non flash-boiling conditions. The engine CFD results highlighted that water injection at 90 degrees before top dead centre (BTDC) showed better vaporization and decreased the formation of liquid wall film on piston surface, cylinder head, and cylinder wall when compared with those for 60 degrees BTDC water injection.

2.6 UMotor Development

2.6.1 Introduction

Nowadays the concerns with environmental problems and the low reserves of petroleum are leading the manufacturers to build less polluting and less consuming engines. The stringent goals for emission reductions and energy efficiency increase proposed by global policies, namely in Europe [66], are pushing the automotive industry towards intense research and development in these fields as never seen before in the automotive history [67]. In this framework, the Academia's ICE research and training has naturally gained a strong focus on these subjects. The formation of college teams participating in vehicle efficiency related contests such as the Shell Eco-Marathon

super-mileage contest has shown to be a good opportunity to promote applied research in this field with highly motivated students and researchers.

Shell organises, on a yearly basis, an event called Shell Eco-marathon. The purpose of this marathon is to race a vehicle on a particular track, at an average speed above 30 km/h with minimum fuel consumption. These vehicles are built by teams of students from different countries and universities. The University of Minho participates in this contest with its car, EconomicUM (Figure 13). A new engine is being developed for this car, called the UMotor (Figure 13).
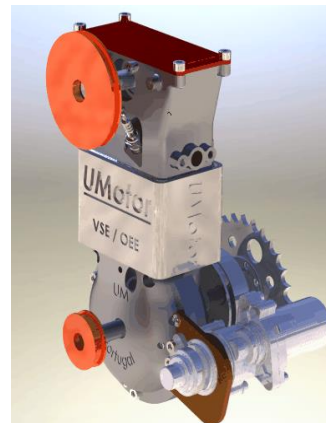
Figure 13 - EconomicUM (left) and UMotor (right).

The UMotor engine is being developed in order to substitute the old engine with the intention of achieving better consumption results. The author has been involved in the development of this engine, with most of the latest engine developments having been made by him. Some unconventional and interesting features were included to the UMotor specifications with the aim of increasing thermal efficiency. The present work has used this engine as basis for the evaluation of several strategies for efficiency improvement. Therefore, the existing engine features and the developments achieved until now will be described in this section.

2.6.2 Engine specifications

The ICE, currently under development, is a spark ignition engine to be running on gasoline. The main principal difference between the UMotor and a conventional ICE is the engine cycle operation and some unusual mechanical specifications. Thus, the UMotor operates under the over-expanded cycle contrary to the Otto cycle present in the conventional spark ignition engines.

Mechanically the over-expanded cycle is accomplished in this engine using a special unconventional hypotrochoid crankshaft that allows different volume variations, where the intake

22

and compressions are the shorter strokes, and the expansion and exhaust the longer strokes. Further, a high swirl generation intake channel and a hemispherical combustion chamber using two spark plugs was developed to enhance combustion efficiency. The engine specifications are listed on Table 2.

Table 2 - UMotor principal specifications.

Engine type	Over-expanded 4 stroke with hypotrochoid crank
Number of cylinders	1
Number of valves	1 intake/ 1 exhaust
Number of spark plugs	2
Bore	39.0 mm
Intake and Compression stroke	19.5 mm
Power and Exhaust stroke	39.5 mm
Connecting rod length	100.0 mm
Intake displacement	23.2 cc
Expansion Displacement	47.2 cc
Expansion ratio	2.0
Compression ratio	11.0:1
Intake valve diameter	14.0 mm
Exhaust valve diameter	14.0 mm

2.6.3 Engine components and relevant features

2.6.3.1 Head design

Small engines have a very unfavourable surface/volume ratio. In order to minimize this a hemispherical chamber was chosen. The combustion chamber was designed to achieve high combustion efficiency, turbulence generation and use two spark plugs (Figure 14). The piston bore is larger than the hemispherical chamber leaving around the combustion chamber a circular ring, which produces high squish turbulence at TDC.
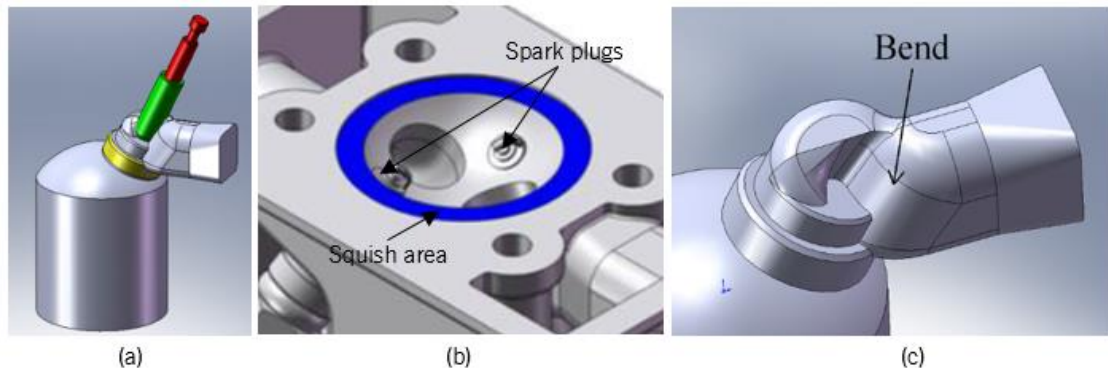
Figure 14 - (a) Intake channel assembly; (b) UMotor combustion chamber showing the squish area and two spark plugs; (c) Working of the helical port.

Intake and exhaust ports are placed on the central axis and valves inclined 50 degrees between them. The intake port is helical for generating a high swirl rate. Swirl turbulence is generated within the intake manifold, around the valve axis. Thus the swirl turbulence is less sensitive to the position of the intake port and it is more intensive.

Two small diameter spark plugs will ignite the mixture. One of the spark plugs is placed near the exhaust port and deflected from the central axis of the combustion chamber.

Sand casting was used to produce the parts to make the head [68]. The cores and moulds were produced by rapid prototyping or by using a core box, which is made of aluminium or wood and created on a 4-axis computer numeric control (CNC) milling machine. But there were some restrictions to the manufacturing process:

- The design cannot have sharp angles on the milled core box because the milling cutter cannot produce sharp angles;
- The design has to be done without undercuts, otherwise the moulds can't be opened;
- Walls that are too thin to be cast should be avoided.

There are also some restrictions on the design of the inlet track:

- Casting restrictions apply;
- The fuel should be injected towards the inlet valve, impinging over its back. As the inlet is curved to create swirl, care was taken to allow a straight path from the injector to the valve;
- Care was taken to reduce pressure losses within the helical duct.

The optimization of the design was continuously improved using CFD studies in a sequence of several enhanced geometries, leading to an optimal final design [68].

After the design was completed it was possible to make the final assembly which consists of Figure 14 (a)): the intake design with cylinder (grey); valve seat (yellow); valve (red) and valve guide (green).

The principle of this geometry is that the air flow is first deflected to the right when it passes the bend (Figure 14 (c)). Then, the air flows around the valve to the left, creating an angular momentum for the intake flow.

The whole engine was designed with a 3D computer aided design (CAD) software. It was designed by parts, and then assembled. Geometric constraints between the components were set in order to simulate the dynamic behaviour of the system. Figure 15 shows the engine head.
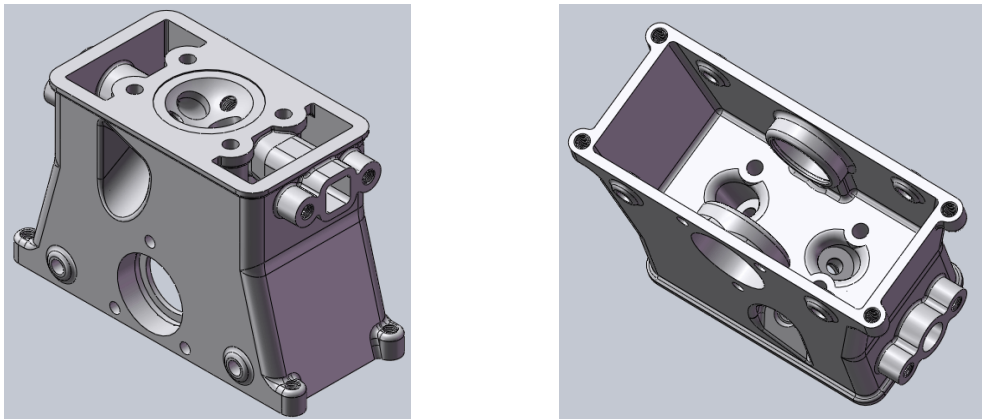
Figure 15 - Engine head bottom view (left) and top view (right).

Subsequently, all the remaining parts of the head engine were designed, including the camshaft, rocker arms, valves, sparkplugs and some other small pieces. The various parts were all assembled, resulting in the final design of the engine head, (Figure 16).
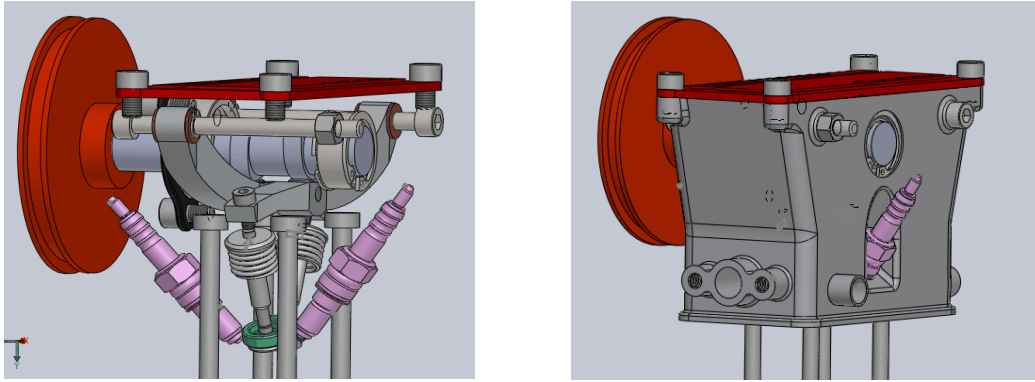
Figure 16 - Engine head interior assembled components (left) and full assembled engine head (right).

To obtain good scavenging control and reduce valve mass single inlet and exhaust valves were elected. A single camshaft with roller bearings is located on the cylinder head, in the same vertical plane as the crankshaft and is driven one end via a timing belt. The rocker arm's contact with the camshaft, valve stem and pivot is made with ball bearings. Both valves have the same dimensions (Ø 12.5 mm) and length (43.5 mm), they are made of stainless steel and are closed by conventional helical springs. Valves are made by Honda [70].

The chosen maximum valve lift was 4 mm to avoid steep cam contours. Valve guides and seats are made of bronze and stainless steel, respectively. Oil splashing lubricates the valve gear train. Figure 17 shows the engine cast head.

Figure 17 - Engine cast head.

2.6.3.2 Cylinder design

The cylinder block (Figure 18) was designed taking into account the existing engine head. The dimensions of the cylinder and the sleeve were defined taking into account the required cylinder capacity and the chosen piston bore (from a Honda GX35 [70]). The volume for the cooling fluid

(water) chamber was calculated in order to enable the cooling of the engine during testing, but also to provide a high thermal inertia to the engine during the race. The Eco Marathon is a consumption race where the engine accelerates the vehicle during a short period ($\approx$5s) and then the car coasts for about 5 min before the engine is fired again. The engine is set to work at a specified temperature (95°C).Therefore, the higher the thermal inertia of the engine, the more stable its temperature will be during the one hour race. Also, the exterior of the engine is to be extensively insulated, as was the case with the current car engine.

The cylinder was machined from a solid aluminium alloy block using a CNC milling machine (Figure 18). The "VSE/OEE" engravement means "Variable Stroke Engine / Over Expanded Engine".

Figure 18 - Engine block.

2.6.3.3 Piston

The design proposed for the piston enables it to be extremely light and to display a reduced liner contact area (Figure 19).
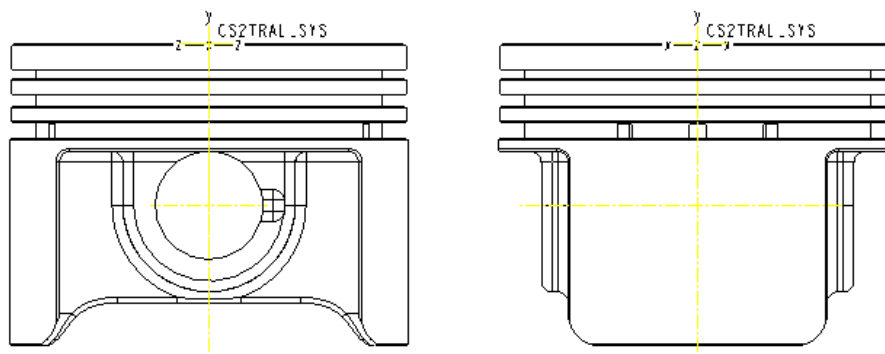
Figure 19 - 2D piston layout.

Figure 20 shows the connecting rod and piston assembly.

Figure 20 - Connecting rod and piston assembly.

2.6.3.4 Crankshaft design

The engine was required to be very efficient with a power of nearly 1.5 kW. For the required power a cylinder capacity of 23 cm^3 was chosen running at 6000rpm. The over-expanded concept was used to enhance efficiency, and as the engine should always work at wide open throttle (WOT) an expansion/compression ratio of 2 was chosen and therefore the total cylinder capacity was 47 cm3. The compression ratio was set at 11:1 (geometric).

This system consists of an internal/hypotrochoid gear set in which two cranks have been included. The main crank is responsible for the main alternative movement of the piston (the base stroke), while the additional one is responsible for the variation of the base stroke between intake and expansion. A fixed annular gear with internal teeth and a smaller interior spur gear operating within the latter were used for the hypotrochoid crank mechanism. To obtain our aim for an expansion/compression ratio of 2:1 the required gear ratio is 2:3. This is necessary so that the small crank completes a quarter of a revolution for each stroke, with each stroke corresponding to half of a revolution of the main crank, as depicted in Figure 21. An unitary module was defined for the internal gear set, enabling a good compromise between gear precision, sliding friction and resistance for the desired application. After studying the dimensions and the desired piston stroke, a large annular gear with 90 inner teeth, and an inner spur gear with 60 teeth were chosen. As the module is one, their pitch diameters, in millimetres, corresponds to their number of teeth.

Figure 21 is a schematic view of the hypotrochoid crank mechanism. The blue dot marks the location where the shaft of the connecting rod connects eccentrically to the inner spur gear. As it may be seen, the difference between the two bottom dead centres (corresponding to the lowest position achieved by the piston in the stroke) is given by twice the distance from the centre of the connecting rod bearing (eccentric hole in the inner spur gear, in blue) to the centre of the main crankshaft bearing. In this case, the distance between centres is 10mm, leading to an expansion stroke that is 20mm longer than the intake stroke. The top dead centre location does not change from the intake to the expansion stroke as the hole of the connecting rod shaft is either to the left or to the right of the centre of the main crankshaft bearing.
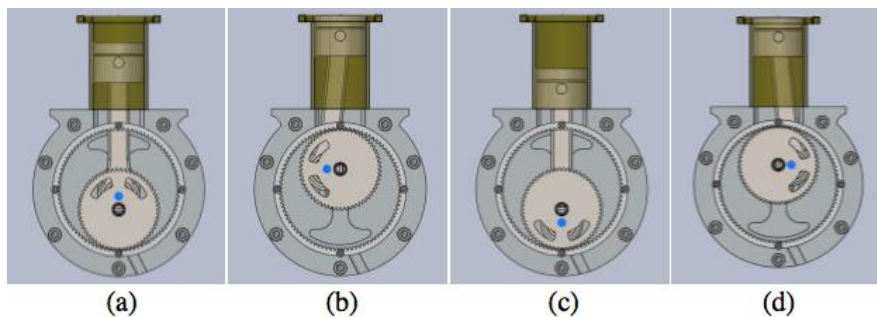
Figure 21 - Hypotrochoid crank mechanism: (a) Intake (short stroke); (b) Compression (short stroke); (c) Expansion (long stroke); (d) Exhaust (long stroke).

The crankshaft design (Figure 22) was made as compact as possible, in order to reduce torsion forces, and to get a small crankcase to minimize volume and weight.

The position of the piston inside the cylinder during two revolutions of the crankshaft, obtained analytically, is shown in Figure 23, completing the 4 strokes of the engine and compared with a 50cc and with a 25cc conventional crankshaft engines. The zero in Figure 23 corresponds to the TDC, the beginning of the intake stroke.
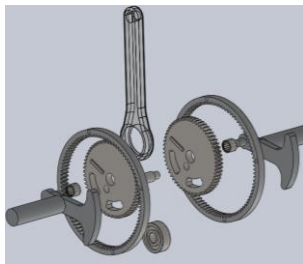
Figure 22 - Exploded view of the crankshaft.
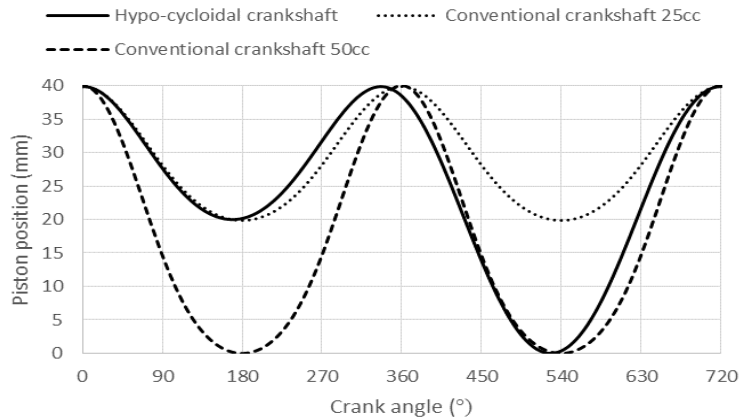
Figure 23 - Piston position vs CA.

With this planetary hypotrochoid crank mechanism it was possible to achieve the required specifications for this engine.

As shown in Figure 24, using the hypotrochoid crank mechanism the connecting rod stays nearly vertical during most of the power stroke. This happens due to the combination of the motion of the two crankpins. This will be further explained in chapter 3.1.1. During expansion it can be seen that when the main crankpin is located to the left, the secondary crankpin will be located to the right, and vice-versa. This will reduce the total offset of the piston connecting rod crankpin from the axis of the cylinder when compared with an epitrochoid or even a conventional crank mechanism.
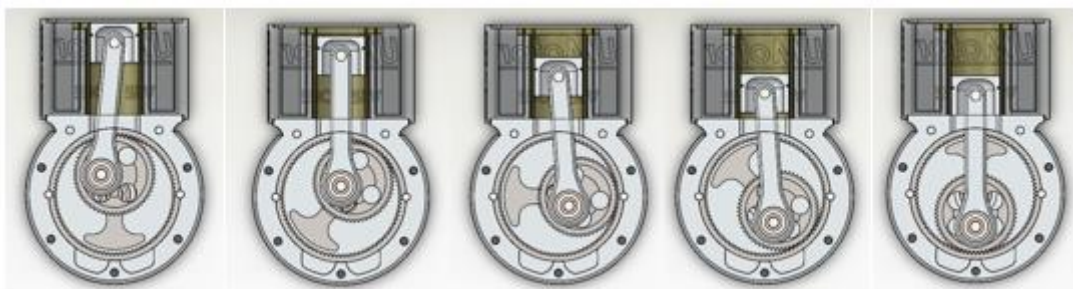
Figure 24 - Verticality of connecting rod during power stroke.

The hypotrochoid crankshaft is composed by the gear train and the output shaft. The latter, like any crank mechanism, is eccentric. The eccentricity between the two axes of the output shaft is 15mm, which is the difference between the large and the small primitive radius of the spur gears. This is necessary in order to achieve the specified gearing.

Both the inner and the outer spur gears were manufactured to the required dimensions in steel, to be rectified and hardened so that needle bearings can be used directly over it. The small spur gears were manufactured with the connecting rod pin hole.

Figure 25 shows the connection between the output shaft and the small spur gear inside the crankcase, the hypotrochoid mechanism. Only half of the crank system, which is symmetric, is here shown. The connecting rod pin connects the two symmetric hypotrochoid mechanisms.
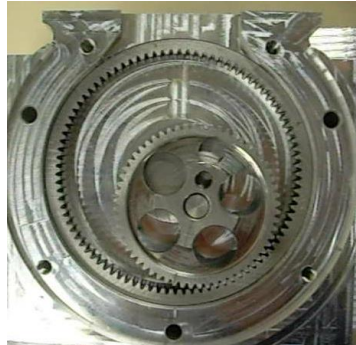
Figure 25 - Hypotrochoid mechanism inside the crankcase

2.6.3.5 Crankcase design

The crankcase (Figure 26) has been designed to accommodate the hypotrochoid system and its components, to ensure a precise fit with the cylinder and its screws holes. It was designed to have a compact geometry, to be light weight and to ensure tight fit. The partition plane is perpendicular to the axis of the crankshaft.
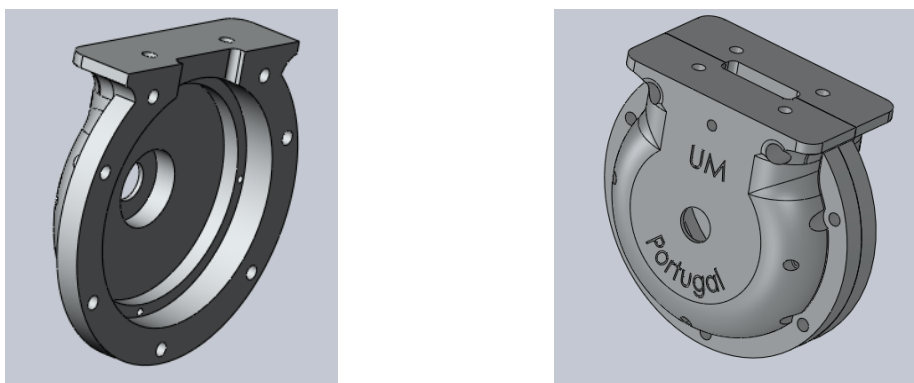
Figure 26 - Crankcase CAD design

The two half crankcases were made by CNC machining (Figure 27).

Figure 27 - Machined crankcase.

2.6.4 Final assembly

The final assembly (Figure 28) shows how the engine will look like. The starter and the clutch had already been designed and assembled, to ensure that all components fit correctly.
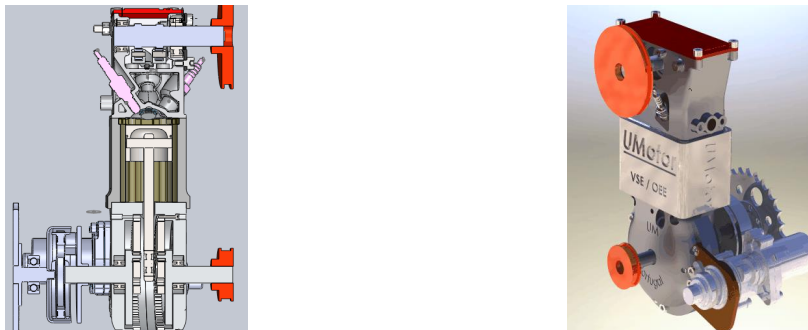
Figure 28 - Section view (left) and rendered view of the full assembled engine (right).

The partial assembly of the crankcase components depicted on Figure 29 illustrates well its working principle and how the variable stroke strategy (and therefore over-expansion) is accomplished.

Figure 29 - Hypotrochoid crank system and connecting rod.

The various components of the disassembled and assembled engine can be seen in Figure 30.

Figure 30 - Exploded view of several parts of the engine and final engine assembly.

2.6.5 Future work

The engine is now in an advanced status of development. The ongoing tasks are the machining of the cams, the valve guides and seats, the finger followers, the rectification and hardening of the various parts of the crankshaft and the ignition and injection systems. Intake and exhaust manifolds, toothed wheels connecting crankshaft and camshaft and the exterior insulation will be the final parts needed for the engine to run.

Theoretically there is still the need to accomplish a full 4 stroke simulation on a CFD software with combustion simulation to correctly estimate the engine performance and evaluate the merit of the several strategies envisioned for the engine.

2.7 Engine modelling

For the processes that govern engine performance and emissions, two basic types of models have been developed. These can be categorized as thermodynamic or fluid dynamic in nature, depending on whether the equations which provide the corresponding model its predominant structure are based on energy conservation computations or on a full analysis of the fluid motion.

Other labels given to thermodynamic energy conservation based models are: zero dimensional (0D) (since in the absence of any flow modelling, spatial features of the fluid motion cannot be predicted), phenomenological (since additional detail beyond the energy conservation equations is added for each phenomenon in turn), and quasi dimensional (where specific geometric features, (e.g., the spark ignition engine flame or the diesel fuel spray shapes), are added to the basic thermodynamic approach). These types of models are used to predict the pressure variation in the

cylinder along time, considering a certain correlation for combustion rate, and evaluate the engine performance, using several parameters.

Fluid dynamics based models are often called multidimensional models due to their inherent ability to provide detailed geometric information on the flow field based on the solution of the governing flow equations.

Engine modelling allows for engine research and design to be less expensive as experimental work can be previously assessed and some set-up conditions to the experiment so defined, thus saving time and resources during the test phase of a project.

The present work focused on the evaluation of engine performance, as translated into several performance parameters (e.g. output torque and power, efficiency, etc.) and also on the evaluation of several design strategies involving spatial flow and heat transfer computations. Hence, single zone and a multiple zone models were used, from simplified custom built spreadsheet models to full CFD commercial packages. The main single zone model used is a thermodynamic model implemented in Matlab Simulink, while the multiple zone model used is the commercial CFD package CONVERGE, which has been especially developed for simulating the various phenomena occurring inside ICEs.

2.7.1 Matlab-Simulink model

A thermodynamic engine model was developed by Ribeiro [71] and implemented in Simulink, a graphical toolbox developed for the Matlab environment. It is a model for simulating single cylinders of 4 stroke engines, and includes instantaneous volume, pressure and temperature calculations, chemical species characteristics, mass exchange, combustion, heat transfer, and friction.

The engine model is divided into different sub-models representing the ICE sub-systems and processes as described below:

- Engine motion;
    - Crankshaft motion/rotation;
    - Piston position and speed;
    - Cylinder (volume, surface area).
- Analysis based on the First Law of Thermodynamics;
- Combustion;
    - Heat release rate.

34

- Gas properties;
- Gas exchange processes;
    - Intake and exhaust processes.
- Heat transfer;
- Valve motion;
    - Open area at each valve position;
    - Valve lift profile.
- Cam profiles;
- Friction;
    - Crankshaft bearings;
    - Connecting rod bearings;
    - Piston and piston rings;
    - Valve train.
- Engine performance parameters.
    - Indicated output work;
    - Power output;
    - Thermal efficiency;
    - Specific fuel consumption;
    - Indicated mean effective pressure (imep);
    - Brake mean effective pressure (bmep).

The model allows to obtain the main engine performance results. The validation and refinement of the results was made with real engine bench tests, with the results being close to experiments, especially under low speeds, where dynamic effects associated with engine breathing are negligible [71].

2.7.2 CONVERGE

The multiple zone model is a computational fluid dynamics software called CONVERGE specially created for ICEs simulation. Described below is the software structure and operation.

Computational fluid dynamics packages allow the simulation of fluid flow, heat and mass transfer among other associated phenomena. Numerical methods are used to solve mathematical equations that describe those phenomena, namely the Navier-Stokes equation and the generalized energy equation.

In CONVERGE, there is no need to supply directly a grid as an input. Instead, it is only needed to supply a triangulated surface and a series of guidelines from which CONVERGE will create the grid at run-time. For simulations with moving boundaries the grid is recreated at each time step.

There are several ways to control the structure of the grid during the simulation. These are:

- Base dx, dy, and dz;
- Fixed embedding;
- Adaptive Mesh Refinement (AMR);
- Grid scaling.

Each of these four methods for controlling the nature of the grid during the simulation are handled through simple input files and are not part of a user grid generation procedure. The setup time in preparing a simulation involves preparing the surface so that it is clean, closed and has the boundaries properly marked.

The methodology followed by CONVERGE for CFD analysis is displayed in Figure 31 [72].
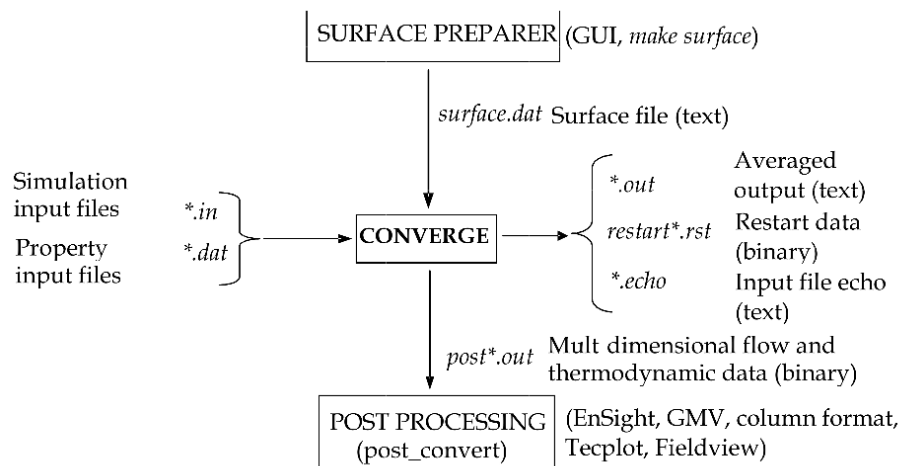
Figure 31 - CONVERGE methodology.

The main models available in CONVERGE for Chemistry and Emissions modelling (combustion), Turbulence Modelling and Energy source modelling (spark energy) are described below.

2.7.2.1 Chemistry and Emissions modelling

The software allows the use of the four general combustion models listed below. Although there is also the possibility of using simplified premixed combustion models that can be used with lower computational effort.

- SAGE Detailed Chemical Kinetics Model;
- Multizone Modeling – Acceleration of Detailed Chemical Kinetics;

- Zero-Dimensional Combustion;

- Chemical Equilibrium – CEQ.

SAGE model was used to simulate the combustion process in the present work thanks to the availability of a very fast computer at the mechanical engineering department.

2.7.2.2 Turbulence modelling

The software allows the use of three different turbulence models, all of them based on the equations of Reynolds Averaged Navier Stokes equations (RANS), being the most utilized models for engineering applications.

- Standard $\kappa - \varepsilon$;

- RNG $\kappa - \varepsilon$;

- Rapid distortion RNG $\kappa - \varepsilon$.

The RNG $\kappa - \varepsilon$ model was used for this work. All these models can only be applied to fully turbulent flow. The best results for the standard $\kappa - \varepsilon$ model are obtained for high Reynolds numbers. The RNG $\kappa - \varepsilon$ model is similar to the standard $\kappa - \varepsilon$, being more suitable for low Reynolds numbers. This is due to a different approach to calculate the effective viscosity formulation. It also has an additional term in the ε equation which improves the accuracy in the calculation of fast flows. Rapid Distortion has a different calculation of the ε equation formulation.

2.7.2.3 Energy source modelling

Source modelling can be used to simulate spark discharge from the sparkplug to initiate combustion. In an actual spark event there are two phases: breakdown and glow/arc. These phases are represented in CONVERGE by specifying two energy sources that briefly overlap. These two overlapping spark phases will cause a step change with respect to time in the energy release. For example, if the spark timing is 15 CA degrees BTDC, the first energy source (the breakdown phase) starts at -15 CA degrees and will have a duration of 0.5 CA degrees. The second source (the glow/arc phase) will start at 15.0 CA degrees and will have a duration of 10.0 CA.

3. Efficiency improvement analysis

While the previous chapters have framed the subject of the present work introducing the several concepts under study and surveying their related literature (including the work done previously by the group), the following chapters properly present and detail the work done during the master thesis. They include the analysis of different ways of thermal efficiency increase on ICEs. The engine used as a basis for this study is the UMotor, the engine described above in chapter 2.6. The analysis includes studies of some of the specificities already implemented in UMotor in order to verify and quantify correctly their merit, and includes also the assessment of new efficiency improvement features which could be implemented if their merit and feasibility would be confirmed.

The features analysed on this work are:

- Over expansion;
    - Friction force analysis during power stroke of the epitrochoid and hypotrochoid crankshaft designs;
    - Thermodynamic analysis, on the Simulink model, of the UMotor using the current hypotrochoid crankshaft.
- Turbulence generation and combustion efficiency improvement;
    - Implementation of a 0D combustion model (heat release rate) on a Excel and Simulink models;
    - CFD analysis of the effects of turbulence generation and combustion chamber design on the combustion efficiency of the UMotor and combustion chamber design improvement;
    - CFD analysis of constant volume combustion using a unconventional crankshaft in the UMotor.
- Direct water injection.
    - 0D Wall temperature model development with heat regeneration using direct water injection over the combustion chamber and over the valve wall during the power stroke;

o Thermodynamic analysis of direct water injection within the gases during combustion and over the engine walls during power stroke after combustion ceasing.

The features analysed and being present on this work can be implemented on any ICE in order to increase its thermal efficiency.

3.1 Over-expansion

3.1.1 Piston friction analysis of the epitrochoid and hypotrochoid crankshaft designs

Different mechanisms can be used to replace the conventional crankshaft in order to get the engine operating under the over-expanded cycle, where the power stroke is longer than the intake stroke. In the UMotor case the over-expansion was attained by the use of a planetary gear mechanism in the crankshaft. Although the final solution was the hypotrochoid mechanism there was another possible solution, the epitrochoid crankshaft mechanism, both illustrated in Figure 32.

Epitrochoid   Hypotrochoid
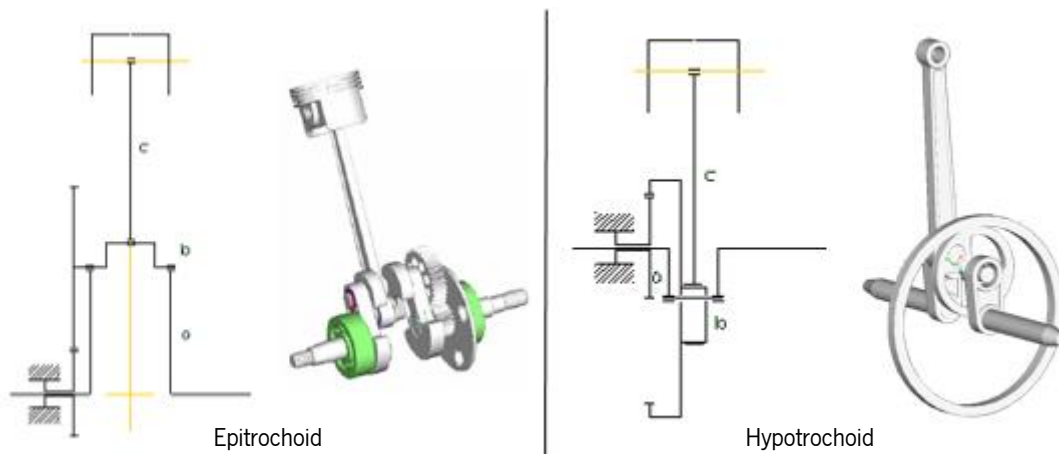
Figure 32 - Epitrochoid and hypotrochoid crankshaft mechanism.

The epitrochoid consist of an inner fixed wheel and the connecting rod is coupled to an outer wheel running on the outside of the fixed wheel. The hypotrochoid consists of an outer fixed wheel (with inner teeth) and an inner wheel runs inside it, coupled to the connecting rod (Figure 33).

Epi-cycloid   Hypo-cycloid
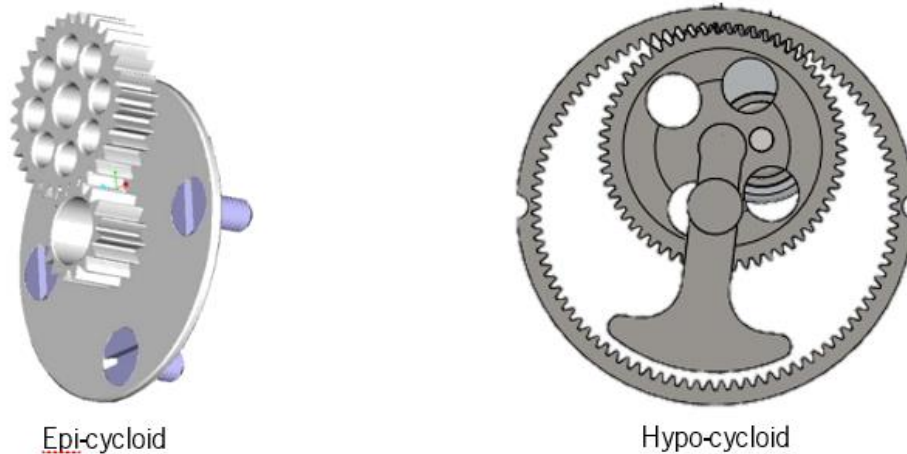
Figure 33 - Epitrochoid (left) and hypotrochoid (right) concepts.

It is possible to implement a 2:1 expansion/compression ratio with both systems. This allows to have a much longer expansion than intake stroke, reducing the waste of exhaust enthalpy. However the centre of the big end bearing of the connecting rod moves differently between the two systems as it is possible to see on Figure 34.
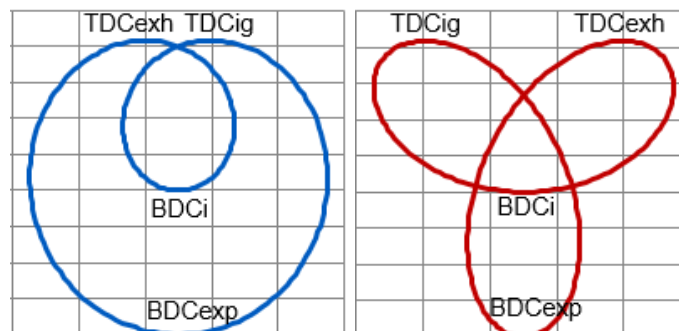
Figure 34 - Epitrochoid (blue) and hypotrochoid (red) centre of the big end bearing of the connecting rod during the 4 strokes.

However, the decision was to use the hypotrochoid for three reasons:

- during combustion the connecting rod is almost vertical (reduces friction with cylinder walls);
- it is easier to control an inner wheel inside an outer wheel than the other way around;
- the internal wheel would lead to lower centrifugal effects.

The first of the aforementioned reasons was dominant for the choice. The more vertical the position of the connecting rod during combustion is, the lower will be the piston to cylinder side thrust, therefore significantly reducing friction. This can be more easily apprehended from Figure 35,

which represents the travel of the centre of the big end bearing of the connecting rod for the hypotrochoid (red line) and the epitrochoid (blue line). Both lines have the same TDC and the same short and long strokes but during expansion (from top to bottom dead centre) the centre of the big end bearing follows a more inner path than the epitrochoid one, being closer to the cylinder axis. Both expansions strokes are represented by wide shaded lines.
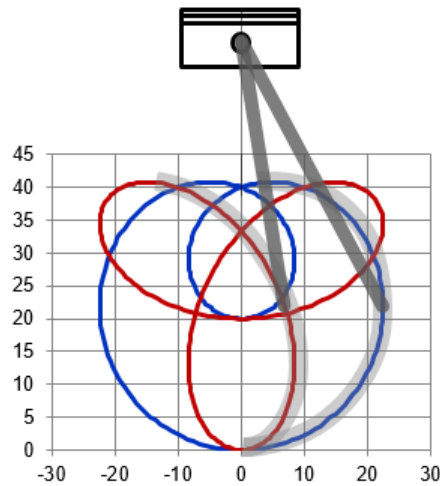
Figure 35 - Comparison between hypotrochoid (red line) and epitrochoid (blue line) crankshafts. Both expansions strokes are represented by wide shaded lines.

However the hypotrochoid solution had a problem: as it can be seen from Figure 36, near TDC the big end bearing of the connecting rod is at a larger distance from the cylinder axis for the hypotrochoid, requiring a longer connecting rod to avoid hitting the bottom of the cylinder liner. However, as it can be seen from that figure, the shorter connecting rod of the epitrochoid results on it being more inclined, leading to higher tangential forces between piston and liner.
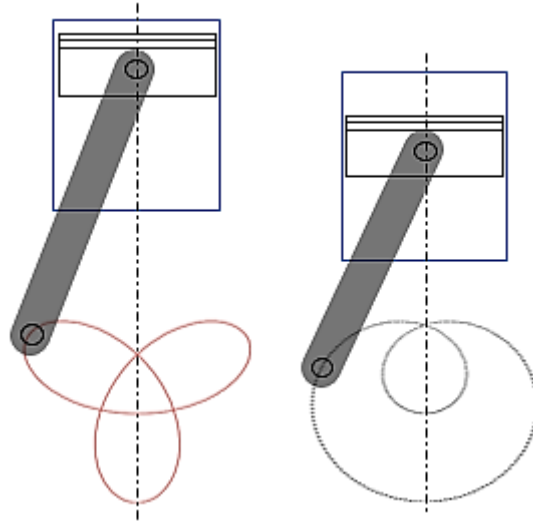
Figure 36 - Comparison of minimum connecting rod length for the hypotrochoid (left) and epitrochoid (right) crankshafts.

The length of the connecting rod was set to be approximately twice the length of the longer stroke, at 100 mm.

In order to verify if the chosen solution was the best one, the piston/cylinder wall friction work had to be compared for both solutions. The data for pressure results from CONVERGE (will be presented later) during expansion was used as a function of time for both solutions, using the same connecting rod length.

Figure 37 shows the integrated friction work done by the piston-liner during the 4 strokes. Near TDC the forces are higher for the hypotrochoid crankshaft because of the higher connecting rod big end deviation from the cylinder axis. During the power stroke after 10 CA degrees ATDC the reverse situation occurs. The friction coefficient was introduced on the calculation of the friction work based on the results achieved by Johansson [73]. The friction coefficient varies during the stroke reaching a maximum value of 0.12 at the reversal points (BDC and TDC) and a minimum of 0.10 at mid stroke.
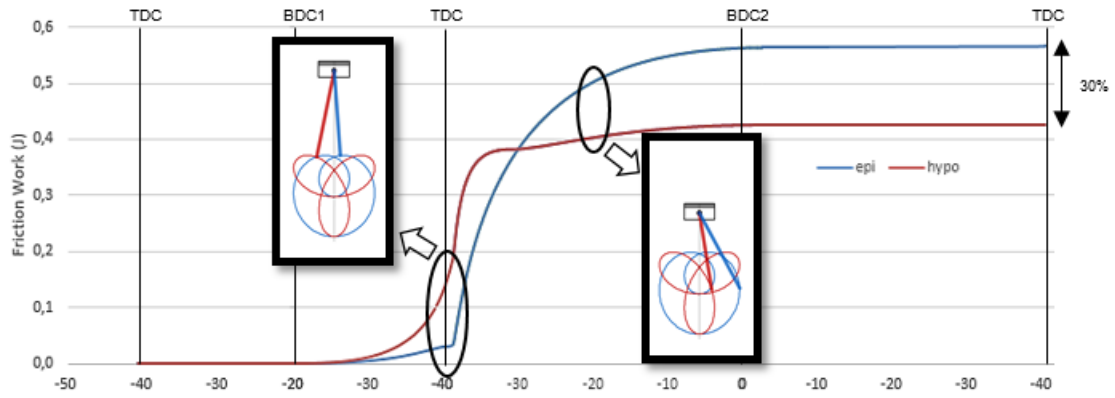
Figure 37 - Friction work comparison between the hypotrochoid and the epitrochoid cranks during the 4 strokes.

Even though the side piston force is higher around TDC for the hypotrochoid case, the friction work is 30% higher for the epitrochoid case at the end of the 4 strokes resulting in higher friction losses decreasing the engines efficiency.

3.1.2 Engine Model Results

Using the numerical Simulink model described in chapter 2.7.1, four different engine were simulated with different geometric characteristics and different working cycles (Table 3). The displacement values are approximate.

Table 3 - Engine cycles simulated using the Simulink engine model.

	Crankshaft	Engine cycle	Intake pressure (bar)	Intake DISP	Expansion DISP	Geometric CR	Trapped CR
1		Otto	0.5	50 cc	50 cc	11:1	11:1
2	Conventional	OE LIVC	1.0	25 cc*	50 cc	22:1	11:1
3		Otto	1.0	25 cc	25 cc	11:1	11:1
4	Hypotrochoid	OE	1.0	25 cc	50 cc	22:1	11:1

* Trapped displacement. The engine is a 50cc engine but it admits only 25cc.

The simulated cycles characterize four different ways of performing the 4 stroke spark ignition cycle, with an expansion displacement of 50 cc (with one exception) and working at similar load. All engine cycles intake the same amount of air during the intake stroke, therefore the same amount of fuel is also used. Two over-expanded cycle engines with different crankshafts and two Otto cycles engines with different loads are compared.

44

Engine #2 works under full load but it has only half of the intake displacement as it works under the over-expanded cycle accomplished through LIVC (using a conventional crankshaft). Engine #4 works also under the over-expanded cycle, not accomplished through intake valve timings but the hypotrochoid crankshaft mechanism. Two engines working under the Otto cycle were also simulated, one working at half load but with the same intake and expansion displacement of 50 cc (#1), and a second working at WOT but with just half of the intake displacement (#3). In all cases it is considered that the intake mixture is stoichiometric. The resulting P-V diagrams of the engine cycles can be seen in Figure 38.
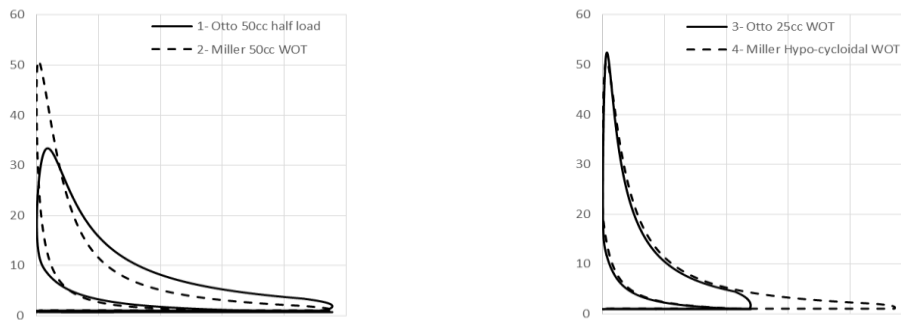
Figure 38 - P-V diagrams for the 4 engine cycles simulated.

Despite of the efficiency improvement (Table 4), engine cycle #2 has almost the same torque (or power) output as the engine performing the Otto cycle at half load (#1). However when the hypotrochoid crank mechanism is used (#4), it produces more power than the engine using the traditional crankshaft with the same intake displacement at full load (#3). Additionally it shows a cycle efficiency improvement of 23% (from 30% to 37%).

Overall the Otto cycled engine got an improvement of 37% (from 27% to 37%) when compared hypotrochoid engine.

The thermal efficiencies (η) and torque at 3000 rpm obtained with this simulation are presented in Table 4.

Table 4 - Efficiency and torque results for the 4 different engine concepts.

	Crankshaft	Engine cycle	Load	η	Torque (Nm)
1		Otto 50cc	50%	27%	1.01
2	Conventional	OE 50cc	100%	35%	1.27
3		Otto 25cc	100%	30%	1.20
4	Hypotrochoid	OE	100%	37%	1.44

The engine using the hypotrochoid crank mechanism to implement the over-expanded cycle (#4) shows the highest efficiency. The lowest efficiency, attained by the Otto cycle at half load (#1) was also expected, as the pumping losses (intake at lower pressure than exhaust) reduces the net work for the same heat of combustion. Also, the trapped compression ratio is lower leading to inferior cycle maximum pressure compared to the other engine cycle simulated.

3.2 Combustion efficiency improvement

3.2.1 Implementation of a 0D combustion model (heat release rate)

The combustion of the fuel/air mixture in an ICE varies from engine to engine, depending on various parameters. The most important are the combustion chamber geometry, the number and position of the spark plugs, the geometric features used to improve the turbulence in the chamber (tumble, squish, swirl), the timing used for the opening and closing of the intake and exhaust valve events, the air temperature, the compression ratio, the ignition advance, the crankshaft geometry, the number of valves, among others.

Nevertheless, the main factors that lead to a variation in the combustion duration are the operating conditions of load, speed and ignition timing.

The combustion in ICEs is a complex phenomenon, so it is not a straightforward task to accurately predict the influence of the operating conditions on engine performance. Based on the analysis done by Bonatesta [74], a simple combustion model was developed and added to a thermodynamic engine model developed in Microsoft Excel. That analysis was based on the findings of several authors who, in an attempt to predict the influence of operating conditions on engine behavior,

performed experimental studies in order to obtain empirical mathematical expressions that reflect this influence on the combustion duration and on the rate of heat release of the burning fuel.

The charge burn process in ICEs can be analytically described using the Vibe function [3] which can be implemented in 0D models because it does not incorporate any reference to the combustion chamber geometry and flame front propagation. Of course, this simplicity highlights the main disadvantage of the Vibe function, as is that it needs input parameters which need to be estimated or at least tuned based on experimental data. These models provide the burn rate and the mass fraction burned (*MFB*) in the crankshaft angles domain.

$$MFB(\theta) = 1 - EXP\left[-a\left(\frac{\theta - \theta_i}{\Delta\theta}\right)^M\right] \tag{2}$$

Where θ is the angle of the crankshaft, θ_i is the location of crankshaft in degrees at the start of the combustion, $\Delta\theta$ is the combustion duration and a and M are adjustable parameters called the efficiency and the form factor respectively.

The total duration of the combustion is calculated by the model as being the time lapse between 0 to 90 % of the total combustion process and not 100%, since 90% of the burned fuel is more easily determined experimentally. This is in particular due to longer combustion durations where the final combustion stage cannot be calculated accurately in experimental analysis of pressure inside the combustion chamber [74].

The value of the efficiency factor can be obtained from the following expression:

$$a = -\ln(1 - \eta_{comb}) \tag{3}$$

Where η_{comb} is the combustion efficiency with the value of 90%, giving a constant efficiency factor whatever the operating conditions, with the value of 2.3026 [74].

As described by Bonatesta [74], empirical correlations for the two independent parameters of the Vibe function, the combustion duration $\Delta\theta$, and the form factor *M,* have been developed calculating the least mean square fits of functional expressions of engine variables to experimental combustion duration data. Whenever possible, power law functions were used in order to minimize the need

for calibration coefficients. The choice of each term was made to best fit the available experimental data.

The 0 to 90% MFB combustion angle is expressed as the product of four functional factors, whose influence is assumed to be independent and separable [74],

$$\Delta\theta = k \times R(\rho_i) \times S(S_p) \times X(x_b) \times T(\theta_i) \tag{4}$$

The dimensional constant k was determined to be 178 when density ρ_i is in kg/m^3, mean piston speed S_p is in m/s, the dilution mass fraction x_b is dimensionless, and the spark timing θ_i is in CA degrees from BTDC.

The correlation used for the total MFB burning duration is written as

$$\Delta\theta = 178 \left(\frac{1}{\rho_i}\right)^{0.34} \left(1 - \frac{1.164}{\sqrt{S_p}}\right) \left(\frac{1}{1 - 2.06\, x_b^{0.77}}\right)^{0.85} (0.00033\, \theta_i^2 \tag{5}$$
$$- 0.0263\, \theta_i + 1)$$

The correlation used for the total MFB M factor is written as

$$M = 3.46 \left(\frac{1}{\sqrt{S_p}}\right)^{0.45} \left(\frac{1}{1 + \sqrt{\theta_i}}\right)^{-0.35} (1 - 1.28\, x_b) \tag{6}$$

Thus, it is possible to establish the combustion duration or the heat released rate in CA for a given total energy released Q_{tot} during a cycle [2],

$$\frac{\partial Q}{d\theta} = Q_{tot} \frac{dMBF}{d\theta} \tag{7}$$

Where,

$$\frac{dMBF}{d\theta} = \frac{(1 - MBF)ma}{\Delta\theta} \left(\frac{\theta - \theta_i}{\Delta\theta}\right)^{m-1} \tag{8}$$

The combustion heat released to the gases inside the cylinder can be expressed as

$$\frac{\partial Q}{d\theta} = (m_{air} + m_{gas})c_v \Delta T \qquad (9)$$

Where m_{air} is the mass of fresh air and m_{gas} is the mass of the remaining hot gases.

Calculating analytically the pressure and temperature of the gases during a working cycle is not a straightforward task because there is heat being released into a space with changing volume. To overcome this complexity, a time discretization was set and the following procedure was considered (Figure 39).
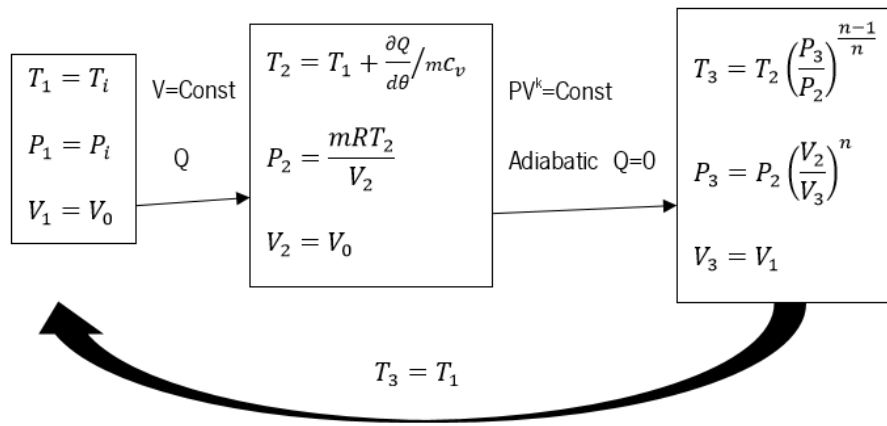
Figure 39 - Combustion model procedure diagram.

At crankshaft location $\theta = 0\ CA$ (BDC), at the beginning of compression stroke, the initial temperature T_1 is assumed to be the inlet air temperature T_i, and the pressure P_i the inlet pressure, same as the engine load.

Then T_2 and P_2, are calculated assuming that the heat released from combustion for each degree of rotation, is supplied at a constant volume. Finally, the final temperature and pressure, T_3 and P_3 is calculated assuming an adiabatic compression or expansion. In this way, it is possible to simplify the problem by virtually separating the heat release and the compression/expansion problems.

The volume calculated at each time step results from the piston motion of a traditional crankshaft.

Since the problem is periodic, the temperature obtained at $\theta = 0\ CA$, will be used as the initial condition for the next iteration, ie, $T_3 = T_1$. The process will be repeated along the subsequent engine strokes.

49

The polytropic index n does vary with engine conditions, but a constant value of 1.3 has been used, knowing that it has yielded acceptable overall results for other similar works [74].

3.2.2 0D combustion model results comparison with CONVERGE results

In order to evaluate the 0D combustion model, results attained with the CONVERGE package were compared with the combustion model results at the same conditions for a conventional 4 stroke spark ignition engine under the same operating conditions with the specifications presented on Table 5. The simulation is from CONVERGE, so the boundary conditions and models used are not displayed and can be consulted in the software manual [72]. The geometry of the ICE was provided by the software package, and was used because it is from a conventional pent roof ICE.

Table 5 - Engine specifications.

Engine type	4 stroke spark ignition
Number of cylinders	1
Number of valves	2 intake/ 2 exhaust
Number of spark plugs	1
Bore	86.0 mm
Stroke	90.0 mm
Connecting rod length	180.0 mm
Displacement	581.5 cc
Compression ratio	9.9:1
Intake valve diameter	35.0 mm
Exhaust valve diameter	30.0 mm

The engine has the pent roof combustion chamber of the conventional "4 valve per cylinder" engines. The spark plug is located on the centre at the combustion chamber as illustrated on Figure 40.
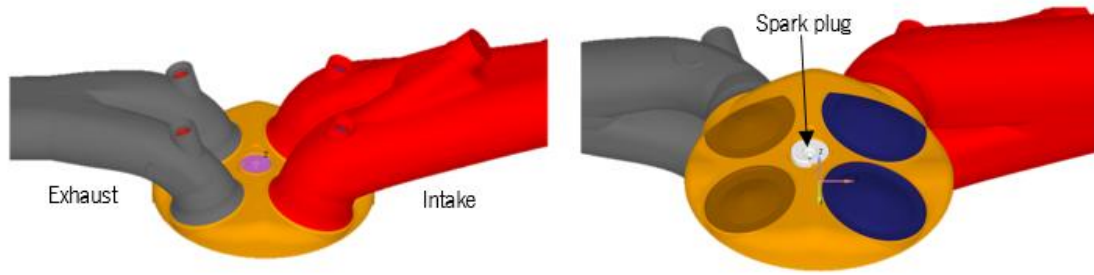
Figure 40 - Engine combustion chamber and inlet (red) and exhaust (grey) ports.

To correctly compare the results both simulations have the same engine conditions presented on Table 6.

Table 6 - Engine conditions.

Engine speed	3000	rpm
Ignition advance	15	CA BTDC
Engine load	1	bar
AFR	14.5	-

The results obtained by both simulations are illustrated on Table 7 and on Figure 41 where the heat release rate and mass fraction burned are plotted.

Table 7 - Combustion results.

-	0D engine model	CONVERGE
Combustion duration (CA)	34	35
Combustion start (BTDC CA)	5	3
Combustion end (ATDC CA)	29	32

51
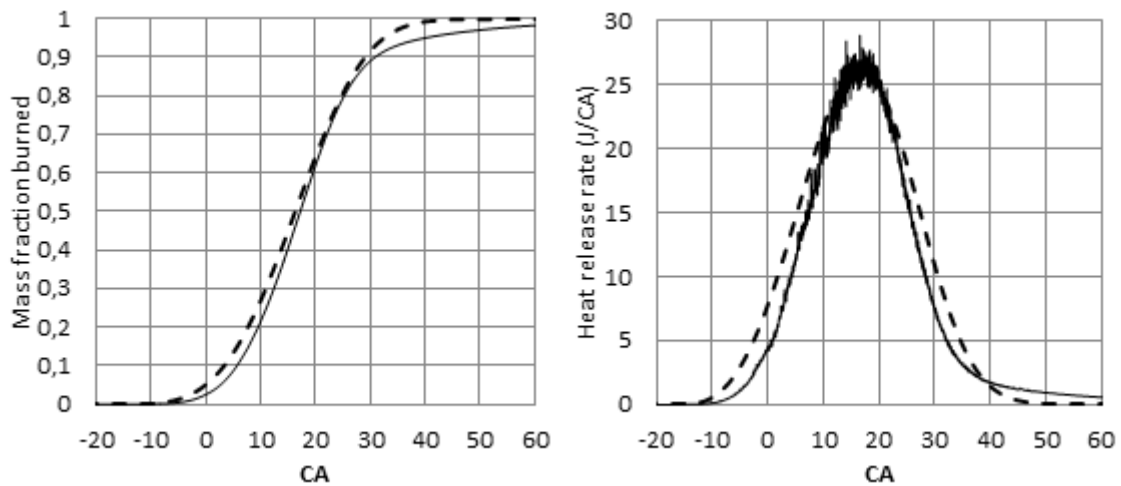
Figure 41 - Mass fraction burned and heat release rate results comparison. 0D engine model (dashed line) and CONVERGE (black line).

On the 0D engine model the combustion starts and ends earlier, although the combustion duration is almost the same, leading to the small differences in the mass fraction burned and in the heat release rate lines for both simulations.

As can be visualized from the results above, the 0D combustion model is very satisfactory showing results very closed to those achieved by the CFD software. Obviously additional simulations should be performed with the CFD software using different combustion shape designs and dimensions should be performed to really evaluate the 0D combustion model performance. Nevertheless, from the results, it is expected that for conventional combustion chambers the results will be very similar.

3.2.3 CFD analysis of the UMotor combustion efficiency

This section assesses the merit of the several features that have been proposed to maximize engine efficiency and a fast combustion process. These strategies include ways of making the combustion chamber more compact, moving the spark plug to a more central location, using two spark plugs, and increasing in-cylinder gas motion by creating swirl and squish during the intake process or during latter stages of compression. A faster combustion process does result in a direct engine efficiency gain as illustrated further ahead in this work. However, of great importance is the fact that the faster burn process is more robust and results in the engine being able to operate satisfactorily at leaner mixtures without decreasing combustion efficiency [3].

The present study uses CONVERGE as the CFD program to model the air flow and the combustion process on the UMotor engine. Some features were already studied and implemented on the

UMotor engine, but a complete 4 stroke engine cycle simulation using turbulence and combustion models was still missing. Until now only air flow simulations had been performed to verify the helical intake channel design performance. This had to do with the difficulty in performing the CFD simulations incorporating valve and piston motion. CONVERGE has not this limitation, being a CFD package specially oriented towards engine simulation.

The CFD simulation will be able to effectively compare the effect of the several features under study and their relative impact in engine performance. Firstly, a normal intake channel and one spark plug will be simulated, secondly with the same normal intake channel and two spark plugs will be simulated, and finally an helical intake channel and two spark plugs will be simulated. Only by changing one feature at a time the combustion efficiency improvement can be correctly quantified.

Before presenting the combustion simulation results, a turbulence analysis of the helical intake channel is proposed in order to verify and quantify the swirl turbulence generation during the intake and compression strokes.

The engine parts were modelled in SolidWorks 2013 environment. They are modelled as a closed surface and then saved as an STL file. After importing it to CONVERGE Studio, the surface was treated and the boundaries were defined as showed on Figure 42.
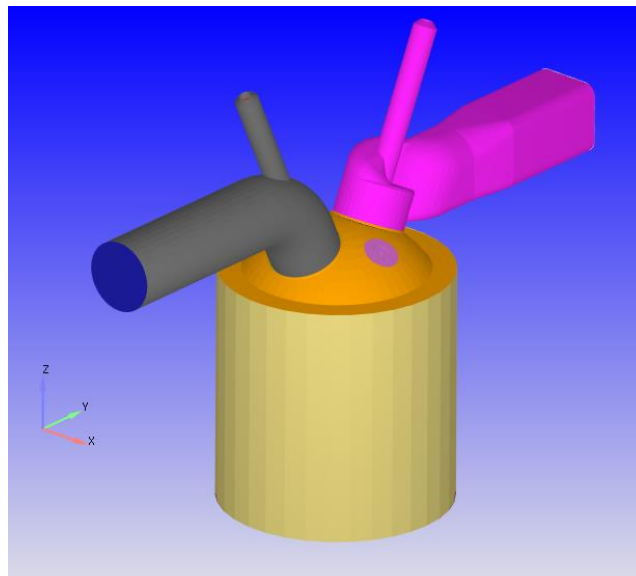
Figure 42 - UMotor surface geometry on CONVERGE Studio.

3.2.3.1   Boundary conditions

The boundary conditions set for different surfaces and interfaces define reciprocal relation in terms of relative (slip, no slip) or absolute (user defined) motion, as well as heat and mass transfer properties. Improper boundary conditions will results in errors during the analysis. Table 8 shows the various boundary conditions used for modelling and their function.

Table 8 - Boundary conditions and functionality.

No:	Boundary Name	Type	Region	Function
1	Piston	Wall Moving	Cylinder	User defined motion
2	Liner	Wall	Cylinder	Moves with piston
3	Cylinder Head	Wall	Cylinder	Stationary wall
4	Spark Plug	Wall	Cylinder	Stationary wall
5	Exhaust Port	Wall	Exhaust system	Stationary wall
6	Exhaust out flow	Outflow/Backflow	Exhaust system	Allows fluid flow
7	Exhaust Valve	Wall Moving	Exhaust system	User defined motion
8	Intake Port	Wall	Intake system	Stationary wall
9	Intake inflow	Inflow	Intake system	Allows fluid flow
10	Intake Valve	Wall Moving	Intake system	User defined motion

Although extensively analysed before, the hypotrochoid crankshaft mechanism used on the UMotor is again described in order to correctly present all the boundary conditions introduced on the simulation.

Figure 43 shows the vertical position of the piston inside the cylinder for two revolutions of the crankshaft, completing the 4 strokes of the engine. The zero in Figure 43 corresponds to the TDC marking the beginning of the expansion stroke.
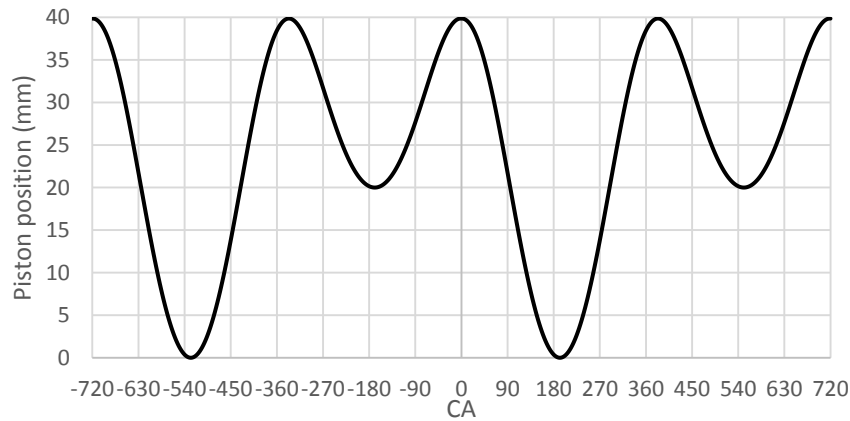
Figure 43 - Hypotrochoid crankshaft mechanism piston position vs CA

With a modest maximum valve lift of 4 mm, the valve motion was modelled analytically and tuned in order to maximize the open time. Table 9 shows the valve motion specifications which have produced the graphic presented on Figure 44. As the engine was not designed for power but for high efficiency, the inlet valve was intentionally left with a small opening lift in order to induce high mixture velocity through the valve even at low engine speeds, to further create turbulence at the cylinder entry.

Table 9 - UMotor valves motion specifications.

Compression stroke duration(°)	168
Power stroke duration(°)	192
Exhaust stroke duration(°)	192
Intake stroke duration(°)	168
Intake valve opening advance (°)	5.0
Intake valve closing delay (°)	25.0
Intake valve maximum lift (mm)	4.0
Exhaust valve opening advance (°)	5.0
Exhaust valve closing delay (°)	30.0
Exhaust valve maximum lift (mm)	4.0
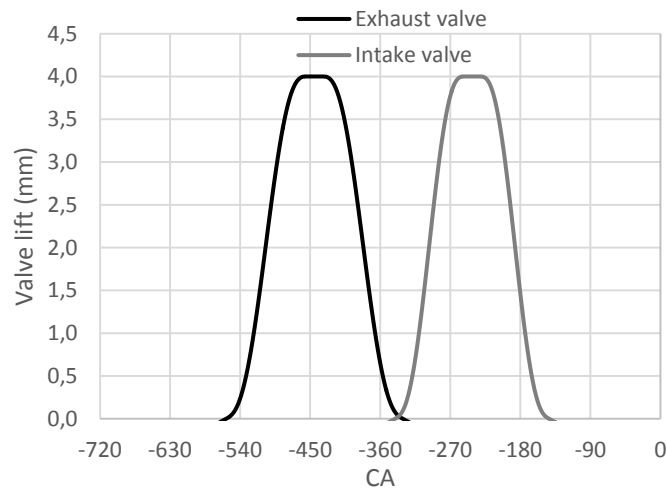
Figure 44 - Intake and exhaust valve motions.

3.2.3.2   Solution procedure

The analysis includes normal engine cycle operation performing all 4 strokes. CONVERGE uses regions to initialize values and each boundary is assigned to a region. The location and orientation of each cell in the mesh is automatically controlled by CONVERGE when the solver generates the grid at the start of the simulation. The open and close events are used to control the flow between two regions (region 1 and region 2) and "disconnect" triangles are created between adjacent regions which are specified as closed (with no mass transfer between them).

Exhaust system, intake system and cylinder are the three regions defined to run the simulation. The close and open events are synchronized with the valve motions (Table 10). Please note that the events are related to Figure 43 and Figure 44, so they all occur before TDC and consequently have negative values. From -341 to -331 (for 10 CA degrees) both valves are open (around TDC at -336).

Table 10 - Region events.

Event start	Region 1	Region 2	Event
-558	Cylinder	Exhaust system	OPEN
-341	Cylinder	Intake system	OPEN
-331	Cylinder	Exhaust system	CLOSE
-143	Cylinder	Intake system	CLOSE

Region initialization values are presented on Table 11.

Table 11 - Region initialization values.

Region	Temperature (K)	Pressure (Pa)	Species
Cylinder	1080	101 325	N_2, CO_2, H_2O
Intake System	383	101 325	IC_8H_{18}, O_2, N_2
Exhaust System	1130	101 325	N_2, CO_2, H_2O

3.2.3.3 Physical models

Turbulence significantly increases the rate of mixing of momentum, energy, and species. For many applications such as ICEs the right specification of turbulence is critical to an accurate simulation.

For the simulation the Rapid Distortion RNG $k - \varepsilon$ of the Reynolds Averaged Navier-Strokes (RANS) model was used. According to Smits [75] this is the best performing model for fluid flow modelling in ICEs.

The SAGE Detailed Kinetics Model incorporated in CONVERGE was used to perform the combustion simulation as it is typically used to more accurately represent the detailed chemical kinetics in combustion [72]. Because SAGE detailed chemistry calculations are computationally expensive, they do not begin until immediately before the spark ignites.

Also, multizone modelling accelerates the solution of detailed chemical kinetics by reducing the number of SAGE calculations. The multizone solver in CONVERGE is based on work conducted at the Lawrence Livermore National Laboratory [76]. The multizone model in this simulation groups cells into zones based on similarities in temperature and equivalence ratio. When the multizone model is activated, CONVERGE completes SAGE calculations for each zone rather than for each individual cell.

3.2.3.4 Intake channel air flow results

Swirl ratio is the ratio of the angular speed of the flow, Ω_{flow}, to the angular speed of the crankshaft, $\Omega_{crankshaft}$, with the direction of swirl being consistent with the right-hand rule [72]. In other words:

$$Swirl\ ratio = \frac{\Omega_{flow}}{\Omega_{crankshaft}} \tag{10}$$

The swirl ratio is calculated for the centre of mass. Figure 45 shows the swirl ratio during the intake stroke (intake valve lift is also plotted) on the UMotor helical intake port. The results presented were done for an engine speed of 3000 rpm.
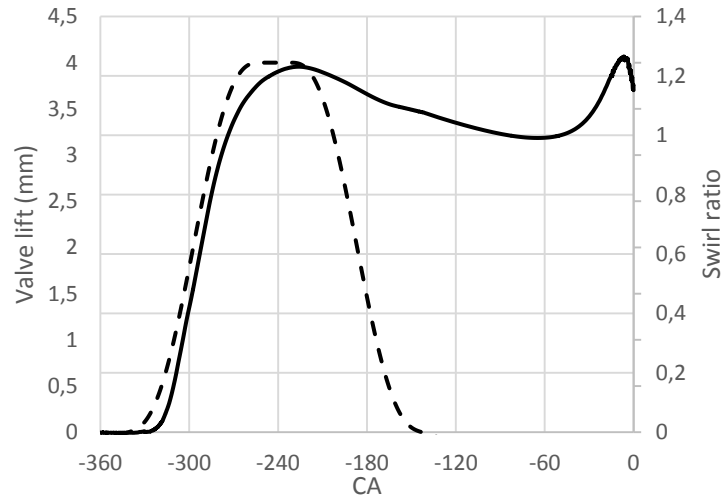
Figure 45 - Swirl ratio (black line) and intake valve lift (black dashed line) vs CA.

After intake valve opening (IVO) the piston speed increases speeding up the intake charge through the helical port and leading to an increase of the swirl ratio. When the intake valve is fully opened the swirl ratio reaches the maximum value of 1.23, a high swirl number. Then the valve starts to close and the piston decelerates towards BDC leading to a nearly constant decrease of the swirl number which continues through the compression stroke until -60 CA degrees, when it is increased by the smaller diameter created by the squish area formed between the piston and the combustion chamber.

Figure 46 shows the pathlines, enabling the visualization of the incoming mixture particles. The pathlines are coloured by velocity module (m/s). The pathlines are swirling through the geometry, showing the direction of the moving fluid. The existence of swirl is evident in these figures.
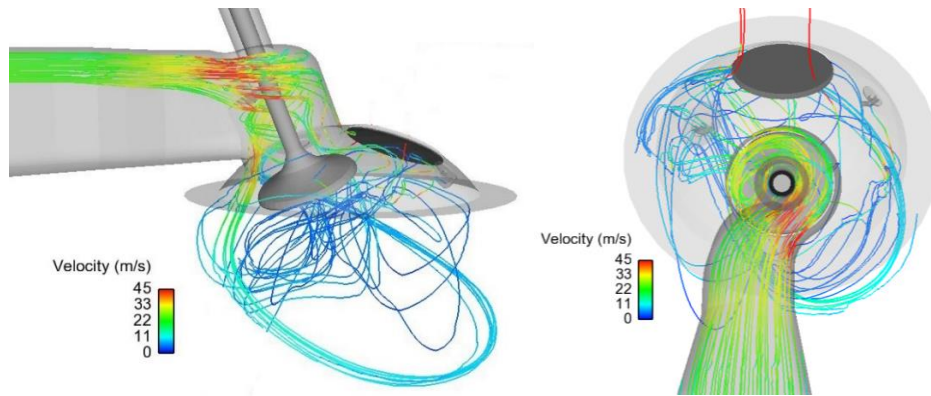
Figure 46 - Two different views of the pathlines of mixture particles swirling through the geometry.

Figure 47 shows the velocity vectors on the top cross section of the cylinder to better visualize the evolution of the swirl within the cylinder during part of the intake stroke. The vectors represent the velocity field direction and magnitude (m/s) in the mesh nodes.

During intake and at -290 CA degrees different vortices can be noticed (Figure 47). This is the result of the air being sucked in through the valve. At -270 CA degrees the vortices are not so visible, but at -250 CA degrees the vortices become clear again, with one big vortex that creates a swirl motion in the cylinder. When the crank angle is above -230 CA degrees the swirl motion is visible in the entire cylinder and the vortex is approximately at the centre of the cylinder.
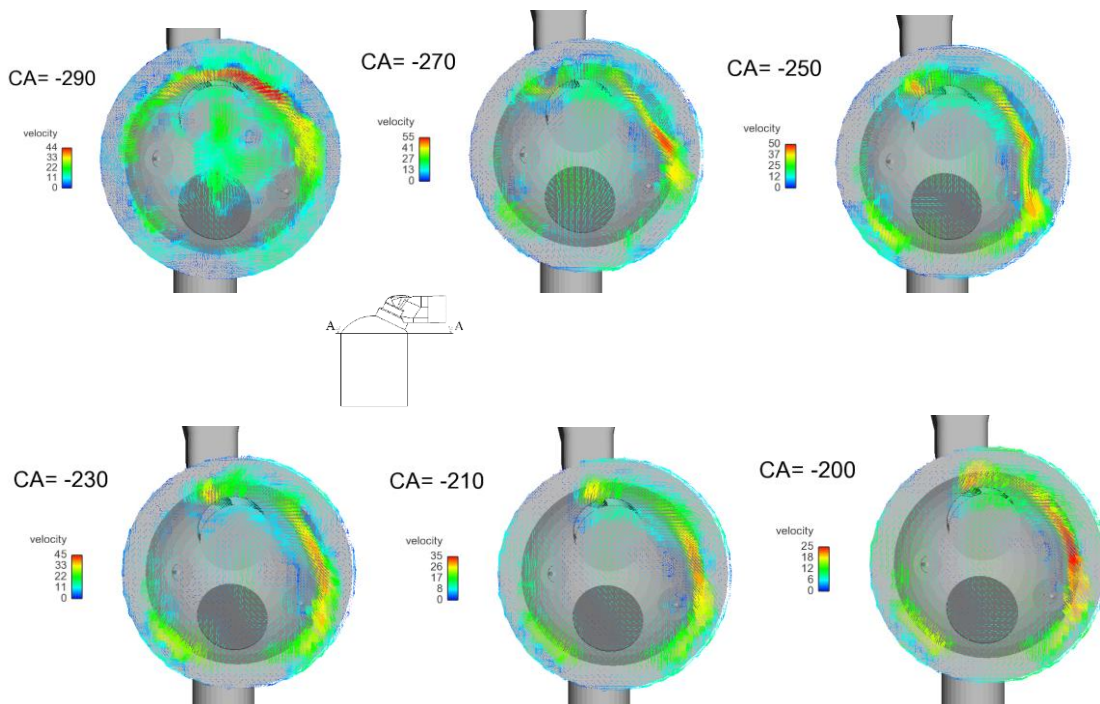
Figure 47 - Top cross section of the cylinder at different piston positions. The vectors represent the velocity field direction and magnitude (m/s) in the mesh nodes. Bottom view.

After BDC, which signals the start of the compression stroke, the swirl velocity is lower and decreases as the piston reaches TDC. However, the swirl motion is still clearly visible during the compression stroke (Figure 48) giving good perspectives for a fast combustions using the high swirl intake channel.
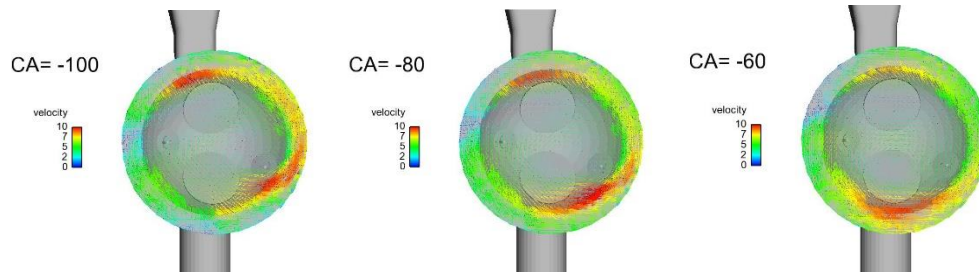
Figure 48 - Top cross section of the cylinder during compression stroke. The vectors represent the velocity field direction and magnitude (m/s) in the mesh nodes. Bottom view.

3.2.3.5 Combustion results

In order to verify and quantify the combustion efficiency improvement using the features described above, three different simulations were performed using the same combustion chamber geometry as described below:

1. High swirl intake channel, 2 spark plugs (HSwirl 2sp);

2. Normal intake channel, 2 spark plugs (Normal 2sp);

3. Normal intake channel, 1 spark plug (Normal 1sp);
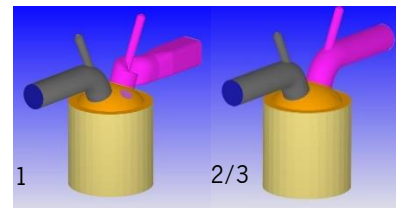
Table 12 shows engine and combustion conditions for the three different simulations performed on CONVERGE. The ignition advance was set to obtain maximum brake torque (MBT) and determined by using a practical method where the ignition timing has to be defined in order to obtain the maximum pressure around 16 CA degrees ATDC [3]. So ignition timing had to be estimated by trial-and-error for each simulation performed.

Table 12 - Combustion results.

	Normal 1sp	Normal 2sp	HSwirl 2sp
Engine load (bar)	1	1	1
Engine speed (rpm)	3000	3000	3000
Ignition advance (CA BTDC)	19	17	15
Combustion duration (CA)	55	42	24
Combustion start (BTDC CA)	10	10	11
Combustion end (ATDC CA)	45	32	13

Adding a spark plug enhances combustion speed and reduces ignition delay. The high swirl intake channel reduces ignition delay in the same level as introducing another spark plug. However, the flame propagation stage is highly reduced and there is a rapid rise in pressure. This is due to the high turbulence in the cylinder which enhances the propagation of the flame front.

Thus it is possible to conclude that the main feature that can be introduce to accomplish a higher combustion efficiency improvement is the high swirl intake channel.

Figure 49 and Figure 50 present the graphical results obtained by the simulation. Figure 49 shows the heat release rate and the integrated heat release rate or MFB resulted from the three simulations to better compare the combustion results.
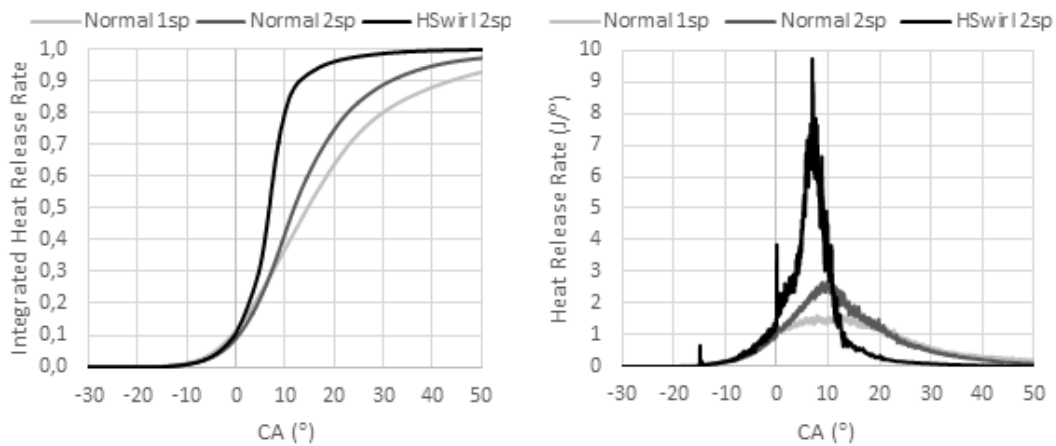
Figure 49 - Heat release rate and integrated heat release rate results for the three simulations performed.

Using a normal intake channel and one spark plug, the ignition advance is long and the combustion is slower than the two other cases, resulting in a maximum pressure of 38 bar. Adding one spark plug makes the ignition advance to be decreased. The combustion is now 13 CA degrees faster and the maximum pressure is 44 bar. With the high swirl intake channel the combustion is extremely fast, the ignition advance has to be decreased and the maximum pressure is 73 bar. Therefore the thermal efficiency improves slightly with the introduction of a second spark plug but it is much increased with the use of the high swirl intake channel. As a result, the area below the P-V diagram is increased (Figure 50), enhancing output torque but mainly efficiency.
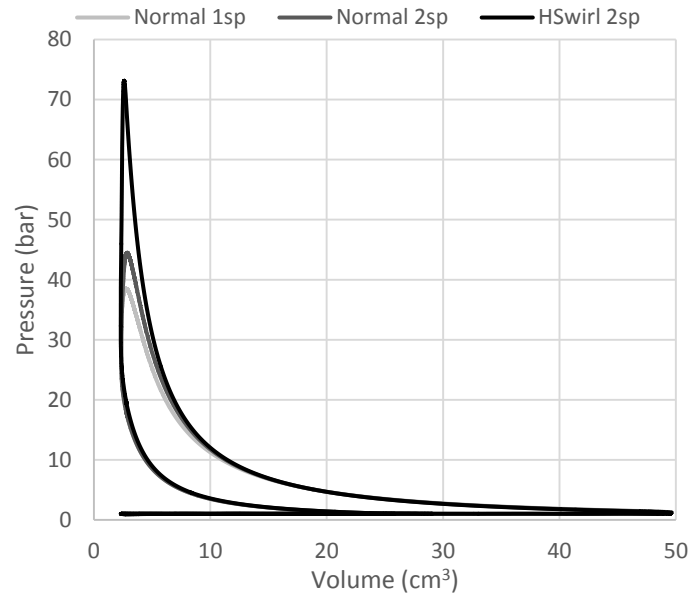
Figure 50 - P-V diagram results from the three simulations performed.

Adding the extra spark plug to the engine with the normal intake channel improves indicated work by 9%, but the introduction of the high swirl intake channel produces an improvement of 26%.

Figure 51 displays a constant temperature isosurface showing the flame front development at different piston positions for the high swirl intake channel, 2 spark plugs (HSwirl 2sp) simulation.
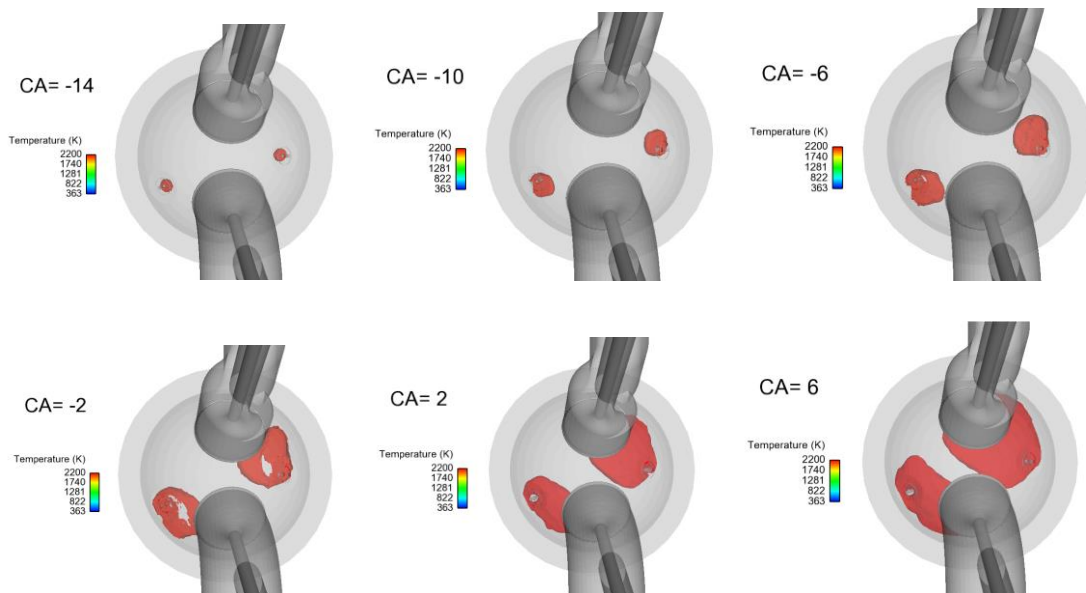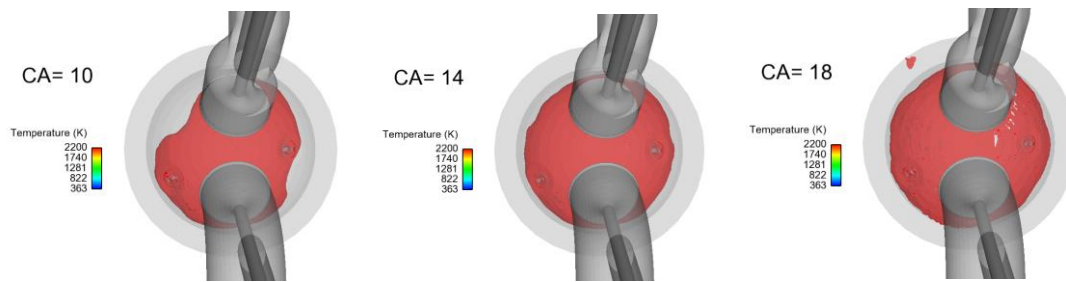
Figure 51 - Constant temperature isosurface showing the flame front development at different piston position. Top view.

As it can be seen the flame development is very fast and, as there are two spark plugs, the duration for combustion is extremely short. From the start of combustion to its completion within the combustion bowl only 32 crank angle degrees have elapsed, which shows how fast this engine can burn its charge.

3.2.4 Constant Volume Combustion

High turbulence, dual spark plug ignition and compact combustion chamber designs, as shown before, are three ways of increasing combustion speed increasing the degree of constant volume of an ICE (the component of the combustion which is made under a nearly constant volume) in order to improve the thermal efficiency. All these methods attempt to reduce the combustion duration in order to approach the ideal Otto cycle.

However, a truly constant volume combustion on an ICE can only be performed using special crankshaft mechanisms that can stop the piston at TDC. This allows the piston to hang, or momentarily pause, at TDC increasing its dwell time. A cam-driven crankshaft can be used to entirely accomplish any kind of piston motion during all strokes of the engine cycle, therefore it can be used to create an isochoric combustion after the compression stroke.

The work presented is being performed along with an American company which has invented a cam crankshaft. Nested coaxial counter rotating cam (NeCCoRC) is the denomination of the crankshaft. The proposed crankshaft is not here described due to disclosure reasons.

The heat release rate during combustion in a conventional engine can be easily predicted and calculated using the Vibe function as stated before. Nevertheless, performing a truly constant volume combustion will enhance the combustion efficiency decreasing its duration. The only way to calculate the heat release rate for a combustion occurring at a constant volume is using a CFD software that includes detailed chemistry in combustion applications like the SAGE model used by

the CONVERGE software. Therefore CONVERGE was used to predict the heat release rate during combustion at a constant volume.

The combustion chamber design used to perform the simulation at constant volume at TDC is the UMotor engine with the normal intake channel and with only one spark plug. Before the presentation of the simulation results, all the inputs and models used are presented.

3.2.4.1 Boundary conditions

Table 13 shows the various boundary conditions used for modelling and their function.

Table 13 - Boundary conditions and functionality.

No:	Boundary Name	Type	Region	Function
1	Piston	Wall Moving	Cylinder	User defined motion
2	Liner	Wall	Cylinder	Moves with piston
3	Cylinder Head	Wall	Cylinder	Stationary wall
4	Spark Plug	Wall	Cylinder	Stationary wall
5	Exhaust Port	Wall	Exhaust system	Stationary wall
6	Exhaust out flow	Outflow/Backflow	Exhaust system	Allows fluid
7	Exhaust Valve	Wall Moving	Exhaust system	User defined motion
8	Intake Port	Wall	Intake system	Stationary wall
9	Intake inflow	Inflow	Intake system	Allows fluid
10	Intake Valve	Wall Moving	Intake system	User defined motion

Figure 52 shows the motion of both a conventional piston and a piston with TDC DWELL used in the simulations. The DWELL duration at TDC was set at 20 CA degrees. In order to standardize the name of the peculiar piston motion to perform constant volume combustion (CVC), from here it will be called unconventional crankshaft.
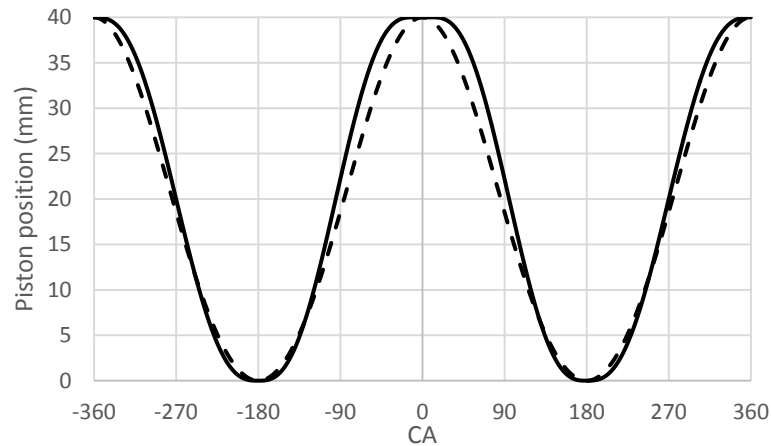
Figure 52 - Conventional piston motion (dashed black line) and piston motion with TDC dwell (black line) used in the simulation.

The valve motion, solution procedure and physical models used were set to be equal to the UMotor combustion simulation.

3.2.4.2 Results

Table 14 shows the engine combustion results for the two different simulations performed in CONVERGE. Figure 53 and Figure 54 present the graphical results obtained by the simulation.

Table 14 - Engine and combustion conditions and results.

	Conventional crankshaft	Unconventional crankshaft
Ignition advance (CA BTDC)	25	13
Engine load (bar)	1	1
Engine speed (rpm)	3000	3000
Combustion duration (CA)	44	38
Combustion start (CA BTDC)	17	9
Combustion end (CA ATDC)	27	29

Once more, the ignition advance was set to obtain MBT and determined by using a practical method where the ignition timing has to be defined in order to obtain the maximum pressure around 16 CA degrees ATDC [3]. So ignition timing had to be estimated by trial-and-error.
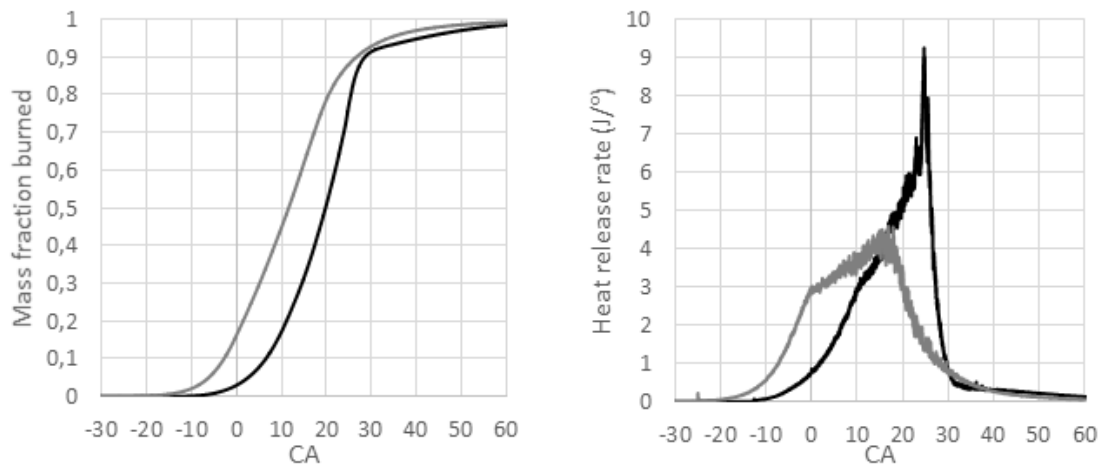
Figure 53 - Mass fraction burned (left) and heat release rate data (right) from the two simulations. Conventional crankshaft (grey line) and unconventional crankshaft (black line).

Using the conventional crankshaft the ignition occurred at 25 CA degrees BTDC and the combustion started at 17 CA degrees BTDC, a delay of 8 CA degrees. On the other hand, using the unconventional crankshaft the ignition advance was reduced to 13 CA degrees BTDC and the combustion started at 9 CA degrees BTDC, a delay of 4 CA degrees. The reduced delay results from a higher density mixture at the moment of ignition. In Figure 53 it can be seen that the heat release rate using the unconventional crankshaft increases much more steeply than in the case of the conventional crankshaft and continues even after the piston leaves TDC (10 CA degrees ATDC).

Therefore, a much faster combustion occurs at constant volume without ignition advance (the ignition is set with the piston already stationary). Consequently the maximum pressure will be much higher, increasing cycle indicated work as shown on Figure 54.
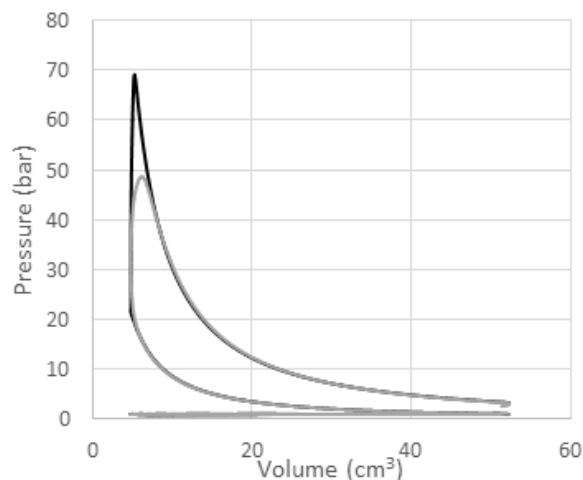
Figure 54 - P-V diagram results from the two simulations. Conventional crankshaft (grey line) and unconventional crankshaft (black line).

After the compression stroke, work improvement is about 1% due to the absence of ignition advance and after the power stroke the work improvement is 6% due to a faster combustion. The efficiency improvement is relatively small from what was expected because performing constant volume combustion leads to an increase of the combustion speed, causing extreme temperature and pressure increases resulting in high heat loss to the engine walls. Therefore the increase in efficiency is not as higher as expected relatively to the Otto cycle using a conventional crankshaft at the same conditions including the higher risk of knock appearance.

The UMotor combustion engine with one spark plug was used to perform the constant volume analysis. Using the helical intake channel is not advantageous when performing a truly constant volume combustion, because the combustion improvement is unnoticeable, while the increase of swirl provided by this geometry will lead only to higher heat losses to the engine walls. Therefore, medium to low combustion speed engines are the ones that could benefit the most from performing constant volume combustion, resulting in an increase on combustion efficiency and speed.

More work and study has to optimize the performance of unconventional crankshaft, namely by performing different piston motions in order to achieve a QCV combustion which has shown good results as presented by Winward [31] and Doric [32].

Nevertheless, the added heat loss to the walls caused by the constant volume combustion strategy can be harvested by internally cooling the engine walls through a direct water injection (a strategy to be assessed below).

3.3 Direct water injection

3.3.1 0D Wall temperature model development with direct water injection

The purpose of the work in this chapter is to create a quasi-adiabatic spark ignition engine by internal cooling using direct water spray injection. The principal aim is to reduce the heat lost by the engine walls by using it to produce work through the expanding vaporizing water. Consequently a wall temperature model was developed in Excel, in order to evaluate the feasibility of this concept.

The purpose of the wall temperature model is to calculate the depth of the wall that is required to "store" the heat from a combustion cycle and to evaluate the required heat transfer rates to accomplish full adiabaticity. Knowing that in reality the combustion does not happen

instantaneously, the combustion model presented above in section 3.2.1 was used as the basis for the wall temperature model. Thus, the engine variables can be changed to affect the combustion duration and the MFB rate. Therefore, the wall temperature model is implemented into the 0D engine combustion model.

Firstly, the wall temperature model is presented with the basic theoretical expressions. Finally the variation of temperature across the combustion chamber wall and exhaust valve during a combustion cycle, with and without water injection, is calculated and presented.

3.3.2 Wall temperature model

The heat transfer to the combustion chamber walls of ICEs is recognized as one of the factors having a great influence both in engine design and operation [3]. Research efforts concerning conduction and convection heat transfer in reciprocating ICEs are aiming, among others, to the investigation of thermal loading of critical combustion chamber components with the target of improving their structural integrity and increasing their safety against fatigue phenomena.

The principal aim in this text, with the creation of a temperature model, is to determinate the capability of water injection to cool the combustion chamber and exhaust valve walls.

3.3.2.1   Heat transfer to the wall

The Annand heat transfer coefficient was used, as it is known to be more accurate when applied to spark ignition engines [2]. The Annand expression separates the convection and the radiation terms but this latter term has not been implemented in the model as it would bring unnecessary complexity and radiation does not represent a very important fraction of the overall heat transfer. The convection heat transfer coefficient h, is related to the Nusselt number, Nu, by

$$h = \frac{k\,Nu}{D} \tag{11}$$

Where D is the cylinder bore and k is the thermal conductivity of the air, quantified by the following expression [2],

$$k = 6.1944 \times 10^{-3} + 7.3814 \times 10^{-5}\,T - 1.2491 \times 10^{-8}\,T^2 \tag{12}$$

The Nusselt number is obtained from the Reynolds number, Re, and a specific constant for 4 stroke engines as follows:

$$Nu = 0.49 \, Re^{0.7} \tag{13}$$

The Reynolds number is calculated as follows:

$$Re = \frac{\rho \, Sp \, D}{\mu} \tag{14}$$

Where Sp is the mean piston speed and μ is the dynamic viscosity of the mixture inside the cylinder [2], calculated by,

$$\mu = 7.457 \times 10^{-6} + 4.1847 \times 10^{-8} \, T - 7.4793 \times 10^{-12} \, T^2 \tag{15}$$

For each heat transfer surface, the expression for the heat transfer rate is given by

$$\dot{Q} = h\left(T_{gas} - T_{wall}\right)A \tag{16}$$

Where A is the heat transfer area, which is constant for the combustion chamber wall and piston surface, and variable for the cylinder wall. $\dot{Q}$ is the heat (thermal power) transferred by the hot gases to the wall.

3.3.2.2 Model description
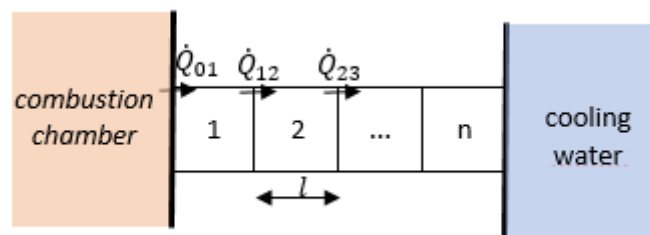
Figure 55 - Model combustion chamber wall section.

Figure 55 represents a section of the combustion chamber wall, which has been divided into *n* lumped sections or cells. The cell #1 is located at the inside of the engine, and is in contact with the hot gases so it represents the combustion chamber wall of the engine. The l is the cell width.

On the left side (combustion chamber) the temperature and the heat transfer coefficient change over time, whereas on the cooling side they are constant.

In the first time step, $t = 0$, the temperature in each cell is defined at a given initial guess value in order to start the iterative temperature calculation that continues in the following time steps (note that the problem is of periodic nature, so the initial conditions must coincide with the final results of the previous engine cycle).

During the subsequent time steps the temperature in each cell is calculated with the following equations, which result from performing an energy balance to the cell and accounting for the thermal heat fluxes (dq) across the cell boundaries and from computing the resulting energy accumulated in the cell during a given time lapse (dt):

$$\frac{dq}{dx} = -\rho c_p \frac{dT}{dt} \tag{17}$$

Where ρ is the gas density, and c_p is its specific heat at constant pressure.

In reality, this is the 1D energy equation for and purely conductive heat transfer. From the definition of heat flux, it can be rewritten as follows:

$$\frac{d}{dx}\left(k\frac{dT}{dx}\right) = \rho c_p \frac{dT}{dt} \tag{18}$$

Or

$$\alpha\frac{d^2T}{dx^2} = \frac{dT}{dt} \tag{19}$$

Where α is the thermal diffusivity.

After the linearization of the previous equations, the temperature at each cell can be calculated with the following equations.

Cell #1,

$$(\dot{Q}_{01} - \dot{Q}_{12})\Delta t = (T_{1f} - T_{1i})mc_p \tag{20}$$

Where,

70

$$\dot{Q}_{01} = h \ (T_{gas} - T_{1i}) \qquad (21)$$

$$\dot{Q}_{12} = \frac{k}{l} \ (T_{2i} - T_{1i}) \qquad (22)$$

Cell #2,

$$(\dot{Q}_{12} - \dot{Q}_{23})\Delta t = (T_{2f} - T_{2i})mc_p \qquad (23)$$

Where,

$$\dot{Q}_{12} = \frac{k}{l} \ (T_{2i} - T_{1i}) \qquad (24)$$

$$\dot{Q}_{23} = \frac{k}{l} \ (T_{3i} - T_{2i}) \qquad (25)$$

The other cells are calculated in the same way as cell number #2.

Is important to state that this is a transient model, so the heat transfer coefficient and the temperature inside the engine (burning mixture) varies for each time step.

Since the problem is periodic (the conditions at end of a cycle must be identical to the conditions at beginning of the next cycle), the temperature distribution obtained at the end of the engine cycle will be used as the initial condition for the next iteration. The process will be repeated until no relevant differences are found between consecutive iterations.

At normal engine operation the cell number n is assumed to be in contact with the cooling water system. It is assumed a medium heat transfer coefficient varying only with engine speed and a constant water temperature of 363 K. The mean heat transfer coefficient $\bar{h}$, can be calculated with the following equation for water flow in a pipe.

$$\bar{h} = \frac{\dot{m} \ c_p}{\pi \ d \ L} \times \frac{(T_{out} - T_{in})}{\Delta T_L} \qquad (26)$$

And,

$$\Delta T_l = \frac{(T_{wall} - T_{out}) - (T_{wall} - T_{in})}{ln\frac{T_{wall} - T_{out}}{T_{wall} - T_{in}}} \tag{27}$$

Where, $\dot{m}$ is the water flow rate, d is the pipe diameter, L is the pipe length, T_{out} and T_{in} is the outlet and inlet water temperature.

The temperature model for the exhaust valve works in a different way. The heat transfer calculation at the exhaust valve face that is in contact with the burning gases is performed similarly with the combustion chamber wall. The main particularity is that the valve stem is ignored in order to allow a 1D analysis (Figure 56).
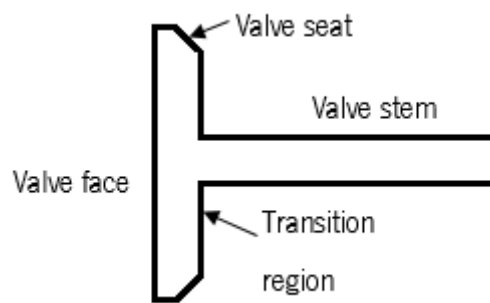
Figure 56 - Exhaust valve description.

The valve seat is generally responsible for most of the heat transfer from the poppet valve. Therefore, when the valve is closed, only the valve seat contact area is considered to allow heat retrieval from the valve rear. When the valve opens all the right side area of the valve (valve seat and transition region) is heated by the passing exhaust gases (Figure 57).
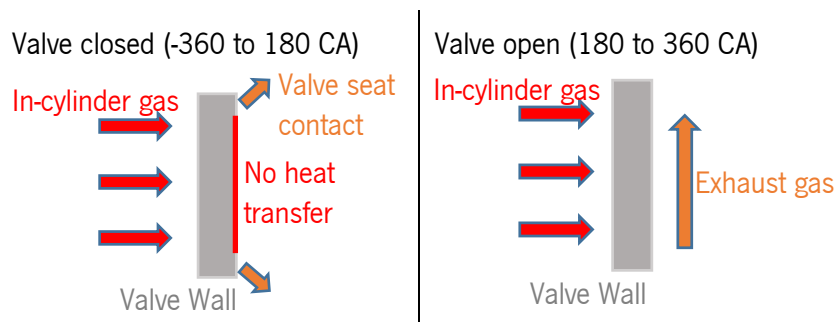
Figure 57 - Exhaust valve model boundaries.

3.3.2.3 Wall surface cooling by direct water injection

The previously described temperature model is complemented with surface cooling by direct water injection. An amount of water is injected in each cycle to the combustion chamber wall and valve face cooling it down during expansion (just after the end of combustion).

During water injection a water film is created between the wall surface and the hot gases leading to an interruption of the heat transfer among the hot gases and the wall surface. When water injection is added the outer side of the wall previously assumed to be in contact with the cooling water, is now assumed adiabatic.

The cooling energy of the injected water can be calculated by the following equation.

$$Q_{water} = m_{water} \times \bar{h}_{fg} \qquad (28)$$

Where m_{water} is the water mass (for one injection), and $\bar{h}_{fg}$ is a mean value for the latent heat of vaporization of water during water injection (internal pressure will vary).

The wall temperature calculation during water injection on the temperature model uses the following equation:

$$\dot{Q}_{01} = -Q_{water}/\Delta w \qquad (29)$$

Where Δw is water injection duration.

3.3.3 Model calculation conditions and inputs

All the model results presented on the result sections have the same fixed model inputs presented below. Table 15 shows the relevant engine specifications.

Table 15 - Engine specifications.

Compression ratio	11:1	
Stroke	39.0	mm
Bore	39.5	mm
Exhaust valve diameter	14.0	mm
Engine load	1	bar
Rod length	100	mm
AFR	14.5	-

The material and geometric characteristics are presented on Table 16 for the combustion chamber and on Table 17 for the exhaust valve.

Table 16 - Combustion chamber material and geometric specifications.

Material	Aluminium	
Cell mass	1.9E-03	Kg
Surface area	6.9E-03	m^2
Density	2700	kg/m^3
Thermal conductivity	205	W/m K
Thermal diffusivity	8.3E-05	m^2/s
Specific heat	910	J/kg K

Table 17 - Exhaust valve material and geometric specifications

Material	Steel	
Valve head diameter	14.0	mm
Valve head face area	2.8E-03	m^2
Valve seat area	1.9E-04	m^2
Density	7830	kg/m^3
Cell mass	2.2E-03	Kg
Thermal conductivity	14.50	W/m K
Thermal diffusivity	9.3E-06	m^2/s
Specific heat	500	J/kg K

74

3.3.4 Engine model validation

Benson [77] shows results for combustion chamber surface temperature using a thermocouple in the cylinder head. These results are presented on Figure 58 and may be compared against the results provided by the model. To compare the results, surface temperature results from model is plotted on the right side. As it can be seen, good agreement exists between measurements and predictions from the present model.
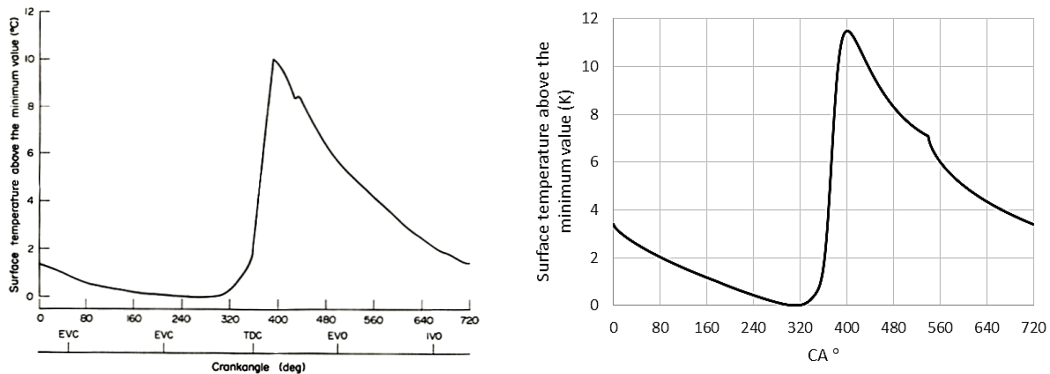
Figure 58 - Measured values [77] (left) and calculated (right) of cylinder head surface temperature.

Figure 59 displays wall surface heat flux measurements made in a cylinder head of a spark ignition engine [3]. The variation of surface heat flux with crank angle for five consecutive individual cycles at 1500 rpm, AFR=18, 40% engine load and MBT timing may be seen in this figure. When comparing it with then model results at the same engine conditions for 1 cycle, it can be seen that the same good agreement was obtained.
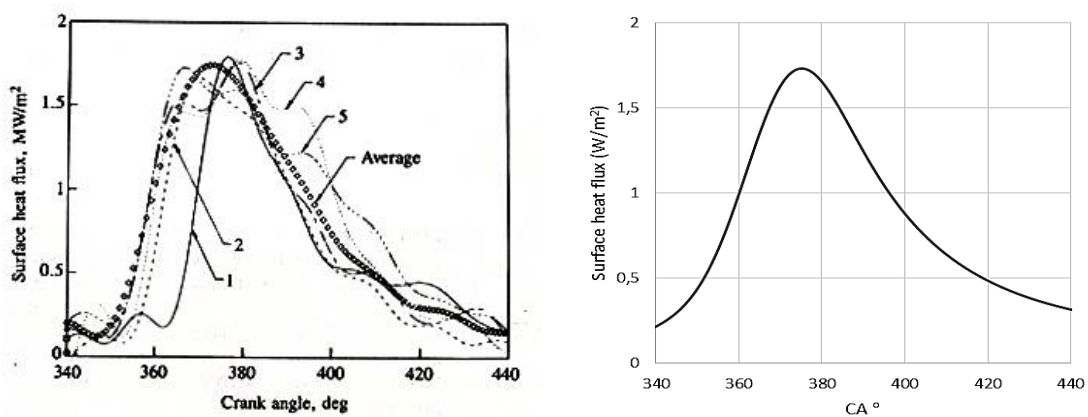
Figure 59 - Heat flux histories for five consecutive individual cycles 198-cycle average 1500 rev/min, AFR=18, Load=40%, MBT timing [3] (left) and surface heat flux model results for same conditions (right).

3.3.5 Combustion chamber temperature results without water injection

The results presented above were done with the sole purpose of comparing the model results with real engine measurements. This section shows the assumptions used in the model in order to evaluate the variations on the wall and valve surface temperature and temperature depth for different engine speed at normal engine operation.

Table 18 presents engine conditions and combustion model outputs for the three different engine speeds modelled using combustion and temperature models.

Table 18 - Combustion model results for 1500, 3000 and 6000 rpm at WOT and ignition advance for MBT.

	Engine speed: 1500 rpm	Engine speed: 2000 rpm	Engine speed: 6000 rpm
Ignition advance (CA BTDC)	14	18	21
Engine load (bar)	1	1	1
Combustion duration (CA)	31.8	40.7	46.6
Combustion start (BTDC CA)	14	18	21
Combustion end (ATDC CA)	17.8	22.7	25.6

Figure 60 shows pressure and temperature results for 1500 rpm. Results for the different engine conditions are very similar and therefore are not shown.
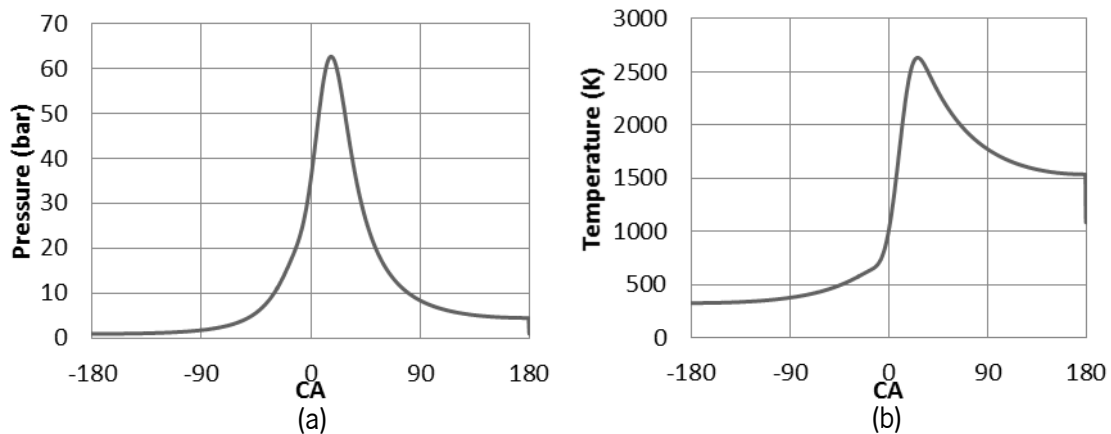
Figure 60 - Pressure (a) and Temperature (b) of the gases as a function of crank angle for MBT.

Results for the envelope of temperatures obtained along the wall depth during one cycle for several operating conditions are presented in Figure 61. Also presented are the results for the evolution of the surface temperature in absolute terms (Figure 62) or relatively to the minimum temperature achieved (Figure 63). These different conditions are plotted on the same graphics in order to better compare the results.

Figure 61 - Envelopes of the temperatures along the wall depth during one cycle for normal engine operation at 1500 rpm (light grey), 3000 rpm (grey), 6000 rpm (black).
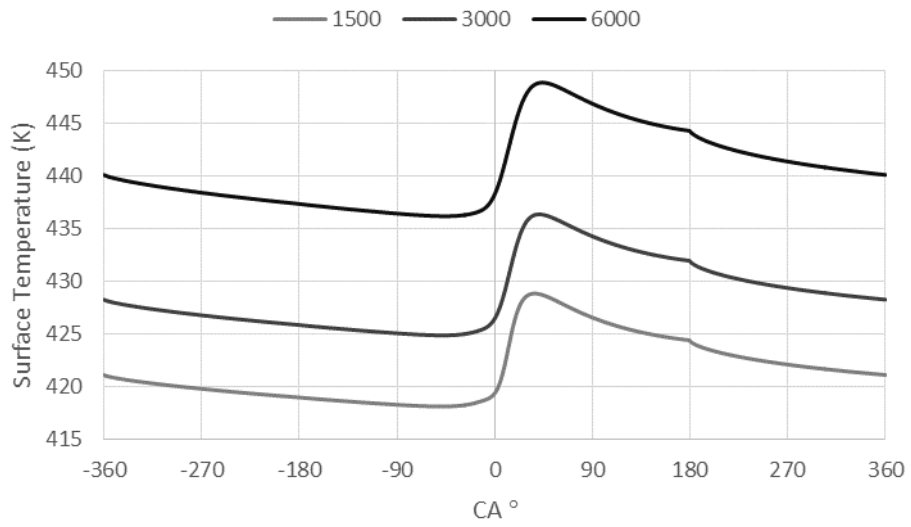
Figure 62 - Wall surface temperature for normal engine operation at 1500 rpm, 3000 rpm, and 6000 rpm.
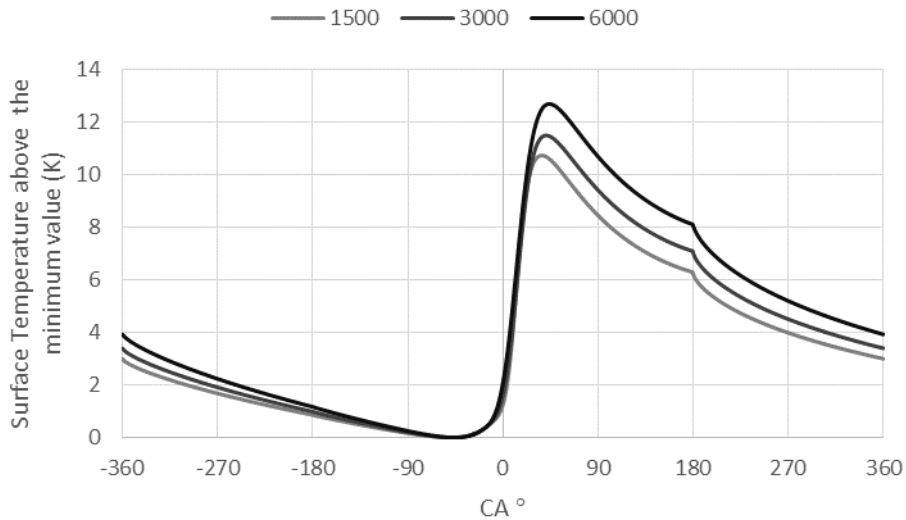
Figure 63 - Wall surface temperature above the minimum value for normal engine operation at 1500 rpm, 3000 rpm, and 6000 rpm.

From the results presented in Figure 61 to Figure 63 it is possible to deduce that surface temperature increases with higher engine speeds due to the enhancement in the heat transfer coefficient. The heat transfer coefficient is correlated to in-cylinder gas velocity. As the engine speed increases, the gas inside the cylinder is forced to move faster and combustion is sped up, further increasing gas speed and consequently the heat transfer coefficient. Under higher engine speeds the faster moving intake gases are capable of cooling down the wall surface at higher rates during intake and compression, and during combustion the higher turbulence produced at higher engine speeds increases the engine cycle temperature.

The model assumes that the cooling water flow rate increases linearly with engine speed, as it happens in real engine operation, in order to maintain the constant temperature at the water side of the wall, as portrayed for 6 mm on Figure 61.

Despite the increase on the wall surface temperature as engine speed increases, indicated engine thermal efficiency increases with engine speed. The temperature model results show that at 1500 rpm the heat lost for the combustion chamber wall was 180 J/cycle, at 3000 rpm it was 143 J/cycle and at 6000 rpm it was 116 J/cycle, which represents 12,4 %, 9,8 % and 8,0 % of the total heat supplied by the fuel, respectively. This phenomenon can be easily clarified. As engine speed increases, the high temperature gases remain in contact with the wall for a shorter period, leading to a decrease in the heat lost despite the increase in the heat transfer coefficient, the higher heat

flows and the higher wall temperatures. Obviously, the total heat transfer rate increases with the increasing speed as the power supply provided by the fuel also increases. Therefore, the power lost to the combustion chamber wall, averaged along a whole engine cycle is 2250 W at 1500 rpm, 3575 W at 3000 rpm and 5800 W at 6000 rpm.

Another influence of the shorter cycle time as engine speed increases is the wall temperature depth. If we look at Figure 61 at 1 mm wall depth it is possible to see that thermal penetration decreases with the increase in engine speed.

There is lower heat loss to the walls since the coolant load is reduced. Therefore, both the brake power (and therefore thermal efficiency) and the exhaust power increase with engine speed due to the lower heat losses through the wall as can be seen on Figure 64 from reference [3].
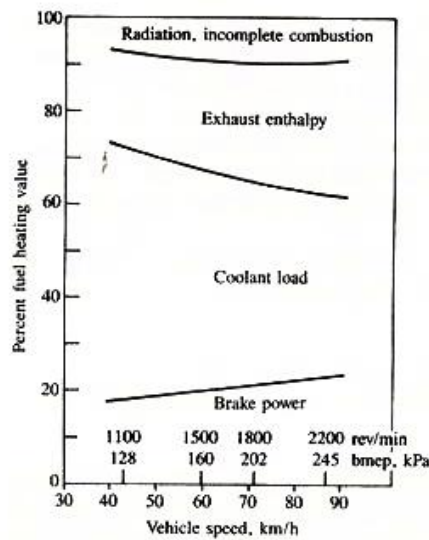
Figure 64 - Distribution of energy on a typical SI Engine as a function of engine speed [3].

Temperature results for the exhaust valve at the same conditions displayed for the combustion chamber wall are presented below. Again, results for temperature along the wall depth (Figure 65) and surface temperature (Figure 66) for these different conditions are plotted on the same graphics in order to better compare the results.
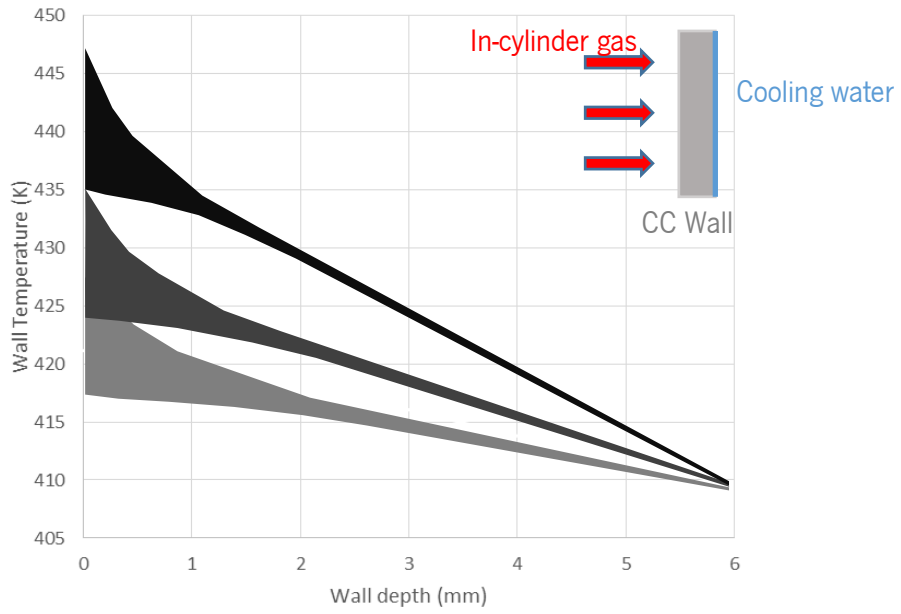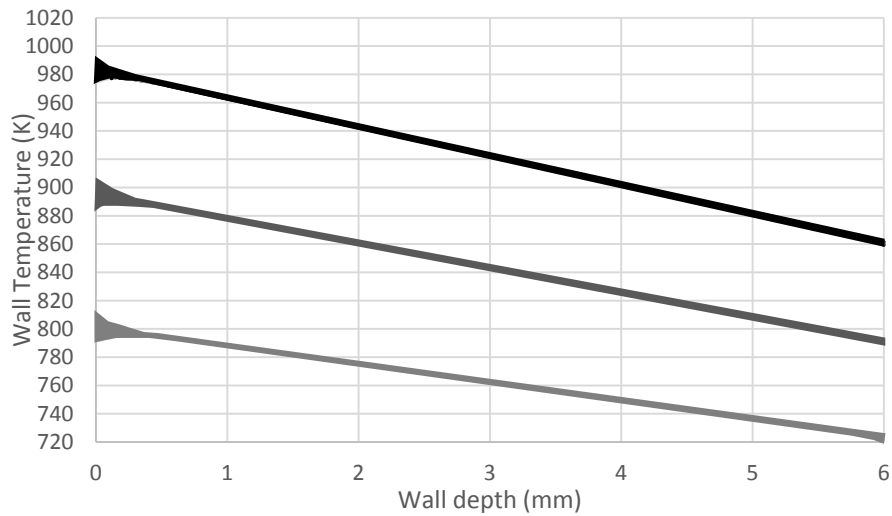
Figure 65 - Envelopes of the temperatures along the valve thickness during one cycle for normal engine operation at 1500 rpm (light grey), 3000 rpm (grey), and 6000 rpm (black).

Similarly to the combustion chamber walls, the exhaust valve face temperatures increase with the increase of engine speed. Nevertheless, the rise in temperature is much higher. This is due to the fact that in conjunction with the increase of the heat transfer coefficient, the valve is in contact with the seat for a shorter period during each cycle, leading to a lower time to cool it down.

As expected the temperature at the right side of the exhaust valve on Figure 65 (valve seat and transition region) is lower than the temperature at left side, as it is cooled by the valve seat (same temperature of the combustion chamber). The rise of the temperature at this region happens at a same rate as the valve face.

The result of the difference on the material properties of the combustion chamber (aluminium) and the exhaust valve (steel) can be seen on Figure 65, where the thermal penetration on the exhaust valve is much lower than for the combustion chamber.
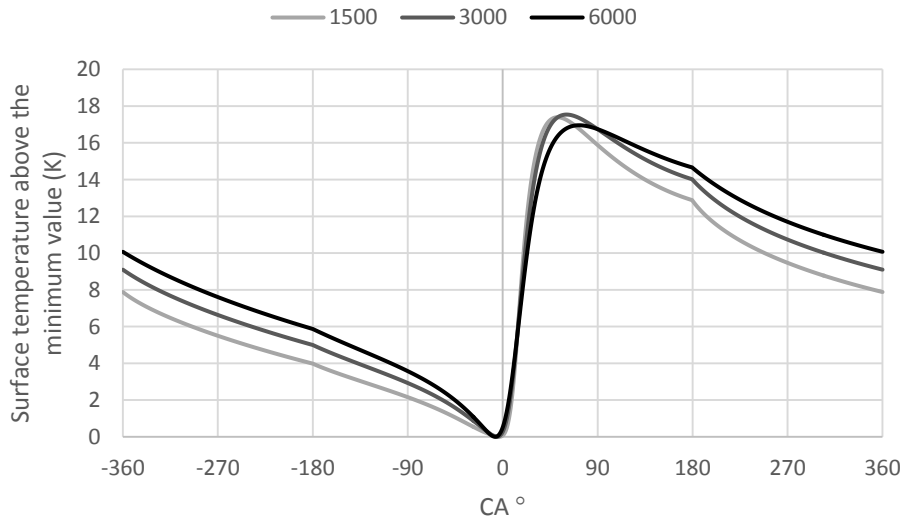
Figure 66 - Exhaust valve face temperature above the minimum value for normal engine operation at 1500 rpm, 3000 rpm, and 6000 rpm.

3.3.6 Cooling effect of water injection at high ambient pressures

Before showing the model results for the water injection condition shall be discussed some of the phenomena associated with water spray injection under high ambient pressures in order to better evaluate the evaporative cooling capability of water jets impinging over the combustion chamber and valve face walls.

The spray simulations done by Issa [78] conducted for a wide range of pressures revealed the following primary key issues regarding to the droplet dynamics, heat transfer and vaporization.

Droplet Dynamics; at pressures higher than ambient air, the larger the droplet size the better is the droplet-wall impaction. With the increase in the drag force (due to the increase in the ambient air density), droplet-drifting behaviour increases. Therefore at higher ambient pressures larger droplets are able to hit the surface and spread better at impaction.

Droplet heat transfer; at higher pressures the Leidenfrost point shifts to a higher temperature. This leads to an increase in the wetting capability of the droplets at impaction and, therefore, to a higher droplet contact heat transfer effectiveness.

Droplet Vaporization; at high ambient pressures more vapour is generated at each droplet impaction on the surface. This is due to the much lower latent heat of vaporization at higher pressures. The result is an increase in the droplet contact heat transfer effectiveness.

The heat transfer effectiveness ε is related to the mass of the droplet (m_{inj}) that is converted into vapour (m_{vap}) during injection. It is defined as the fraction between the heat that is released during partial evaporation and the maximum possible heat that can be released when complete droplet evaporation occurs:

$$\varepsilon = \frac{m_{vap}}{m_{inj}} \tag{30}$$

A numerical model was developed by Issa [78] to simulate the impingement of liquid sprays on surfaces heated at temperatures ranging from nucleate to film boiling. The model was used to simulate high ambient pressure conditions as expected in an ICE during the power stroke (hot gas expansion).

In order to check for the sensitivity and validity of the model to the various operating pressures the spray experiment conducted by Halvorson [79] was simulated by Issa [78]. In this experiment a single stream of droplets impinges on a heated plate with wetting contact. The droplet injections were made in a pressurized chamber using three different gauged needles. The model was simulated for chamber pressures of 0.1, 0.5, 1, 2, 5, 10, 30 and 50 atm. Experimental data by Halvorson were available for comparison at 0.1, 0.5, 1, and 2 atm. At 5, 10, 30 and 50 atm, the results were based on model predictions for high operating pressure conditions.

The results revealed a good agreement between Halvorson experimental data and the model predictions. At high pressures the sub-cooling of the droplet has a significant effect on the absorption of heat. This is because of the fact that the saturation temperature increases with the increase in pressure and, therefore, a larger portion of heat is needed to increase the droplet temperature towards the saturation temperature. At 50 atm the droplet sub-cooling accounts to 35% of the maximum possible heat removal by the droplet, compared to 11% at atmospheric pressure. The increase in the droplet sub-cooling is also accompanied by the decrease in the latent heat of evaporation, much easier at higher pressures.

Figure 67 shows the model predictions at 5, 10, 30 and 50 atm (in addition to the results achieved by Halvorson) for the total heat flux as function of the mass flow flux.
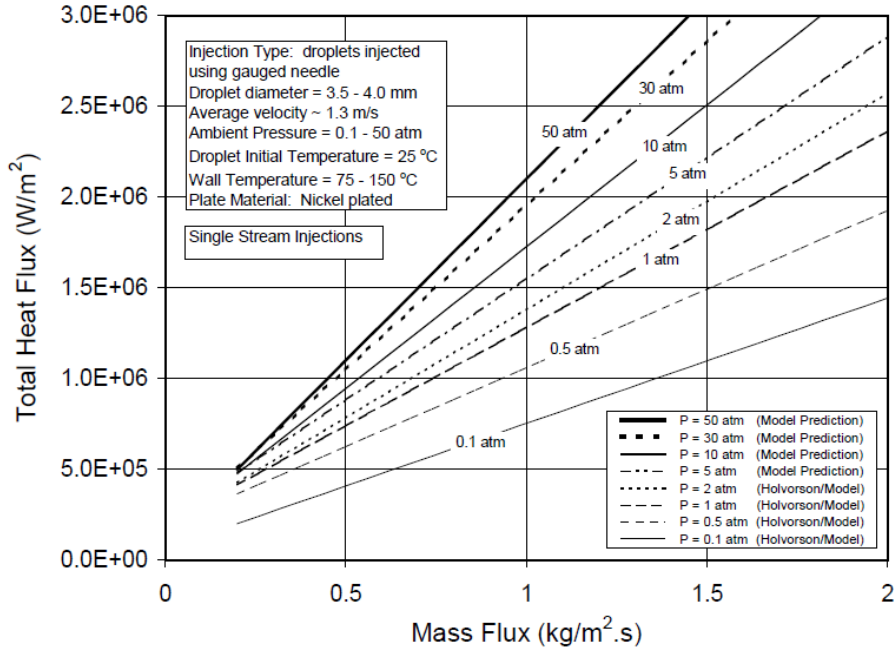
Figure 67 - Model predictions at 5, 10, 30 and 50 atmospheres (in addition to the results achieved by Halvorson [79]) [78].

The mass flux and total heat flux were calculated and compared with the results achieved by Issa [78] model on Figure 67, in order to verify if water injection duration for the water fuel ratio imposed is feasible.

The relationship between the total heat flux and the mass flux is almost linear, so it is possible to predict values of mass flux and total heat flux higher than the ones appearing in Figure 67.

Along with the graphical results presented by Issa [78], correlations for the droplet contact heat transfer effectiveness were also established as a function of the ambient pressure.

For 10 atm ambient pressure:

$$\varepsilon = 0.715 + 0.285 \cos\left(\frac{\pi}{523.8}\left[\left(T_{wall} - T_{drop}\right) - 242.2\right]\right) \tag{31}$$

For 30 atm ambient pressure:

$$\varepsilon = 0.74 + 0.26 \cos\left(\frac{\pi}{522.2}\left[\left(T_{wall} - T_{drop}\right) - 345.1\right]\right) \tag{32}$$

Droplet contact heat transfer effectiveness for ambient pressures between 10 and 30 atm can be calculated interpolating the above equations, where T_{wall} and T_{drop} are the wall and droplet temperature respectively.

Another research regarding water spray to cool hot walls was carried out by Ciofalo [80]. The results are shown on Figure 68, where maximum heat fluxes of 10^7 W/m^2 may be attained using different types of injectors and specific flow rates between 10 and 80 kg/m^{2}s.
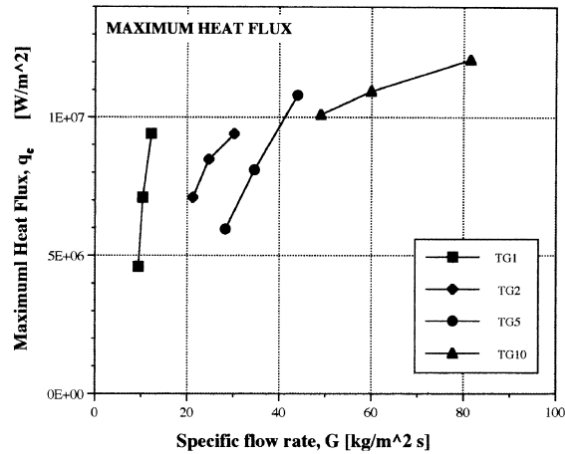
Figure 68 - Investigation of the cooling of hot walls by liquid water sprays [80].

However, in order to obtain maximum heat fluxes above 10^7 W/m^2 the flow rate has to be extremely high. In a system where the water mass and pressure have to be extremely limited this value is extremely high.

3.3.7 Results with water injection

The target of this work is to inject a precise amount of water after combustion cessation in order to cool the combustion chamber wall and exhaust valve down to the intended temperature levels. The vapour thus created will induce a rise in gas pressure after combustion ending promoting the expansion work.

At normal engine operation the combustion chamber wall temperature should not exceed 450 K. At that temperature the saturation pressure of water is lower than 10 bar. At WOT gas pressure is lower than 10 bar only after 80 CA degrees ATDC, becoming too late to start the water injection. The solution is to raise the combustion chamber wall temperature in order start water injection at 40 CA degrees ATDC (Table 19). At this position combustion should be completed and there is the possibility to place the water injector on the cylinder liner pointing upwards.

The same problem doesn't occur on the exhaust valve surface temperature since it is extremely high comparatively to the combustion chamber wall. On the other hand, reducing the exhaust valve

temperature is beneficial, since it is possible to raise the compression ratio without increasing the likelihood of knock onset which is sensible to engine hotspots.

Another benefit of increasing the wall temperature of the combustion chamber is the fact that less water has to be injected in order to cool down the walls since less heat is transferred from the hot combustion gases. Obviously there are some drawbacks of increasing the wall temperatures to extremely high values, such as material problems, lubricant degradation and hotspots (knock).

Table 19 - Temperature model conditions.

Engine speed	3000	rpm
Water injection start	40	CA
Water injection finish	90	CA
Water Fuel ratio (WFR)	1.66	

As displayed on Table 19, water injection started at 40 CA degrees, so that the water/steam does not interfere with combustion, which theoretically ends at approximately 23 CA degrees.

The different heat transfer modes occurring during part of the engine cycle are illustrated on Figure 69.
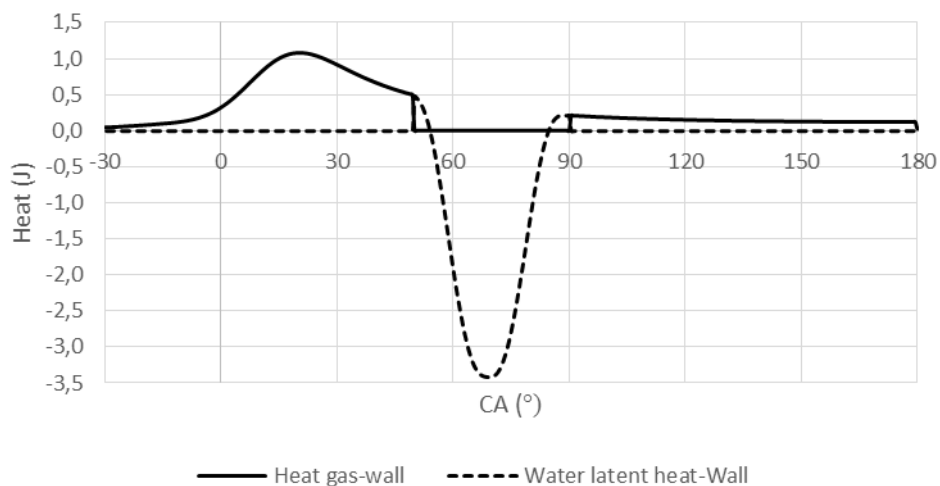
Figure 69 - Heat release from the gases to the wall and heat retrieved from the water injection.

The heat released to the combustion chamber surface is considered to halt when water is injected until it dries out. It is assumed that all the latent and sensible heat from the water is retrieved from the wall. Although part of the heat transferred to the water could come from the hot gases, as the

steam is produced on the surface and moves away from it, it is considered that there is no heat transfer (sensible or latent) from the hot gases to the vaporizing water.

Results for the wall temperature along its thickness are presented on Figure 70 and results for the wall surface temperature are presented on Figure 71. During combustion the wall temperature increases to a maximum of 510 K. Water injection drops the surface temperature dramatically, reaching a minimum of 391 K. Then, after the water injection ends, the hot gases heat the surface back to the initial temperature of 500 K. As the right wall is adiabatic, the inner wall temperature tends to the referred 500 K, and it is constant after approximately 2 mm.
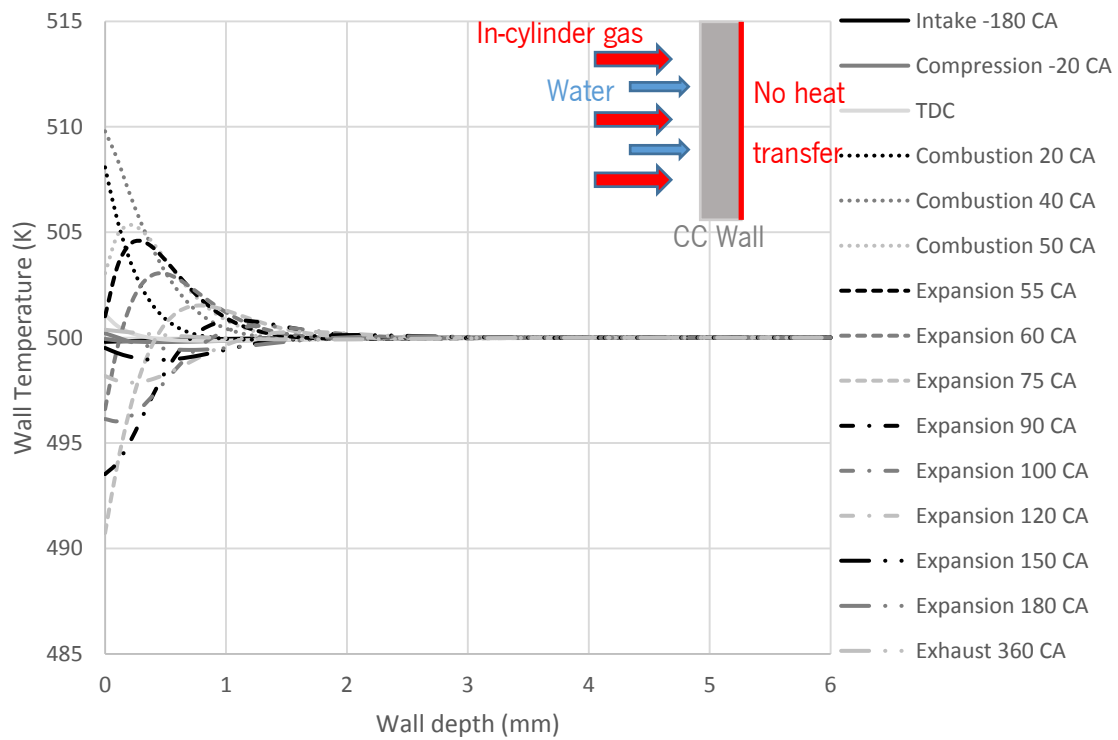
Figure 70 - Envelopes of the temperatures along the combustion chamber thickness during one cycle with water injection for different CA.

Figure 71 - Inner wall surface temperature during one engine cycle.

More detailed conditions for water injection are presented on Table 20. The average cylinder pressure during water injection is 20 bar. The mass flux and total heat flux required to cool down the combustion chamber wall are presented on Table 21 for those conditions.

Table 20 - Water injection conditions.

Water injection start	40.0	CA
Water injection finish	90.0	CA
Water Fuel ratio (WFR)	1.66	
Q heat water injection ($\varepsilon = 1$)	109	J
Water injection mass	0.057	g
Q heat transferred to wall	109	J
% heat transferred to wall	7.2	%

Table 21 - Mass and heat flux required.

Mass flux	2.95	kg/m^2 s
Total heat flux	5.62E+06	W/m^2

When water injection starts (40 CA degrees ATDC) in-cylinder pressure is nearly 32 bar, for which the saturation temperature of water is 237 °C (510 K). When the water injection ends (90 CA degrees ATDC) in-cylinder pressure is 8 bar for which the saturation temperature of water is approximately 170 °C (443 K).

Figure 72 shows the operation point (OP) from Table 21 on the projection of the Figure 67 for $\varepsilon = 1$ (see Eq. 30).
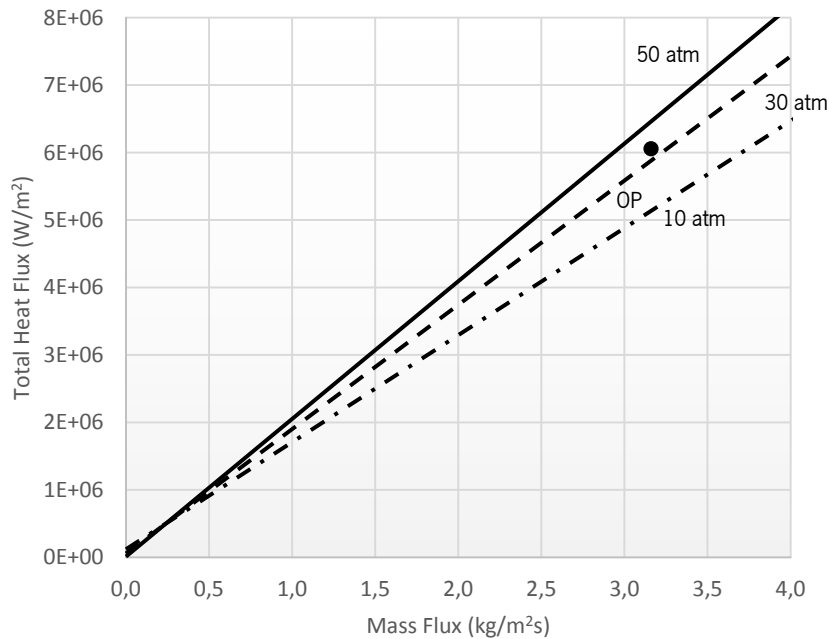
Figure 72 - Total Heat and mass flux for ε=1

This figure shows that in order to effectively cool the combustion chamber wall with the imposed mass flux, the water injection should be done during in-cylinder mean pressures above 30 atm (OP). Consequently more water mass (higher mass flux) has to be added to cool effectively the combustion chamber wall at medium pressures around 20 bar.

Obviously, adding more water would reduce even further the combustion chamber wall surface. Using the correlations (31) and (32) the droplet contact heat transfer effectiveness, for a medium ambient pressure of 20 bar and a mean wall surface temperature of 500 and a droplet temperature of 300 K is 94% ($\varepsilon = 0.94$).

Water fuel ratio has to be raised from 1.66:1 to 1.77:1 in order to have a mass flux of 3.14 kg/m^{2}s to obtain the required cooling effect (in-cylinder pressure of 20 bar) as can be seen on Figure 73 (OP).
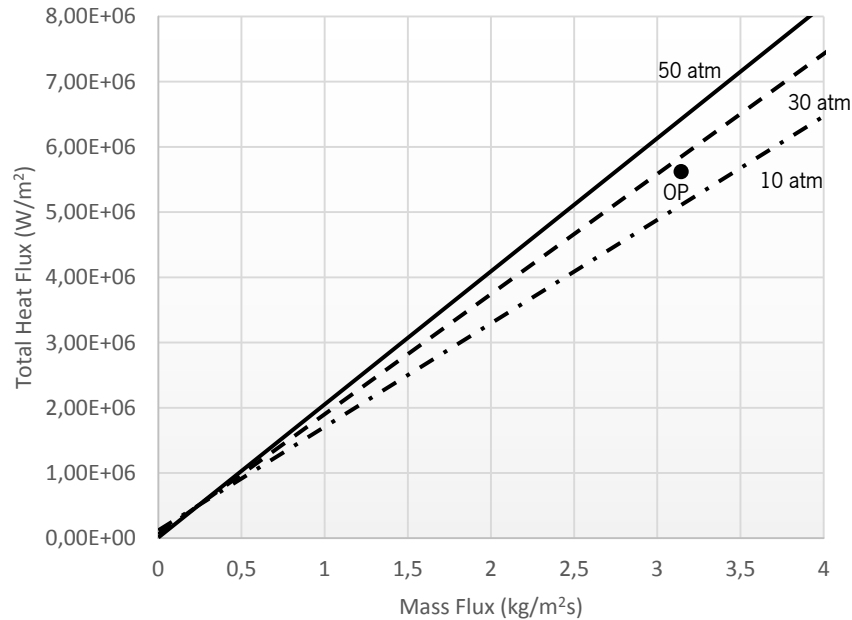
Figure 73 - Total heat and mass flux for ε =0.88

Below are the temperature results for the exhaust valve at the same conditions displayed for the combustion chamber wall. The model boundary with water injection are displayed on Figure 74.
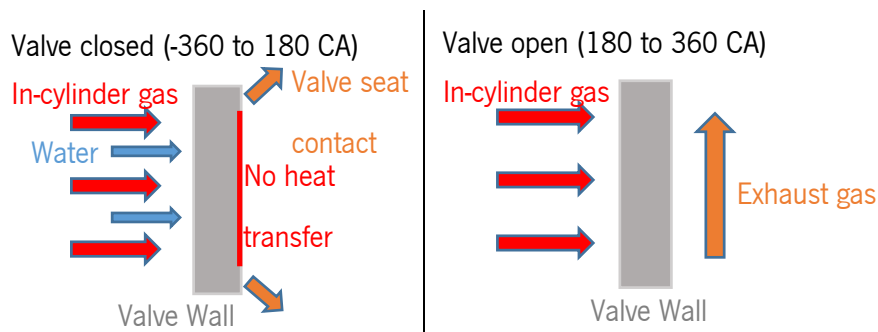
Figure 74 - Exhaust valve model boundaries with water injection.

Results for valve temperature along its thickness are presented on Figure 75 and Figure 76. During combustion the wall temperature increases to a maximum of 520 K. Water injection drops the surface temperature dramatically, reaching a minimum of 485 K. Then, after the water injection ends, the hot gases heat the valve face back to the initial temperature of 500 K. The seat temperature is assumed to be at a constant temperature of 500 K (combustion chamber

temperature with water injection). The right side of the valve on Figure 75 stabilizes at 512 K approximately.
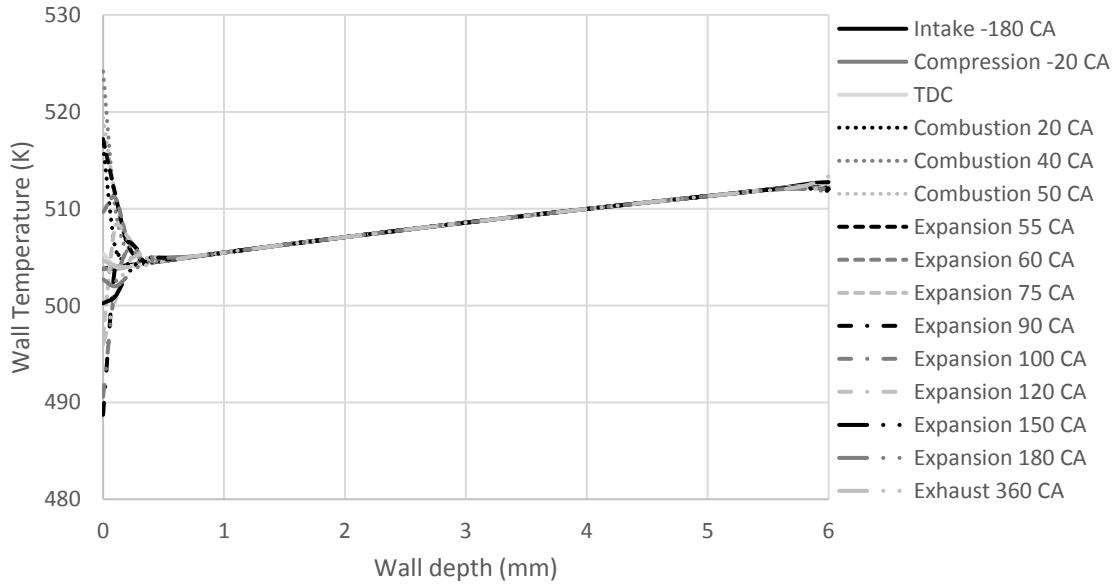
Figure 75 - Envelopes of the temperatures along the valve thickness during one cycle with water injection for different CA.
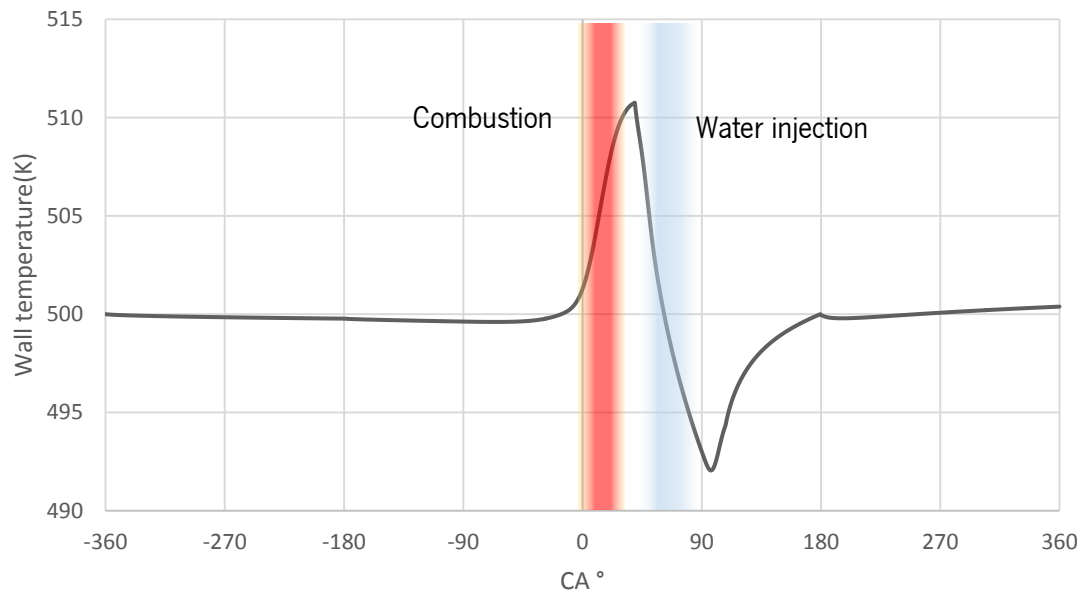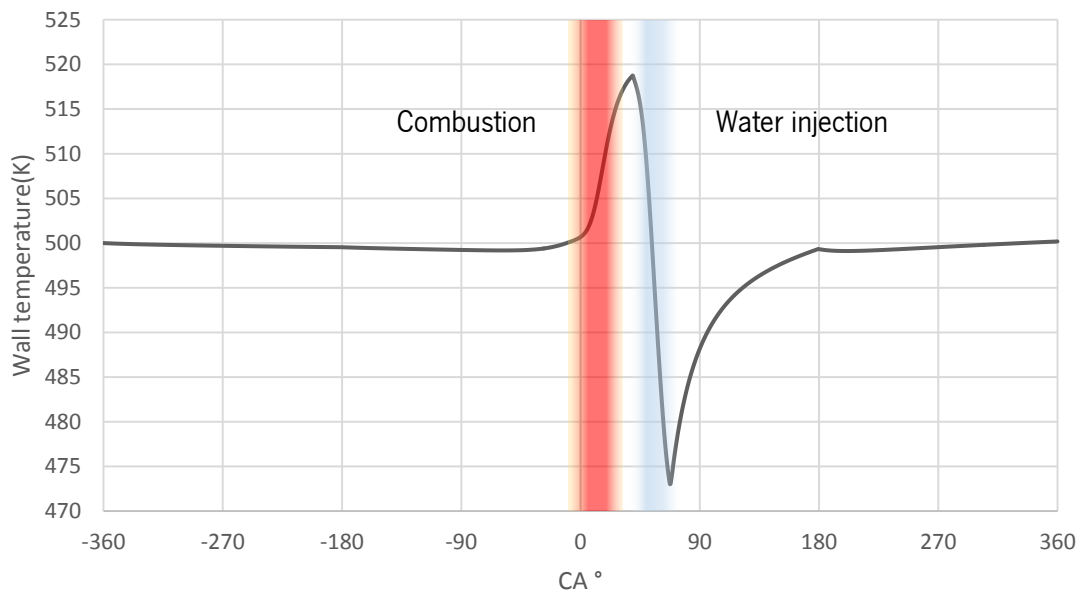

Figure 76 - Valve face temperature during one engine cycle.

The conditions for water injection are presented on Table 22, the average cylinder pressure during water injection is 20 bar. The mass flux and total heat flux required to cool the combustion chamber wall are presented on Table 23 for those conditions.

Table 22 - Water injection conditions.

Water injection start	40.0	CA
Water injection finish	90.0	CA
Water Fuel ratio (WFR)	0.65	
Q heat water injection ($\varepsilon = 1$)	44	J
Water injection mass	0.022	g
Q heat transferred to wall in cylinder surface	41	J
% heat transferred to wall	2.7	%

Table 23 - Mass and heat flux required.

Mass flux	2.38	kg/m^2 s
Total heat flux	4.38E+06	W/m^2

When water injection starts (40 CA degrees ATDC) in-cylinder pressure is nearly 32 bar, for which the saturation temperature of water is 237 °C (510 K). When the water injection ends (90 CA degrees ATDC) in-cylinder pressure is 8 bar for which the saturation temperature of water is approximately 170 °C (443 K).

On Figure 77 is displayed the operation point (OP) from Table 23 on the projection of Figure 67 for $\varepsilon = 1$ (see Eq.30).
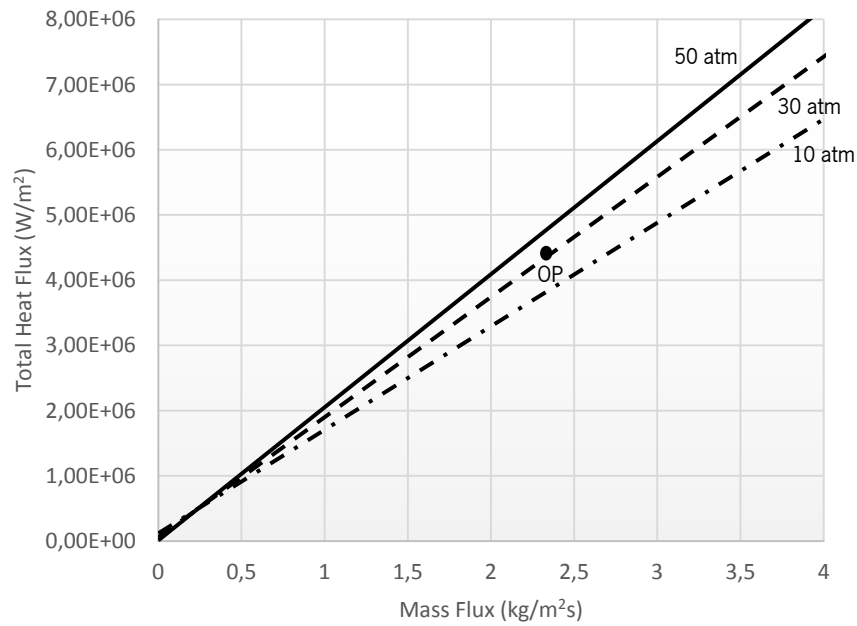
Figure 77 - Total Heat and mass flux for ε =1.

Figure 77 shows that in order to effectively cool the exhaust valve with the imposed mass flux, the water injection should be done during in-cylinder medium pressures of 30 atm (OP). Consequently more water mass (higher mass flux) has to be added to effectively cool the exhaust valve at medium pressures around 20 bar.

Obviously, adding more water would reduce even further the exhaust valve temperature if the droplet contact heat transfer effectiveness was 100% ($\varepsilon = 1$). Using the correlations (31) and (32) the droplet contact heat transfer effectiveness, for a mean ambient pressure of 20 bar and a mean wall surface and droplet temperature of 300 and 500 K respectively, is 94% ($\varepsilon = 0.94$).

Water fuel ratio has to be raised from 0.65:1 to 0.70:1 so that a mass flux of 2.56 kg/m^2 s is obtained and the required cooling effect (in-cylinder mean pressure of 20 bar) is achieved, as can be seen on Figure 78 (OP).
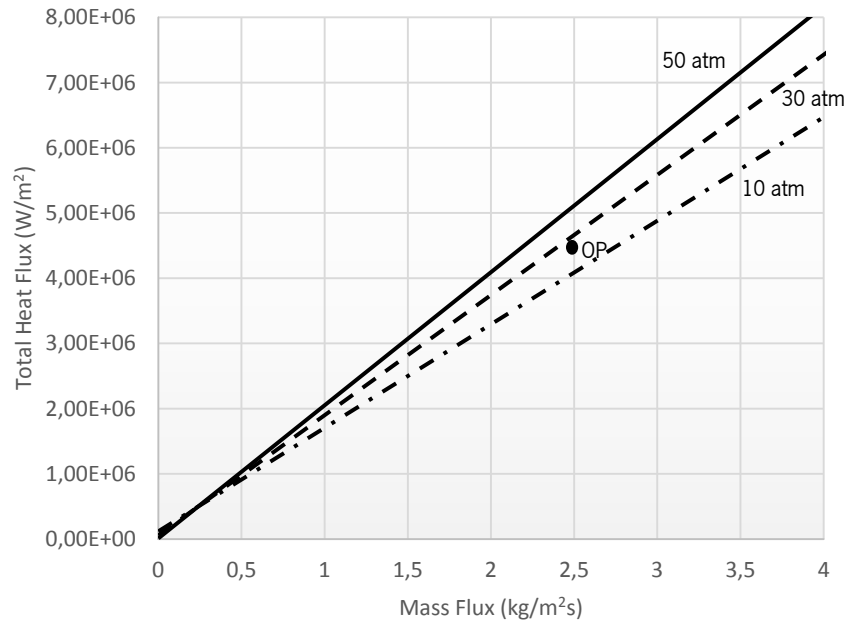
Figure 78 - Total heat and mass flux for ε=0.94.

3.3.8 Results with water injection and varying engine speed

The results presented above, were assessed to explore the possibility of internally cooling the combustion chamber and exhaust valve walls by water injection for a limited set of operating conditions. The model will now be used to evaluate the variations on WFR and water injection duration for different engine speeds.

As shown previously, the increase in engine speed decreases the heat lost to the walls. This fact leads to a reduction in the WFR as engine speed increases. Another aspect resulting from the reduction of the duration of the engine cycle with increasing speed is the maximum heat flux required to cool down the combustion chamber wall by water injection. Establishing a maximum heat flux of 6.0E6 W/m^2K, it is expected that water will have to be injected during a longer period (in terms of CA) as engine speed increases.

Figure 79 shows the model WFR results under varying engine speed for the combustion chamber and exhaust valve. As expected, the increase in engine speed results in a decrease in WFR. Nevertheless, the evolution decrease in WFR is different between combustion chamber and exhaust valve. This is due to the fact that the outer side (right side) of the combustion chamber wall is considered to be adiabatic, and the valve is also cooled by the seat. As engine speed increases

less heat is transferred through the valve seat, leading to an almost linear curve for the exhaust valve and an almost constant WFR with the increase in engine speed above 5000 rpm.
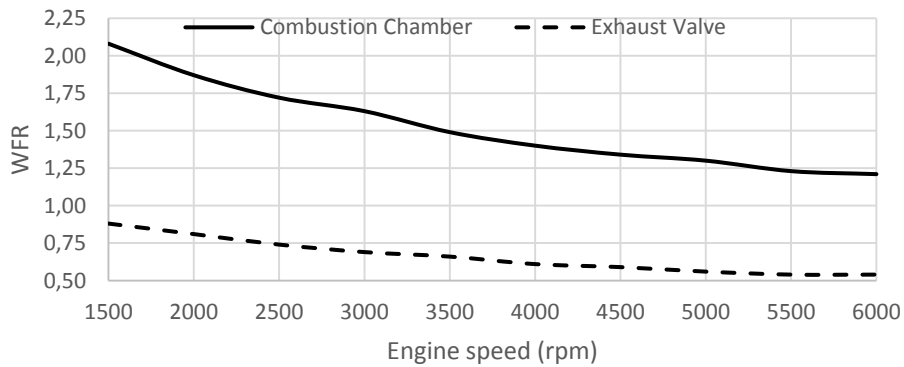
Figure 79 - WFR varying engine speed for the exhaust valve (dashed black line) and combustion chamber (black line).

Figure 80 shows water injection duration as a function of engine speed for the combustion chamber and exhaust valve. The increase in duration of the water injection is nearly linear with the engine speed increase.
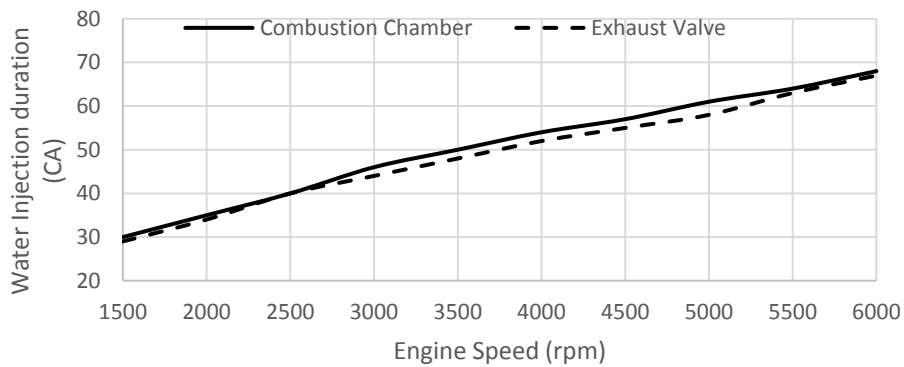
Figure 80 - Water Injection duration varying engine speed for the exhaust valve (dashed black line) and combustion chamber (black line).

Although the results shown above illustrate the already expected outcome, there is a particular phenomenon occurring inside the ICEs that is not being accounted for. As engine speed increases friction losses rise exponentially and all of the energy lost in friction is transformed into heat, heating up the engine oil and part of the cylinder walls. The objective in the future will be to harvest part of this energy to pre-heat the water that will be injected closest to its saturation temperature as possible.

Conventional spark ignition engines suffer from heat created by friction at a level of 10% [3]. The amount of heat required to raise the temperature of the water injected per cycle at 1500 rpm (highest WFR) between 298 K and 373 K is 22 J, which represents almost 2% of the heat supplied by the fuel per cycle. This means that only 20% of the heat created by engine friction is required for the referred goal of warming the water to the saturation temperature.

3.3.9 Thermodynamic analysis of the direct water injection technology

The engine Simulink model was update with the water injection feature in order to evaluate the rise in pressure due to the water mass added to the cycle and predict the increase in engine efficiency and power output.

The next logic step would be to introduce a subsystem were a mass of water could be added to the engine combustion chamber at a specific rate during a given duration, where all gas variables are changed in order to simulate the water injection.

Water injection can be performed in two ways. During combustion with a fine mist (1st water injection) and during the power stroke (2nd water injection).

The 1st water injection is done in order to vaporize the water in the combustion hot gases reducing the temperature and increasing the pressure due to the higher compression ratio generated by the increase in mass inside the cylinder. The 2nd water injection (which is being extensively studied) is performed in order to cool down the combustion chamber walls from the inside of the engine. It is assumed that all the heat needed to vaporize the water comes from the hot combustion chamber walls. Because of the fact that the water spray has to travel through the hot gases, part of it will be vaporized before reaching the walls reducing gas temperature. The amount of water that is vaporized during this process is still being evaluated using CONVERGE, although in this simulation it was assumed to be 25% of the water mass.

The amount of water used in the 1st injection is assumed to be the same as the mass of fuel injected, while the water amount of the 2nd water injection is calculated using the temperature model created in Excel. The next step will be to implement the temperature model in the Simulink model which hasn't been done during this work.

Due to the extensive modifications done on the Simulink model in order to simulate the water injection feature only the results achieved are presented on this work on the next section.

4. Results comparison

All the results of the features analysed and presented on this work are hereafter illustrated and compared using the engine cycle P-V diagram which easily shows the overall amount of work delivered by the thermodynamic cycle performed with the ICE.

Summarizing, increasing engine efficiency may be accomplished by the combination of 4 procedures:

1. Over-expanded cycle;

2. High turbulence generation;

3. Constant volume combustion;

4. High compression ratio obtained by;

    4.1. Over-expanded cycle;

    4.2. Cooling by water injection to be vaporized within the gases during combustion;

5. Extra-expansion of steam from.

    5.1. Steam created by water injection to be vaporized within the gases during combustion;

    5.2. Steam created by water injection onto the combustion chamber walls after combustion;

    5.3. Steam created by water injection onto the exhaust valves after combustion.

The summarized features listed above can be accomplished by the corresponding technologies presented on Table 24.

Table 24 - Features and corresponding technologies.

	1.	2.	3.	4.1.	4.2.	5.1.	5.2.	5.3.
Crankshaft design	x		x	x				
1st water injection					x	x		
2nd water injection							x	x
High swirl intake channel		x						

The intention of this chapter is to calculate to what extent each one of these points has an impact effect on engine efficiency. So there is the necessity to evaluate this point by point.

Listed on Table 25, are the cycles simulated to better understand the increase in efficiency that each feature can provide.

	Crankshaft	Cycle	Geometric CR	Load	Fuel mass (g)	Water inj (1st or 2nd)	Water mass (g)
1	Conventional	Otto		50%		-	-
2	Hypotrochoid	OE		100%			
3	Conventional					1st	1.2E-6
4			11.5:1	50%	1.2E-6	2nd	4.0E-6**
5		Otto				-	-
6	Unconventional *			50%		1st	1.2E-6
7						2nd	4.0E-6**

*Unconventional crankshaft. Piston DWEEL at TDC during 20 CA degrees creating constant volume combustion.

** Mass of water required to cool the combustion chamber walls calculated at conditions present at point 2.

Below are the P-V diagrams obtained by the simulations done and presented on Table 25. Each figure is labelled with the cycle efficiencies and the efficiency improvement (Eff$_i$). Each simulation is compared with simulation number (#1) (conventional crankshaft Otto cycle).

4.1 Hypotrochoid crank over-expanded cycle

The P-V diagram (Figure 81) shows the differences between the Otto cycle at half load (#1) and the over-expanded cycle at WOT using the hypotrochoid crankshaft (#2). Both cycles have the same mass of air trapped in the cylinder after intake. Due to the fact that the over-expanded cycle performs an expansion greater than the Otto cycle there is a significant improvement in engine efficiency. Furthermore the over-expanded has lower exhaust gas temperature and pressure when the exhaust valve opens leading to an overall efficiency improvement of 28%.
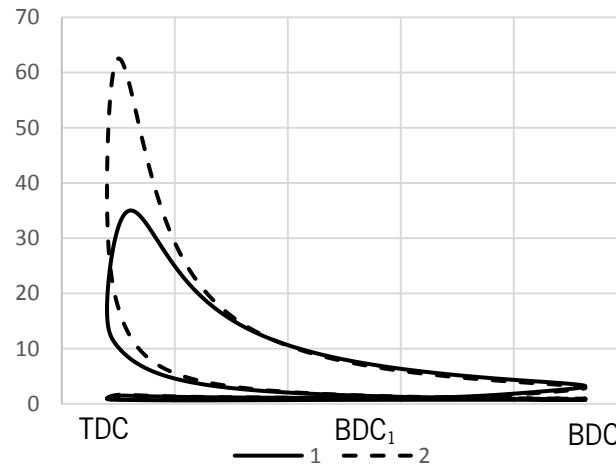
Figure 81 - Engine cycle P-V diagram. 1 – Otto cycle Eff_1=29%; 2 – Over-expanded cycle Eff_2=37%; Eff_1=28%.

4.2 Conventional crank Otto cycle with 1st and 2nd water injection

The P-V diagram presented on Figure 82 show the differences between the Otto cycle at half load with (#3) and without (#1) the first water injection during combustion. The injection of water during combustion increases the cycle's maximum pressure and reduces gas temperature. The fine mist of water spray is vaporized by the hot gases reducing their temperature. The decrease in gas temperature could reduce pressure, however due to the fact that water vapor is generated in a small volume (combustion chamber volume with piston at TDC) the compression ratio increases due to the mass of vapor added to the system resulting in a pressure increase. The increased surface area of the graph representing the positive work of the engine cycle is due to the higher pressure generated and less heat transferred to the engine walls. Therefore cycle efficiency is improved by 7%.
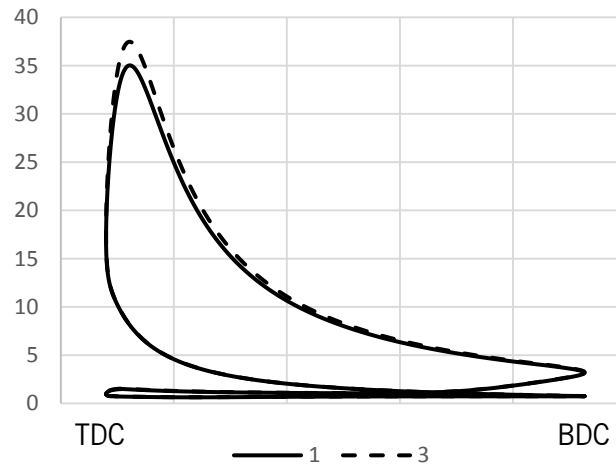
Figure 82 - Engine cycle P-V diagram. 1 – Otto cycle $Eff_1=29\%$; 3 – Otto cycle with 1st water injection $Eff_3=31\%$; $Eff_i=7\%$.

The P-V diagram presented on Figure 83 show the differences between the Otto cycle at half load with (#4) and without (#1) the second water injection during power stroke to cool the engine walls. Water is injected after the combustion occur, starting at 50 CA degrees ATDC and ending at 90 CA degrees ATDC. Due to the fact that the heat used to vaporize the water comes almost from the engine walls, a rise in pressure can be observed on the P-V diagram. Cycle efficiency is improved by 10%. However, when exhaust valve opens, there is a higher gas pressure comparatively to the basic Otto cycle which is wasted. Therefore, in order to increase even further the cycle efficiency over-expansion should be implemented. The cycle efficiency is improved by 10%.
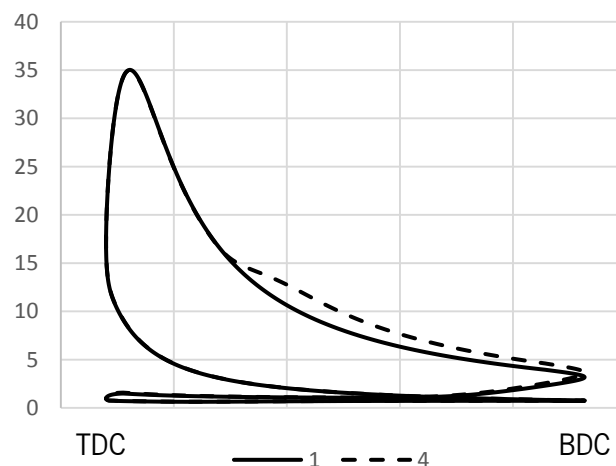

Figure 83 - Engine cycle P-V diagram. 1 – Otto cycle $Eff_1=29\%$; 4 – Otto cycle with 2nd water injection $Eff_4=32\%$; $Eff_i=10\%$.

100

4.3 Unconventional crank Otto cycle

The P-V diagram presented on Figure 84 shows the differences between the Otto cycle at half load (#1) and the Otto cycle at half load using the unconventional crankshaft which performs isochoric combustion (#5). Despite of the higher pressure attained performed by the constant volume combustion, the efficiency improvement is small (6%). This results from the higher heat losses to the engine walls which are a consequence of the higher gas pressure and temperature.
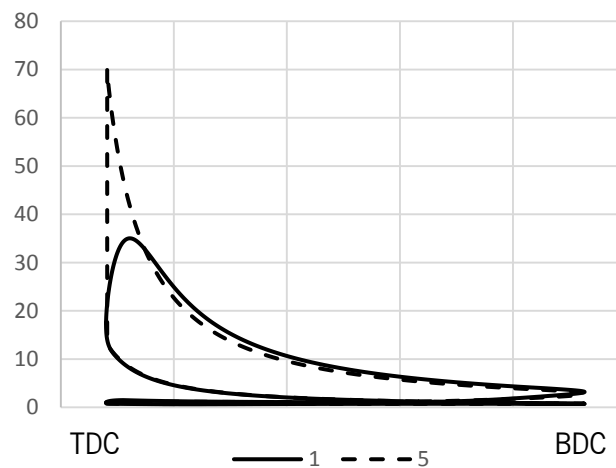
Figure 84 - Engine cycle P-V diagram. 1 – Otto cycle Eff$_1$=29%; 5 – Otto cycle with CVC Eff$_5$=31%; Eff$_i$=6%.

4.4 Unconventional crank Otto cycle with 1st and 2nd water injection

The P-V diagram presented on Figure 85 shows the differences between the Otto cycle at half load (#1) and the Otto cycle at half load using the unconventional crankshaft with the first water injection during combustion (#6). The P-V diagram presented on Figure 86 show the differences between the Otto cycle at half load (#1) and the Otto cycle at half load using the unconventional crankshaft with the second water injection during power stroke to cool the engine walls (#7). The same amount of water spray and duration, performed on the Otto cycle using the conventional crankshaft, were used to simulate the latter cycles.

Similar results were achieved with the 1st and 2nd water injections comparatively with the simulations performed with the Otto cycle using the conventional crankshaft. Nonetheless, some improvements could be done to increase cycle efficiency which could not be done using the conventional crankshaft. For instance, more water could be injected during combustion to lower the gas temperature in order decrease heat lost to the engine walls. On the other hand, as more

heat is transferred to the engine walls, more water has to be injected to cool it down. The fact of being able to inject more water will result in higher efficiency improvement.
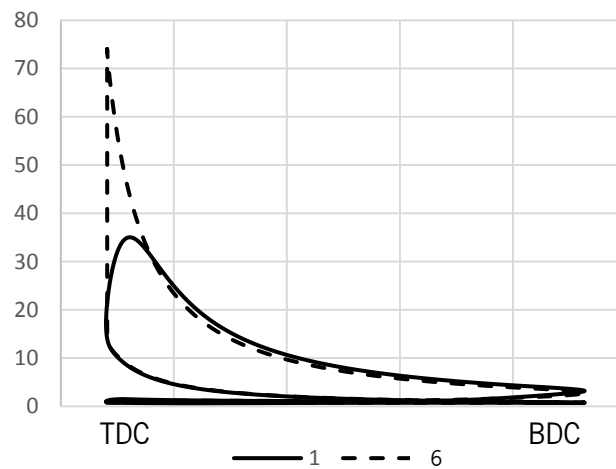
Figure 85 - Engine cycle P-V diagram. 1 – Otto cycle Eff_1=29%; 6 – Otto cycle with CVC and 1st water injection Eff_6=33%; Eff_i=13%
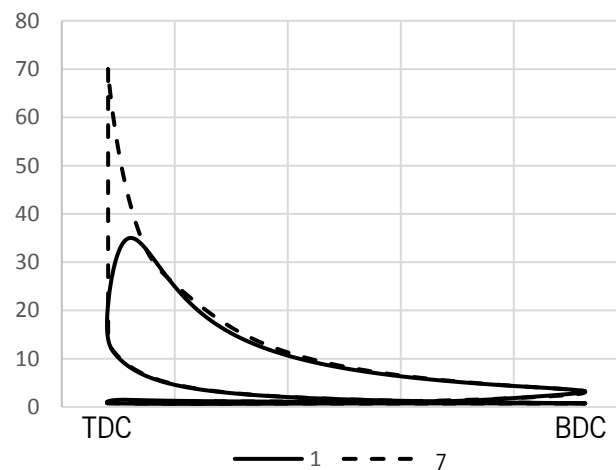
Figure 86 - Engine cycle P-V diagram. 1 – Otto cycle Eff_1=29%; 7 – Otto cycle with CVC and 2nd water injection Eff_7=35%; Eff_i=20%

4.5 Combined cycle

In conclusion, the next logic step would be to combine all the features simulated creating an engine cycle using the unconventional crankshaft which produces over-expansion (performed by the crankshaft), constant volume combustion, and run the 1st and 2nd water injection creating an adiabatic engine. Although more work and study has to be done in order to quantify all the variables involved to produce the most efficient cycle, it is expected that the thermal efficiency might reach values close to 50% (Figure 87).

102
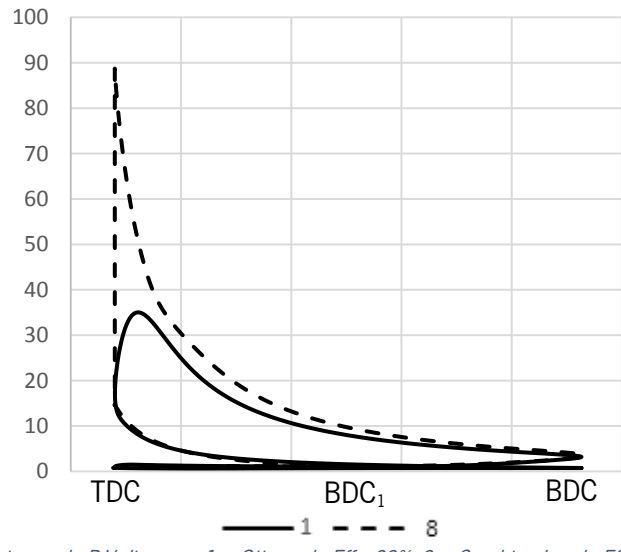
Figure 87 - Engine cycle P-V diagram. 1 – Otto cycle Eff$_1$=29%; 2 – Combined cycle Eff$_8$=50%; Eff$_i$=72%.

104

5. Conclusions and Future Work

Different features are proposed and analysed in order to increase the ICE efficiency. Supported by 0D models and a commercial CFD software it was possible to quantify the efficiency increment that each feature can provided (Table 26).

Table 26 - Calculated cycle efficiencies.

	Crankshaft	Cycle	Water injection (1st or 2nd)	Eff
1	Conventional	Otto	-	29%
2	Hypotrochoid	OE	-	37%
3	Conventional	Otto	1st	31%
4	Conventional	Otto	2nd	32%
5	Unconventional	Otto	-	31%
7	Unconventional	Otto	1st	33%
8	Unconventional	Otto	2nd	35%

Before being presented the features studied on this work, the UMotor specifications and development was presented. This helped to understand its design and to show all the peculiar features introduced in order to achieve a high efficient ICE. Also the commercial CFD software and the 0D engine model were briefly introduced in order to show their capabilities.

5.1 Over expansion

A detailed piston skirt friction analysis and comparison between the epitrochoid and the hypotrochoid crankshaft had clearly show that the hypotrochoid crankshaft was the best choice for the UMotor crankshaft due to the lower friction work produced during the whole power stroke. Using the hypotrochoid crankshaft mechanism the engine efficiency achieves higher levels (37%) than using other techniques to produce an over expanded cycle.

Work needs to be done in order to fully assess the dynamics of the hypotrochoid crank mechanism and the friction losses associated with it. In the present work only the friction associated with the piston/cylinder walls was accounted for.

5.2 Combustion efficiency improvement

The 0D combustion model was developed in order to be implemented on the wall temperature model. A result comparison with the commercial CFD software shows good results, being a reasonably good way to calculate the heat release rate from combustion using a fast and straightforward technique.

The UMotor already designed intake channel and combustion chamber was simulated on the CFD software in order to predict the swirl generation and its influence on the combustion efficiency. The generation of turbulence really improves the engine efficiency even if the heat losses are higher. A dual spark plug system also improves the efficiency although in a more modest way. Both features speed up the combustion, increasing the component of the combustion which is made under a nearly constant volume condition. This result in a higher cycle maximum pressure increasing the cycle indicated work. Therefore, the UMotor intake channel really does what is supposed to, and will improve significantly the real engine combustion efficiency.

An alternative way to increase combustion efficiency is by performing combustion at a constant volume using an unconventional crankshaft which creates the ability of performing the piston motion desired during the 4 strokes. Simulating the engine cycle using the UMotor combustion chamber with a normal intake channel and one spark plug on the commercial CFD software opens the ability to quantify the combustion efficiency improvement performing constant volume combustion. This feature was found to increase the heat release rate, creating a faster combustion and providing the ability of igniting the air-fuel mixture without the need for any advance and creating no negative work during the compression stroke.

Nevertheless, the increment on thermal efficiency was lower than expected due to the higher heat losses during combustion. More work has still to be done, tuning the piston motion in order to enhance the engine thermal efficiency without being limited by the conventional engine piston motion.

5.3 Direct water injection

The direct water injection feature is a great engineering idea, but is extremely complex to be study in a short period of time. There is a lack of scientific studies presented about the subject, and even information on water spray injection and cooling at high atmospheric pressures is relatively scarce.

Water injection could be performed in two ways. During combustion with a fine mist (1st water injection) and during the power stroke (2nd water injection).

The 1st water injection is done in order to vaporize the water in the combustion hot gases reducing the temperature and increasing the pressure due to the higher compression ratio generated by the increase in mass inside the cylinder. This feature is still being evaluated using CONVERGE, and no development is presented in this work about this subject.

The 2nd water injection (which was extensively studied) is performed in order to cool down the combustion chamber walls from the inside of the engine. It is assumed that all the heat needed to vaporize the water comes from the hot combustion chamber walls.

The purpose of the work was to create a quasi-adiabatic spark ignition engine by internal cooling using direct water spray injection. The principal aim is to reduce the heat lost by the engine walls by using it to produce work through the expanding vaporizing water. Consequently a wall temperature model was developed in Excel, in order to evaluate the feasibility of this concept.

The work done until now allowed the estimation of the amount of water that has to be used to cool the combustion chamber and exhaust valve walls to the desire temperature levels and the rise in thermal efficiency that can be achieved with that strategy.

Work has still to be done using CFD software and experimental studies focusing on the spray injection under high ambient pressures and temperatures in order to verify the feasibility of this technology.

6. References

[1] H Ealey, L. A., Mercer, G. A., Tomorrow's cars, today's engines, Mckinsey Quarterly, Number 3, 2002.

[2] Martins, J., Motores de Combustão Interna, Publindústria, Porto, 2005. (in portuguese)

[3] Heywood, J., Internal Combustion Engines Fundamentals, 1988, McGraw-Hill.

[4] Harry, R., The high-speed internal-combustion engine, London, 1968.

[5] Poulos, S. G., and Heywood, J. B., The Effect of Chamber Geometry on Spark-Ignition Engine Combustion, SAE paper 830334, SAE Trans., vol. 92, 1983.

[6] Brunt, M.F.J., The effect of combustion chamber design on the combustion rate in an SI engine, Doctoral Thesis, 1980.

[7] CARIS, D.F., MITCHEL, B.J., McDUFFIE, A.E. and WYCZALEK, r.A. Mechanical Octanes for Higher Efficiency. S.A.E. Transactions, VOL 64, 1956.

[8] QUADER, A.A. Lean Combustion and the Misfire Limit in Spark Ignition Engines. S.A.E. paper 741055.

[9] OBLANDER, K., ABTHOFF, J. and FRICKER, L. From Engine Testbench to Vehicle - An Approach to Lean Burn by Dual Ignition. Pap8r C8B/79, I.Mech.E. Conference on Fuel Economy and Emissions of Lean Burn Engines, London, 1979.

[10] NAKAJIMA, Y., SUGIHARA, K. and TAKAGI, Y. Lean Mixture or EGR - Which is Better for Fuel Economy and NO Reduction? Paper C94/79, x I.Mech.E. Conference on Fuel Economy and Emissions of Lean Burn Engines, London, 1979.

[11] Blair, G. P., Design and Simulation of Four-Stroke Engines, Warrendale (U.S.A), SAE, 1999.

[12] Stone, R., Motor Vehicle Fuel Economy, Middlesex (England), Macmillan education LTD, 1989.

[13] Lumley, J. L., Early work on fluid mechanics in the IC engine, Annual Reviews, Annual Review of Fluid Mechanics Volume 33, Issue 1, 2001.

[14] RIBEIRO, B., MARTINS, J., Direct Comparison of an Engine Working under Otto, Miller and Diesel cycles: Thermodynamic Analysis and Real Engine Performance, Technical Paper Series, nº 2007-01-0261, included in 'New SI Engine and Component Design and Engine Lubrication and Bearing Systems', edited by SAE (ISBN Number:978-0-7680-1883-7), 2007

[15] Baker, T.G., Nightingale, C. J. E., Port Throttling and Port De-activation Applied to a 4-Valve SI Engine, SAE 960587, 1996.

[16] NAGAYAMA, I. ARAKI, Y. and IIOKA, Y. Effects of Swirl and Squish on S.I. Engine Combustion and Emissions. S.A.E. 770217.

[17] Kutlar, O. A., Arslan, H., Calik, A. T., Methods to improve efficiency of four stroke, spark ignition engines at part load, Energy Conversion and Management 46 (2005) 3202-3220, 2005.

[18] Ribeiro, B., Martins J., Desenvolvimento do Conceito de Motor Sobre-Expandido – análise teórica, numérica e experimental", 8° Congresso Iberoamericano De Engenharia Mecanica (CIBIM 8), Cuzco, October 23rd – 25th, 2007.

[19] Martins, J., Uzuneanu, K, Ribeiro, B., Jasansky O., Thermodynamic Analysis of an over-Expanded Engine, SAE 2004-01-0617, 2004.

[20] Ribeiro, B., Martins, J., Nunes, A., Generation of Entropy in Spark Ignition Engines, Int. J. of Thermodynamics (ISSN 1301-9724), Vol. 10 (No. 2), pp. 53-60, June, 2007.

[21] Martins, J., Ribeiro, B., Ion, I., Thermodynamic Analysis of Spark Ignition (SI) Engines Using the Entropy Generation Minimisation Method, Int. J. Exergy, Vol. 6, No. 1, pp 93-110, 2009

[22] Martins, J., Ribeiro, B., Motor com Ciclo Sobre-Expandido com Taxa de Compressão Efectiva Constante, Patente Nacional nº103363, concedida a 11 de Abril de 2008 (Boletim da Propriedade Industrial no. 73/2008 de 11 de Abril de 2008).

[23] Takita, Y., Kono, S., Naoi, A., Study of Methods to Enhance Energy Utilization Efficiency of Micro Combined Heat and Power Generation Unit-Equipped with an Extended Expansion Linkage Engine and Reduction of Waste Energy," SAE Technical Paper 2011-32-0574, 2011.

[24] Hitomi, M., Sasaki, J., Hatamura, K., Yano, Y., Mechanism of Improving Fuel Efficiency by Miller Cycle and Its Future Prospect, SAE 950974, 1995.

[25] Hirose, K., Ueda, T., Takaoka, T., Kobayashi, Y., The high-expansion-ratio gasoline engine for the hybrid passenger car, JSAE Review 20 (1999), 13-21.

[26] Liquid Piston Website, Available: www.liquidpiston.com/technology/hehc-cycle/ Last accessed 15th September 2014.

[27] Shkolnik, N., Shkolnik A. C., High Efficiency Hybrid Cycle Engine, ICEF2005- 1221, Proceedings of ICEF2005, ASME.

[28] Scuderi Group Website, Available: http://www.scuderigroup.com/engine-development/ Last accessed 15th September 2014.

[29] Suzuki, M., et al, Effect of Piston Speed around Top Dead Center on Thermal Efficiency, Article of Honda R&D Technical Review, Vol.18, No.1, 2006.

[30] Doric, J. et al, Constant volume combustion cycle for IC Engines, FME Transactions, pp 37-104, 2011.

[31] Winward, R. et al, Quasi-Constant Volume (QCV) Spark Ignition Combustion, SAE Technical Paper 2009-01-0700.

[32] Doric, J., Klinar, I., Efficiency Characteristics of a New Quasi-Constant Volume Combustion Spark Ignition Engine, In Thermal Science, Vol. 17, No. 1, pp. 119-133, 2012.

[33] Wei-Xin, X., Liang-Fang, Z., The thermal conductivity of ceramic piston, heat-insulation effect of air layer and their influence upon thermal load in adiabatic engine, In Heat and Mass Transfer in gasoline and diesel engines, London, UK, 1987.

[34] R. B. Melton, JR., S. J. Lestz, R. D. Quillian, JR. DIRECT WATER INJECTION COOLING FOR MILITARY ENGINES AND EFFECTS ON THE DIESEL CYCLE, U.S. Army Fuels and Lubricants Research Laboratory, Southwest Research Institute, San Antonio, Texas.

[35] Weatherford, JR., Quillian, JR., Total Cooling of Piston Engines by Direct Water Injection, SAE Technical Paper 700880, 1970.

[36] Rothrock, A., Krsek. A., Jones, A., The induction off water to the inlet air as means of internal cooling in aircraft-engines cylinders, NACA report no. 756

[37] Vandeman, J., Heinicke, O. Effect of water-alcohol injection and maximum-economy spark advance on knock-limited performance and fuel economy of a large air-cooled cylinder. Aircraft engine research Laboratory Cleveland, Ohio. NACA report E5H12, 1945.

[38] Chasselut, P. HIGHLIGHTS 1997 ITALIAN FORMULA 1 WORLD CHAMPIONSHIP RENAULT F1, 1977 1997:THE ITALIAN GRAND PRIX. Available: http://www.aquamist.co.uk/dc/coollinks3/index/race/renaultf1/renault.html Last accessed 10th February 2013.

[39] Bedford, F. et al., Effects of Direct Water Injection on DI Diesel Engine Combustion. SAE Technical Paper 2000-01-2938.

[40] Conklin, J., Szybist, J., A highly efficient six-stroke internal combustion engine cycle with water injection for in-cylinder exhaust heat recovery, In "Energy 35", pp 1658–1664, Elsevier, 2010.

[41] Kiran, P., A Feasibility Study on Waste Heat Recovery in Six Stroke IC Engine, In "International Journal on Mechanical Engineering and Robotics (IJMER)", Volume-1, Issue-1, pp 113-117, 2013. ISSN 2321-5747

[42] Kandari, S., Gupta, I., Six Stroke Engine. In "International Journal of Engineering Research & Technology (IJERT)", Vol. 2, Issue-10, pp 884-889, 2013. ISSN: 2278-0181

[43] Pirault, J., Split-Cycle engine with water injection. International Publication Number WO 2008/106007 A1, 2008.

[44] Thorpe, D., Evaporative In-Cylinder Cooling. United States Patent Number US 7,299,770 B2. 2007.

[45] Mulye, N., Internally Cooled High Compression Lean-Burning Internal Combustion Engine. United States Patent Number US 2012/0260886 A1. 2012.

[46] Keays, S., Internal combustion water injection engine. European Patent Application Number 08005402.6. 2009.

[47] Binion W., In-Cylinder Water Injection Engine. United States Patent Number 5,718,194. 1998.

[48] Zemer, D., Engine Having Direct Water Injection During Power Stroke. Patent Number WO1998003779 A3. 1998.

[49] Crower, H., Method and Apparatus for Operating an Internal Combustion Engine. United States Patent Number US 2007/0022977 A1. 2007.

[50] Yuki, A. et al., Method of Operating Internal Combustion Engine Injected with Critical Water. European Patent Application Number 02713301.6. 2008.

[51] Maro, R. Matousek, R., Advanced Internal Combustion Engine. United States Patent Number US 8,479,690 B2.

[52] Gothenburg, L. Horred, B., Turbo Charged Combustion Engine with Water Injection. United States Patent Number 4,558,665.

[53] Leone, T. et al., Engine with Water and/or Ethanol Direct Injection Plus Gas Port Fuel Injectors. United States Patent Number US 7,730,872 B2.

[54] Connor, M., Coordinated Water and Fuel Injection System. United States Patent Number 5,148,776.

[55] Hobbs, C., Water Introduction in Internal Combustion Engines. United States Patent Number 5,125,366.

[56] McAlister, R., Systems and Vehicles Incorporating Improved Engine Cooling and Energy Generation. United States Patent Number US 2013/0291826 A1.

[57] McAlister, R. et al., Systems and Methods for Improved Engine Cooling and Energy Generation. United States Patent Number US 2013/0206082 A1.

[58] Freiberg, H., Reciprocating Piston Combustion Engine With Water Injection. United States Patent Number 4,502,420.

[59] Eaubonne, D., Device For Injecting Water Into The Cylinders Of An Internal Combustion Engine, Particularly For Reducing The Degree Of Pollution Of The Latter. United States Patent Number 4,120,268.

[60] Jepsen, M., Combined Internal Combustion and Steam Engine. United States Patent Number 4,322,950.

[61] Eft, S., Water Injection System for I.C. Engines. United States Patent Number 4,018,192.

[62] Dunlap, C. et al., Water Injection System for an Internal Combustion Engine. United States Patent Number 3,845,745.

[63] McKinley, F., Water Injection Apparatus. United States Patent Number 2,879,753.

[64] Schechter, M., Airless Engine With Gas and Water Recycling. United States Patent Number US 7,958,872 B1.

[65] Meghraj Bhagat, M. et al., Experimental and Numerical Study of Water Spray Injection at Engine-Relevant Conditions, SAE Technical Paper 2013-01-0250.

[66] European Commission, EU Climate and Energy Package, 2010, Available: http://ec.europa.eu/clima/documentation/package/docs/climate_package_en.pdf, Last accessed 15th September 2014.

[67] Jost, K., Upfront (Editorial): Green Innovations, Automotive Engineering International, 118-3, p. 4. 2010

[68] Martins, J., Monteiro, A., Barbosa, J., Engine Design Using Rapid Prototyping Techniques, Proceedings of COBEM 2005, 18th International Congress of Mechanical Engineering, Ouro Preto, MG, Brazil, 2005

[69] Coene, Inlet Design for Optimal Swirl in an IC Engine, MSc thesis, University of Minho, Portugal, 2008.

[70] Honda Parts, Available: http://www.hondaparts-direct.com/, Last accessed 15th September 2014.

[71] Ribeiro, B., Thermodynamic optimisation of spark ignition engines under part load conditions, Doctoral Thesis, Unversity of Minho, 2006.

[72] Converge 2.1.0 Theory Manual, Convergent Science, 2013.

[73] Johansson, S., et al, Experimental friction evaluation of cylinder liner/piston ring contact, Wear 271, p. 625-633, 2011.

[74] Bonatesta, F., Premixed Combustion in Spark Ignition Engines and the Influence of Operating Variable. Chapter 1 of "Advances in Internal Combustion Engines and Fuel Technologies", edited by Hoon Kiat Ng, pp 3-51, Intech, 2013, ISBN 978-953-51-1048-4

[75] Smits, J. J. M., Modeling of a fluid flow in an internal combustion engine, Eindhoven, 2006.

[76] Babajimopoulos, A., et al, A fully coupled computational fluid dynamics and multi-zone model with detailed chemical kinetics for the simulation of premixed charge compression ignition engines, International Journal of Engine Research, Vol. 6, 5: p. 497, 2005

[77] Benson, R., Whitehouse, N., Internal Combustion Engines, Vol. 1, Pergamon Press, 1979.

[78] Issa, R., Numerical Modeling of the Dynamics and Heat Transfer of Impacting Sprays for a Wide Range of Pressures., Doctoral Thesis, University of Pittsburgh, 2003.

[79] Halvorson, P. J., On the Heat Transfer Characteristics of Spray Cooling, Doctoral Thesis, Georgia Institute of Technology, 1994.

[80] Ciofalo, M., Investigation of the cooling of hot walls by liquid water sprays, International Journal of Heat and Mass Transfer 31, pp 1157-1175, 1999.